THE UNIVERSITY OF ALABAMA
COLLEGE OF ENGINEERING
BUREAU OF ENGINEERING RESEARCH

Interim Report
Contract Number MASG-R/ES4

HYDRODYNAMICS OF MOBILE BAY AND MISSISSIPPI SOUND

by
Gary C. April
Donald C. Raney
co-principal investigators

and

Lih Chern
John P. Jarrell
Der-Jang Lou
Yieng-Chiang Wu
graduate research assistants

prepared for
Mississippi-Alabama Sea Grant Consortium

March 1980

BER Report No. 247-112

MASGP-79-020

UA . . . UNIVERSITY, ALABAMA 35486

BUREAU OF ENGINEERING RESEARCH

Members of the faculty who teach at the undergraduate and graduate levels, along with their graduate students, generate and conduct the investigations that make up the College's research program. The College of Engineering of The University of Alabama believes that research goes hand in hand with teaching. Early in the development of its graduate program, the College recognized that men and women engaged in research should be as free as possible of the administrative duties involved in sponsored research. Therefore, the Bureau of Engineering Research (BER) was established and assigned the administrative responsibility for such research within the College.

The director of BER—himself a faculty member and researcher—maintains familiarity with the support requirements of both proposals and research in progress. He is aided by the College of Engineering Research Committee which is made up of faculty representatives from the academic departments of the College. This committee serves to inform BER of the needs and perspectives of the research program.

In addition to administrative support, BER is charged with providing certain technical assistance. Because it is not practical for each department to become self-sufficient in all phases of the supporting technology essential to present-day research, BER makes services available through support groups such as the machine shop, the electronics shop, and publication services.

INTERIM REPORT

HYDRODYNAMICS OF MOBILE BAY AND MISSISSIPPI SOUND

Prepared by

Donald C. Raney, Co-Principal Investigator
Gary C. April, Co-Principal Investigator
Lih Chern, Research Assistant
J. Phillip Jarrell, Research Assistant
Yieng-Chiang Wu, Research Assistant
Der-Jang Lou, Research Assistant

College of Engineering
The University of Alabama
P.O. Box 1968
University, Alabama 35486

Prepared for

Mississippi-Alabama Sea Grant Consortium
P.O. Box Drawer AG
Ocean Springs, Mississippi 39564

March 1980

This work is a result of research sponsored in part by NOAA Office of Sea Grant, Department of Commerce under Grant No. NA79AA-D-00049 and the Mississippi-Alabama Sea Grant Consortium. The U. S. Government is authorized to produce and distribute reprints for governmental purposes notwithstanding any copyright notation that may appear hereon.

TABLE OF CONTENTS

LIST OF FIGURES

I. SUMMARY

Previous work at The University of Alabama dealing with the numerical modeling of Mobile Bay has demonstrated the value of a predictive capability describing water movement and elevation in coastal waters. The extension of that concept to include the Mississippi Sound is both logically and technically correct. Each of these water bodies influences the circulation within the other. That has been demonstrated in field-survey studies during the '70s. The nature of the coastal zone adjacent to these waters is such that rapid industrial, commercial, residential and recreational development is expected. Major goals of this project are, therefore, directed at providing information responsive to this development.

During 1979, successful adaptation of the WIFM II models to Mississippi Sound and Mobile Bay has been achieved. Trend calibration studies in the Mobile Bay system have been completed using historical field survey data. Results from a Sea Grant-sponsored field survey designed for trend calibration in Mississippi Sound is anticipated during the early period of 1980. In addition, data from a detailed 6-month survey program to be conducted by the Corps of Engineers in mid-1980 may be made available for comprehensive calibration and verification of the models.

Preliminary investigations have been initiated into water-quality models, storm-surge models, three-dimensional models and sediment-transport processes. These areas will become of increasing importance once the hydrodynamic model WIFM II has been verified and calibrated for Mobile Bay and Mississippi Sound.

II. OBJECTIVES OF THE STUDY

The objective of this study is to establish a baseline methodology from which water-resources management, water-quality assessment and water-related projects in the Mobile Bay-Mississippi Sound region can be achieved. This objective will be accomplished by implementing the specific tasks listed as follows:

1. To extend the mathematical modeling capabilities developed for the Mobile Bay system to the Mississippi Sound area shown in Figure 1.
2. To review the historical data base, to integrate the field data information provided in a parallel physical oceanographic study, and to use this information to establish preliminary trend behavior for water-movement patterns and water levels under mid-range meteorologic and hydrologic conditions.
3. To apply the developed trend analyses in better defining field data survey locations that complement the math modeling effort.
4. To calibrate and verify the model with the physical oceanographic data, thus providing a sound starting point from which three-dimensional models can be evaluated and/or material transport, water-quality and economic models can be applied to better describe the system.

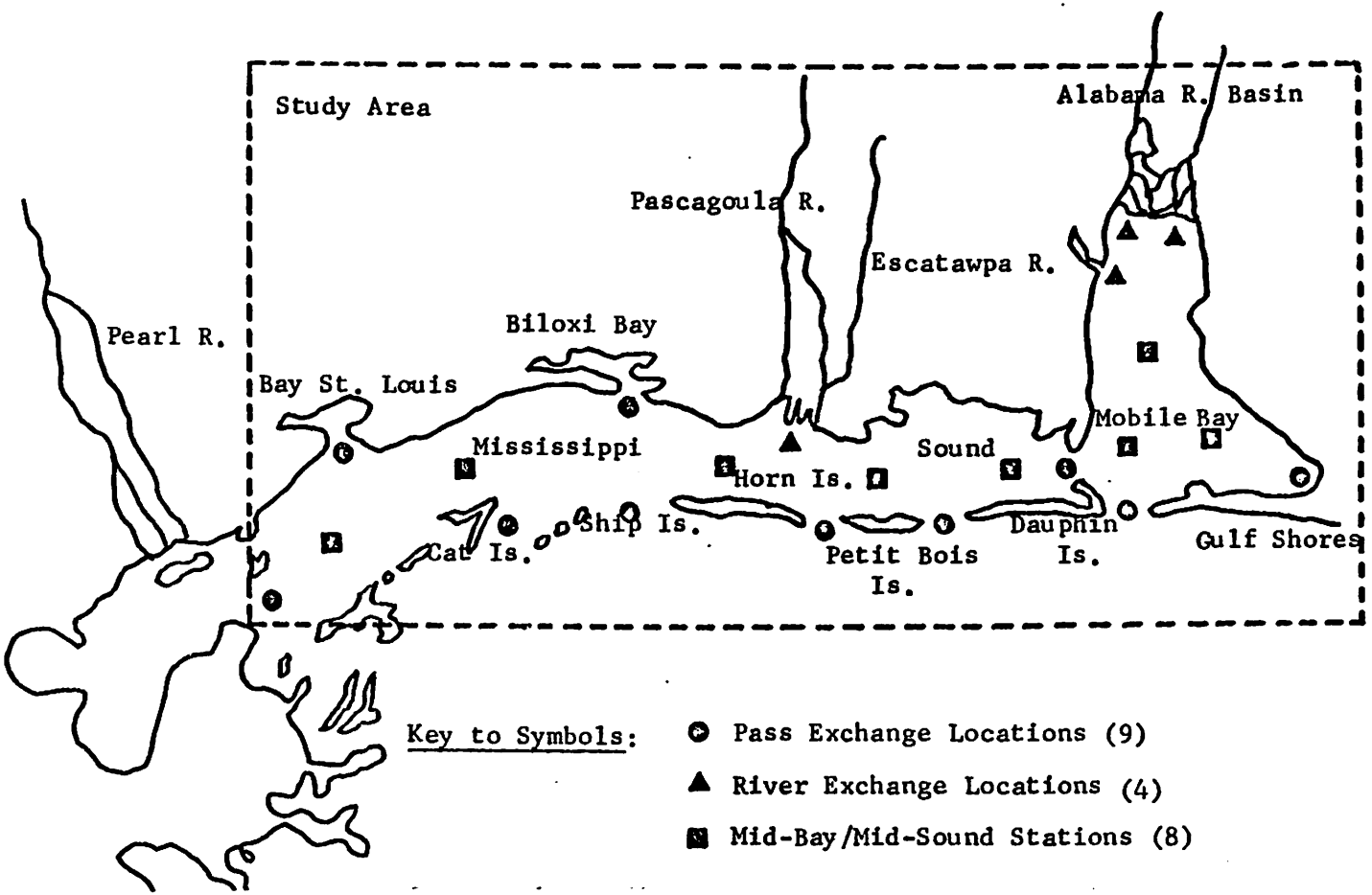

Figure 1. Mobile Bay-Mississippi Sound Study Area

III. APPROACH

It seems only logical that a basis from which the mathematical modeling effort should begin is the 7-year experience of Mobile Bay modeling at The University of Alabama. This experience, plus the additional numerical modeling experience of the co-principal investigators, insures that the proposed work will proceed in an expedient manner. Although data-limited in many areas, the hydrodynamic description of the bay has proven to be a good representation of behavior suitable for trend analysis, and in some cases, detailed subsystem (isolated bay areas) analysis. This background, along with accumulated data collected in conjunction with the various bay studies, provides a valuable starting point from which capabilities can be applied to the Mississippi Sound.

Additionally, a search of historical data (river flow, storm frequency, wind, rainfall, etc.) that could provide insight and knowledge of the coastal zone is important. This information, while limited in the ability to assist in detailed mathematical modeling calibration/verification, can provide trend behavior patterns for initial exercises of the formulated models. Such was the case in the Mobile Bay project, during which valuable information concerning where field data surveys could provide supportive data was established. This will likewise be done during the first year (Phase 1 of the project - Figure 2). Field data from the Sea Grant programs will be interfaced with the model with the intention of beginning calibrating studies. Also, during this period, information concerning the location, time and frequency of data-collection planned for the second year will be generated.

Figure 2

WORK SCHEDULE

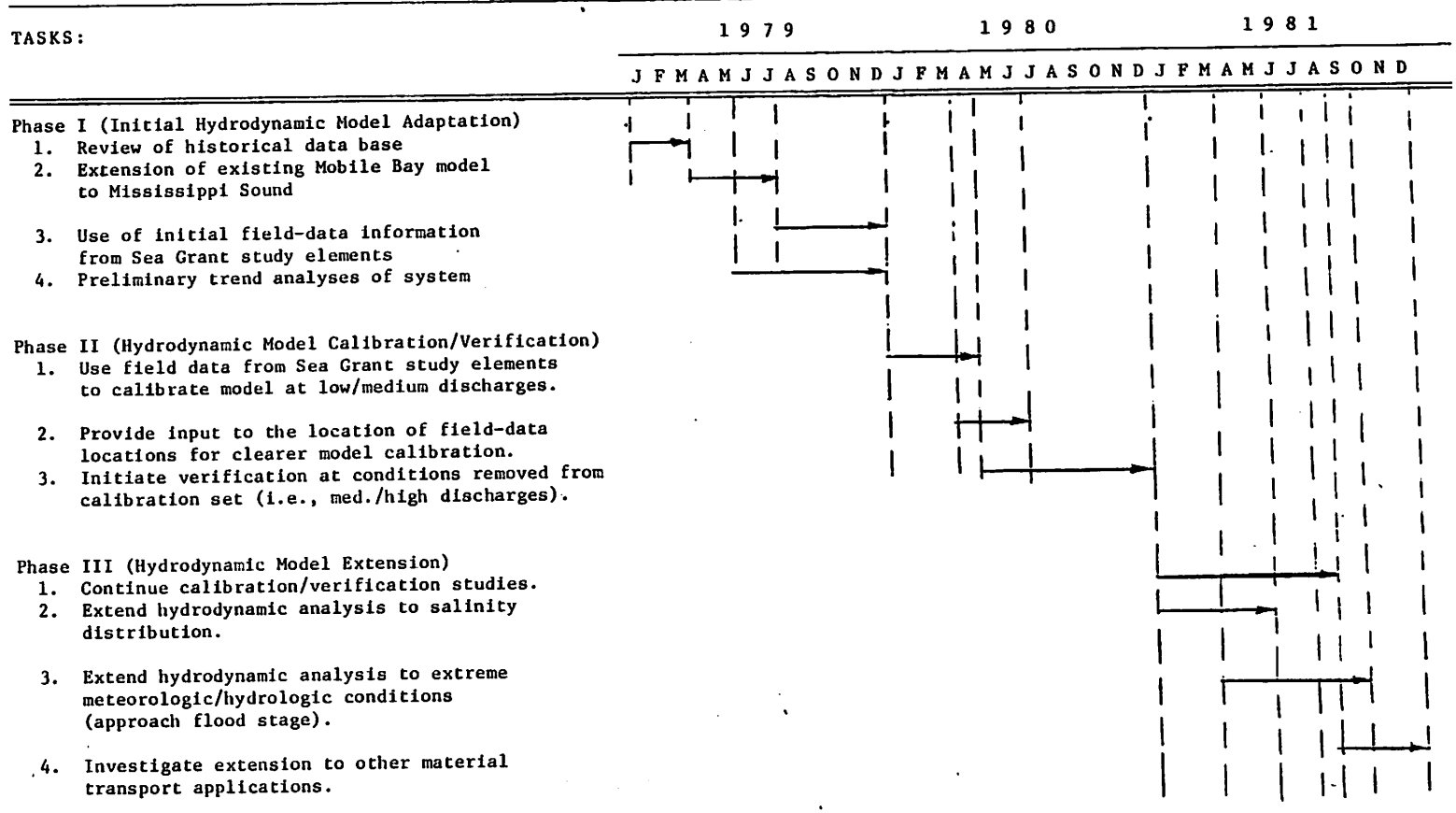

Phase II of the project (second year) will be designed to calibrate and verify the model for the coastal water masses. This phase of the project will rely on the field surveys for data (including pass exchange, water movement and level, conductivity, temperature, etc.) to provide an accurate description of water movement and level (hydrodynamic behavior) under mid-range or lower meteorological and hydrologic conditions. Although calibration and verification are an ongoing effort in a project such as this one, it is anticipated that sufficient data will be available to permit the application of the hydrodynamic model in describing limited material transport properties of the water mass (i.e., salinity).

Phase III of the project (3rd year) will deal with the description of overall material transport properties within the bay. Beginning with salinity distribution patterns, this study will rely on field data collected during Phases I and II for calibration and verification of both conservative and non-conservative bulk transport. Success with this part of the project will allow the further extension of the model to describe (i) hydrodynamic and material transport properties at extreme conditions, (ii) water quality within the estuarine system, or (iii) other transport descriptions for selected species such as bacteria, nutrients, chemical pollutants, etc. Also, during Phases II and III, evaluation of three-dimensional models will be made, especially where needed to describe stratification within the system.

Thus in three years, a sound mathematical model base, supported by field data collected specifically for model use, will be established. Directed studies aimed at particular, pressing issues will be able to be addressed with a high degree of confidence and reliability - factors which are not now available. This report covers the completed tasks under Phase I of the program objectives.

Several of the tasks in Phase II and Phase III are heavily dependent upon prototype data. It may be necessary to shift some activities between Phase II and Phase III to accommodate the prototype data-acquisition schedule.

IV. NUMERICAL SIMULATION MODELS

A. Introduction to Finite-Difference Modeling

Numerical modeling is a rapidly developing discipline which can be attributed in part to the general availability of fast, large-memory digital computers. A fast, large-memory computer is generally necessary to obtain the desired resolution from the model results in a reasonable amount of computer time. Prior to the 1970s, access to large, fast computers was restricted to the larger government or university research laboratories; however, this type computer is now generally available at most universities. As a consequence, development and use of state-of-the-art numerical models are now common within the academic community.

A numerical model basically consists of a numerical algorithm which has been developed from the differential equations governing the physical phenomena. Several methods exist for developing the numerical algorithm, falling generally into two types of formulation: finite-difference and finite-element. Finite-element techniques are used extensively in solid mechanics but to a much smaller extent in fluid mechanics. For a variety of reasons, finite-difference techniques have gained greater acceptance in hydrodynamic modeling. A one-dimensional, two-dimensional or three-dimensional model formulation may be required, depending on the individual problem to be considered.

Numerical fluid mechanics is a separate discipline, with many features distinct from experimental fluid mechanics and theoretical fluid mechanics. The numerical modeler, however, does have many problems in common with the physical modeler. The numerical modeler (as does the

physical modeler) must interface with individuals involved in the collection of prototype data to provide information for "verification" of the numerical model. Any model must be verified by demonstrating that the model can produce results which agree with measured values for some set of boundary conditions before much credibility can be associated with the model results. Only after a model has been verified can it be used with reasonable confidence as a predictive tool.

There is a wide range of numerical models; however, certain features and concepts are common to most models. The phenomena to be modeled is governed by certain differential equations. To apply a finite-difference solution technique, the physical system must be discretized or divided into smaller "cells" using a (generally) rectangular grid. This may be a one-, two-, or three-dimensional grid or model. Each of these cells' behavior is governed by certain differential equations and appropriate boundary conditions. Using finite-difference techniques, the various derivatives in the differential equations are approximated numerically in terms of distinct values of the variables at the cells. The differential equations are thus replaced by a numerical algorithm which can be solved numerically for values of the flow variables for each cell in the system. The derivative representations are not unique. The finite-difference representation of the governing differential equations can, therefore, be represented in several forms. Choosing the most appropriate representation for a particular differential equation involves the "art" of numerical modeling as opposed to the science of numerical modeling. Some of the difficulties in numerical modeling arise because some very logical finite-difference representations do not work and some apparently minor changes in the finite-difference equations can produce significantly different results.

The governing equations for the generalized three-dimension flow of a fluid represent a complex system of non-linear partial differential equations. The formulation and calculation process for a three-dimensional numerical model is involved. In addition, three-dimensional models require a large quantity of prototype data for the verification and calibration process.

Fortunately, many hydrodynamic events can be satisfactorily represented by a simplified system of governing equations, rather than the generalized three-dimensional equations. For example, for flow in a river, only the river elevation and the volumetric flow rate passing a point at any time may be of interest. Thus, only one spatial dimensional is involved. This problem can be formulated so that only the variables flow rate and surface elevation are dependent variables in the problem. A system of two equations, one momentum equation and the continuity equation, are required to be solved to obtain a solution. This problem would obviously require fewer finite-difference cells and would be much simpler to solve than the general three-dimensional system of equations. This solution will also fail to provide any detailed variation of the velocity with depth or the velocity variation across the river. However, if only flow rate and surface elevations are of interest, then a satisfactory solution can be obtained from this model.

There are also problems where the essential character of the flow is two-dimensional. This problem is best illustrated by the unstratified tidal circulation problem. For tidal circulation flow in an estuary or harbor, obviously the flow varies with position in the harbor. However, as illustrated in Figure 3, in many cases there is relatively little variation of flow across the depth of the water column, and an average

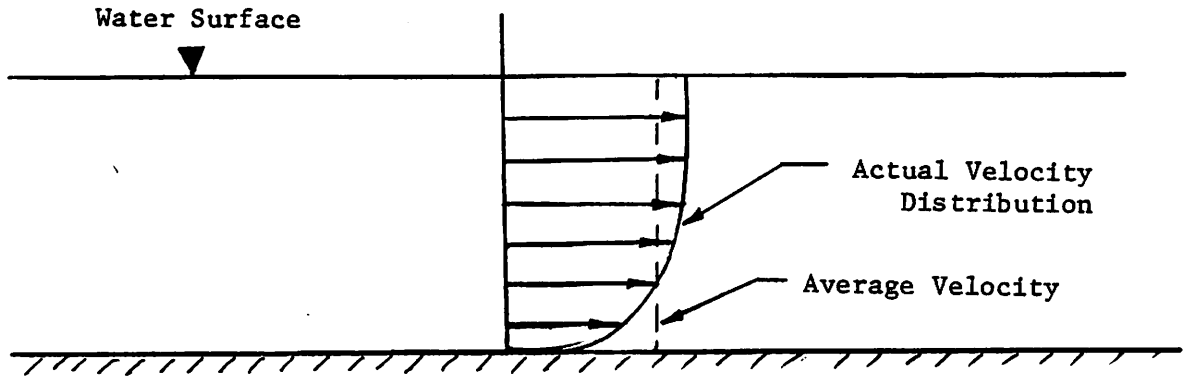

Figure 3. Typical Velocity Distribution Over the Water Depth for Unstratified Tidal Circulation

velocity over the depth has physical significance. This problem can thus be formulated as a two-dimensional flow. This problem will involve two momentum equations and the continuity equation. The problem is still much simpler to formulate, operate and verify than the general three-dimensional flow problem. At the same time, for those problems where the velocity does not vary greatly over depth, very satisfactory results can be obtained.

The three-dimensional model is the most involved. A three-dimensional array of cells is required. There are, however, certain problems (lakes, stratified estuaries, etc.) where it is necessary to use a three-dimensional model to satisfactorily define the flow field. For example, circulation in a lake is primarily due to wind stress. The surface velocity in the lake is thus basically in the same direction as the wind. The velocity, however, varies greatly with depth and indeed the bottom velocity in the lake may be essentially opposite in direction to the wind. This is illustrated in Figure 4. Obviously, an average velocity over the depth has little physical relationship to the actual velocity distribution.

Three-dimensional models require large numbers of finite-difference cells, the calculation procedure is involved, and the model is difficult to verify.

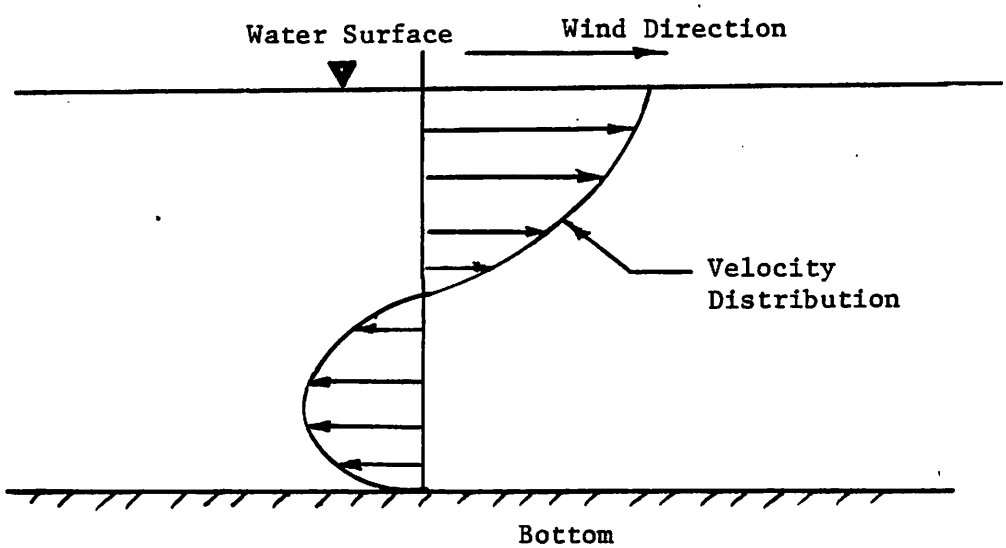

Figure 4. Typical Three-Dimensional Velocity Distribution

A similar situation can occur if salinity and/or temperature gradients produce a stratified estuary. An estuary may be stratified locally and a three-dimensional model may be necessary for detailed investigation of the resulting flows.

The numerical model provides a valuable tool in fluid mechanics, but careful attention must be directed to the limitations imposed by model assumptions. Also, one cannot overstate the need for a numerical model to be calibrated and verified using experimental data.

B. Two-Dimensional-Depth-Averaged Model-WIFM II

For this investigation, the WES Implicit Flooding Model, Version II (WIFM II) is used to simulate tidal circulation in Mobile Bay and

Mississippi Sound. WIFM II is a two-dimensional-depth-averaged model appropriate for application to unstratified estuary systems. WIFM II was developed at the U.S. Army Engineer Waterways Experiment Station (WES) by H. Lee Butler, Reference (1). WIFM II represents the current state-of-the-art in tidal circulation models. A variable grid capability, the ability to flood and dry cells during the tidal cycle, and the ability to represent sub-grid features significantly increase the simulation capability of this model.

Several graphical programs have been developed or modified to display model results in an appropriate format for study and analysis. These graphical programs plot the variable grid overlay for the coastal chart, plot velocity vector flow fields for the entire model area or some portion of the area at desired times in the tidal cycle and plot hydrodynamic variables at specific locations in the study area as a function of time.

The theoretical analysis and development of the governing equations for WIFM II are not original. These discussions are included for completeness since portions of this material are not available in the open literature.

1. Equations of Motion

The hydrodynamic equations used in WIFM are derived from the classical NAVIER-STOKES equations in a Cartesian coordinate system. The coordinate system used is shown in Figure 5.

The following assumptions have been made in the WIFM II model:

(1) The water column is incompressible and homogeneous.

(2) Vertical acceleration of the fluid is neglected.

(3) Horizontal flow over the fluid depth is reasonably uniform.

These assumptions result in the classical, vertically integrated long wave equations of motion and mass conservation. A detailed derivation of these equations is given in reference (2). These equations provide a basis for solving numerous problems dealing with the behavior of long-period waves. Long-period waves are those whose wave length is large compared with the water depth. Applications include, in part, simulation of tidal circulation, storm surge, open-sea tsunami propagation, tsunami inundation, and landslide-generated water waves. Sound engineering judgment must be exercised to assess the applicability of these equations to a given problem.

The basic equations for the two-dimensional-depth-averaged hydrodynamic model are:

a. Momentum Equations

$$\frac{\partial U}{\partial t} + \frac{\partial}{\partial x}\left(\frac{U^2}{d}\right) + \frac{\partial}{\partial y}\left(\frac{UV}{d}\right) - fV + gd\,\frac{\partial}{\partial x}(\eta-\eta_a) + F_x + \frac{gU}{c^2d^2}(U^2+V^2)^{\frac{1}{2}} - e\left(\frac{\partial^2 U}{\partial x^2} + \frac{\partial^2 U}{\partial y^2}\right) = 0 \tag{1}$$

$$\frac{\partial V}{\partial t} + \frac{\partial}{\partial x}\left(\frac{UV}{d}\right) + \frac{\partial}{\partial y}\left(\frac{V^2}{d}\right) + fU + gd\,\frac{\partial}{\partial y}(\eta-\eta_a) + F_y + \frac{gV}{c^2d^2}(U^2+V^2)^{\frac{1}{2}} - e\left(\frac{\partial^2 V}{\partial x^2} + \frac{\partial^2 V}{\partial y^2}\right) = 0 \tag{2}$$

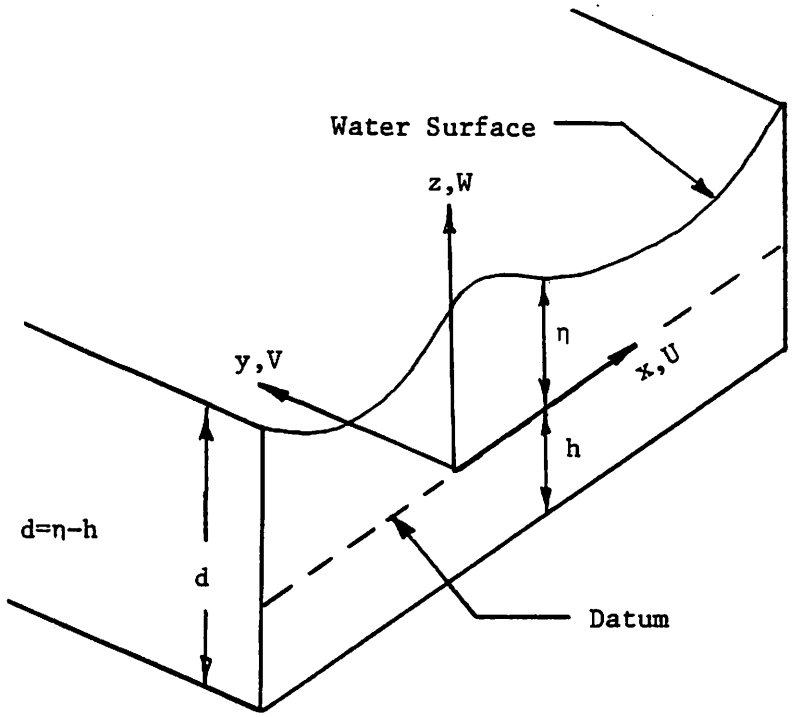

Figure 5. Coordinate System for Problem Formulation

b. Continuity Equation

$$\frac{\partial \eta}{\partial t} + \frac{\partial U}{\partial x} + \frac{\partial V}{\partial y} = \hat{R} \qquad (3)$$

where

η: the water surface elevation

η_a: the hydrostatic elevation corresponding to the atmospheric pressure anomaly

U, V: the vertically integrated transports per unit width at time t in the x and y directions, respectively

$d = \eta - h$: the total water depth

h: the still water elevation

f: the Coriolis parameter

C: the Chezy frictional coefficient

g the acceleration of gravity

e: the generalized eddy viscosity coefficient

$\hat{R}$: the rate at which additional water is introduced into, or taken from, the system (for example, through rainfall and evaporation)

F_x, F_y: external forcing functions such as wind stress in the x and y directions

2. Stretched Coordinates

A major advantage of WIFM II (3) is the capability of applying a smoothly varying grid to the given study region. Independently for each direction, a piecewise reversible transformation is used to map prototype or real space into computational space. The transformation takes the form:

$$x = a + b\alpha^c \tag{4}$$

where a, b, and c are arbitrary constants. The transformation is such that all derivatives are centered in α - space. A time-share program is available to calculate the mapping defined by equation (4) allowing complete control of grid resolution at any point along each grid axis.

By using equations similar to (4), the equation of motion in α - space can be written as:

MOMENTUM EQUATION

$$\frac{\partial U}{\partial t} + \frac{1}{\mu_1}\frac{\partial}{\partial \alpha_1}\left(\frac{U^2}{d}\right) + \frac{1}{\mu_2}\frac{\partial}{\partial \alpha_2}\left(\frac{UV}{d}\right) - fV + \frac{gd}{\mu_1}\frac{\partial}{\partial \alpha_1}(\eta - \eta_a) + F_{\alpha_1} + \frac{gU}{C^2 d^2}(U^2 + V^2)^{\frac{1}{2}} - T_1 = 0 \tag{5}$$

$$\frac{\partial V}{\partial t} + \frac{1}{\mu_1}\frac{\partial}{\partial \alpha_1}\left(\frac{UV}{d}\right) + \frac{1}{\mu_2}\frac{\partial}{\partial \alpha_2}\left(\frac{V^2}{d}\right) + fU + \frac{gd}{\mu_2}\frac{\partial}{\partial \alpha_2}(\eta - \eta_a) + F_{\alpha_2} + \frac{gV}{C^2 d^2}(U^2 + V^2)^{\frac{1}{2}} - T_2 = 0 \tag{6}$$

CONTINUITY EQUATION

$$\frac{\partial \eta}{\partial t} + \frac{1}{\mu_1}\frac{\partial U}{\partial \alpha_1} + \frac{1}{\mu_2}\frac{\partial V}{\partial \alpha_2} = \hat{R} \tag{7}$$

where

$$\mu_1 = \frac{\partial x}{\partial \alpha_1} = b_1 c_1 \alpha^{c_1 - 1} \tag{8}$$

$$\mu_2 = \frac{\partial y}{\partial \alpha_2} = b_2 c_2^{\,c_2 - 1} \tag{9}$$

T_1, T_2 = the transformed flux terms

Quantities μ_1 and μ_2 define the stretching of the regular spaced computational grid in α space to approximate a study region in real region.

Many investigators have found it difficult to obtain meaningful solutions when advective terms (second and third terms of equation 5 and 6) are included. Proper representation of these terms is still being investigated but is not included in the basic WIFM II model. The last terms in the momentum equations are representative of equivalent internal stress resultants due to turbulent and dispersive momentum flux. They provided a mechanism for dissipating wave energy of wavelength on the order of twice the spatial step by smoothing curvatures developing in the solution. Since energy is transferred to this scale by the non-linear advective terms and these terms have been neglected in this presentation, the flux terms have also been omitted in the basic WIFM II model. Both terms are presented here for completeness.

C. Computational Techniques

1. Implicit Formulation

To form the finite difference approximations of the differential equations, a space-staggered scheme shown in Figure 6 is used where flows and water levels are defined at different locations in the grid.

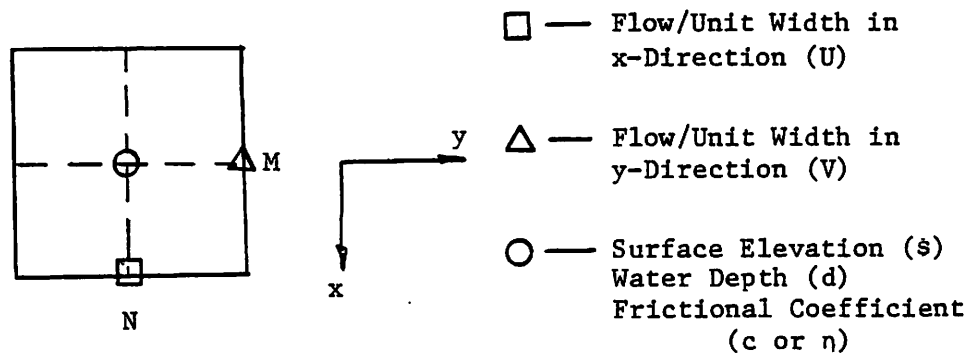

Figure 6

Definition of Variables in Finite-Difference Cell

A multi-operational alternating-direction technique is used to develop an appropriate algorithm. Computations are separated into two cycles corresponding to a sweep of the grid in both directions. The first operation computes η and U implicitly, advancing the time from $K\Delta t$ to $(K + \frac{1}{2})\Delta t$. Applying a centered difference operator to the momentum equation (5), and the continuity equation (7), along a grid line parallel to the x-axis, results in a system of linear algebraic equations whose coefficient matrix is tridiagonal. The form of the difference expressions for the first cycle is given by:

a. Momentum Equation

$$U^{K+\frac{1}{2}}_{n,m+\frac{1}{2}} = U^{K-\frac{1}{2}}_{n,m+\frac{1}{2}} + \Delta t \left\{ f\bar{\bar{V}}^{K}_{n,m+\frac{1}{2}} + F^{K}_{\alpha_1} - \frac{g}{2\Delta\alpha_1}\left(\frac{d^*}{\mu_1}\right)_{n,m+\frac{1}{2}} \left\{ \eta^{K+\frac{1}{2}}_{n,m+1} \right.\right.$$

$$\left. - \eta^{K+\frac{1}{2}}_{n,m} + \eta^{K-\frac{1}{2}}_{n,m+1} - \eta^{K-\frac{1}{2}}_{n,m} - 2\left[(\eta_a)^{K}_{n,m+1} - (\eta_a)^{K}_{n,m}\right] \right\} \qquad (10)$$

$$\left. - \frac{g(U^{K+\frac{1}{2}}_{n,m+\frac{1}{2}} + U^{K-\frac{1}{2}}_{n,m+\frac{1}{2}})}{(2\, d^*\, \bar{\bar{C}}^{K})^2} \left[(U^{K-\frac{1}{2}}_{n,m+\frac{1}{2}})^2 + (\bar{\bar{V}}^{K}_{n,m+\frac{1}{2}})^2\right]^{\frac{1}{2}} \right\}$$

b. Continuity Equation

$$\eta^{K+\frac{1}{2}}_{n,m} = \eta^{K}_{n,m} - \frac{\Delta t}{2}\left[\frac{1}{\Delta\alpha_1(\mu_1)_m}\left(U^{K+\frac{1}{2}}_{n,m+\frac{1}{2}} - U^{K+\frac{1}{2}}_{n,m-\frac{1}{2}}\right)\right.$$

$$\left. + \frac{1}{\Delta\alpha_2(\mu_2)_n}\left(V^{K}_{n+\frac{1}{2},m} - V^{K}_{n-\frac{1}{2},m}\right)\right] + \frac{\Delta t}{2}\hat{R}^{K}_{n,m} \qquad (11)$$

where

$$d^* = \bar{\eta}^{K} - \bar{h}$$

Δt = the time step for completing two cycles.

A single bar represents a two-point average and a double bar represents a four-point average. The subscripts m and n correspond to spatial locations and subscript K to time levels.

Gathering terms to be completed along line n at time level $(K+\frac{1}{2})\Delta t$, equations 10 and 11 can be written as

$$-a_m \eta^{K+\frac{1}{2}}_{n,m} + \bar{a}_{m+\frac{1}{2}}\, U^{K+\frac{1}{2}}_{n,m+\frac{1}{2}} + a_{m+1}\, \eta^{K+\frac{1}{2}}_{n,m+1} = B_{m+\frac{1}{2}} \qquad (12)$$

$$-a_{m-\frac{1}{2}}\, U^{K+\frac{1}{2}}_{n,m-\frac{1}{2}} + \eta^{K+\frac{1}{2}}_{n,m} + a_{m+\frac{1}{2}}\, U^{K+\frac{1}{2}}_{n,m+\frac{1}{2}} = A_m \tag{13}$$

where

$$A_m = \eta^K_{n,m} - \frac{\Delta t}{2(\mu_2)_n\, \Delta\alpha_2}\,(V^K_{n+\frac{1}{2},m} - V^K_{n-\frac{1}{2},m}) + \frac{\Delta t}{2}\,\hat{R}^K_{n,m} \tag{14}$$

$$B_{m+\frac{1}{2}} = U^{K-\frac{1}{2}}_{n,m+\frac{1}{2}} + \Delta t \left\{ f\bar{\bar{V}}^K_{n,m+\frac{1}{2}} - \frac{gd^*}{2(\mu_1)_m \Delta\alpha_1} \left\{ \eta^{K-\frac{1}{2}}_{n,m+1} - \eta^{K-\frac{1}{2}}_{n,m} - 2 \right.\right.$$

$$\left.\left. [(\eta_a)^K_{n,m+1} - (\eta_a)^K_{n,m}] \right\} + (F_{\alpha_1})^K_{n,m} - \frac{gU^{K-\frac{1}{2}}_{n,m+\frac{1}{2}}}{2(\bar{C}^K d^*)^2} \right.$$

$$\left. [(U^{K-\frac{1}{2}}_{n,m+\frac{1}{2}})^2 + (\bar{\bar{V}}^K_{n,m+\frac{1}{2}})^2]^{\frac{1}{2}} \right\} \tag{15}$$

where

$$\bar{\bar{V}}^K_{n,m+\frac{1}{2}} = \tfrac{1}{4}(V^K_{n+\frac{1}{2},m} + V^K_{n-\frac{1}{2},m} + V^K_{n+\frac{1}{2},m+1} + V_{n-\frac{1}{2},m+1}) \tag{16}$$

$$\bar{C}^K = \tfrac{1}{2}(C^K_{n,m+1} + C^K_{n,m}) \tag{17}$$

$$d^* = \tfrac{1}{2}(\eta^K_{n,m+1} + \eta^K_{n,m} - h_{n,m+1} - h_{n,m}) \tag{18}$$

$$a_{m-\frac{1}{2}} = a_{m+\frac{1}{2}} = \frac{\Delta t}{2(\mu_1)_m \Delta\alpha_1} \tag{19}$$

$$a_m = a_{m+1} = \frac{g\Delta t d^*}{2(\mu_1)_m \Delta\alpha_1} \tag{20}$$

$$\bar{a}_{m+\frac{1}{2}} = 1 + \frac{g\Delta t}{2(\bar{C}^K d^*)^2}\,[(U^{K-\frac{1}{2}}_{n,m+\frac{1}{2}})^2 + (\bar{\bar{V}}^K_{n,m+\frac{1}{2}})^2]^{\frac{1}{2}} \tag{21}$$

Assuming that $\eta_M^{K+\frac{1}{2}}$ is a given water level at the lower boundary and $U_{L+\frac{1}{2}}^{K+\frac{1}{2}}$ is a given flow in the upper boundary, the matrix form of the equations for line n can be written as follows:

$$\begin{bmatrix} \bar{a}_{M+\frac{1}{2}} & a_{M+1} & 0 & 0 & \cdots & 0 \\ -a_{M+\frac{1}{2}} & 1 & a_{M+\frac{3}{2}} & 0 & \cdots & 0 \\ 0 & -a_{M+1} & \bar{a}_{M+\frac{3}{2}} & a_{M+2} & \cdots & 0 \\ & & & & \cdots & \\ & & & & \cdots & \\ & & & & \cdots & \\ 0 & 0 & 0 & \cdots & -a_{L-\frac{1}{2}} & 1 \end{bmatrix} \begin{bmatrix} U_{M+\frac{1}{2}}^{K+\frac{1}{2}} \\ \eta_{M+1} \\ U_{M+\frac{3}{2}} \\ \cdot \\ \cdot \\ \cdot \\ \eta_L \end{bmatrix} = \begin{bmatrix} \hat{B}_{M+\frac{1}{2}}^{K} \\ A_{M+1} \\ B_{M+\frac{3}{2}} \\ \cdot \\ \cdot \\ \cdot \\ \hat{A}_L \end{bmatrix} \tag{22}$$

The system of equations is noted to be tridiagonal and can be solved with a minimum number of operations by defining the process of elimination as a set of recursive formulas. Starting with the first equation:

$$U_{m+\frac{1}{2}}^{K+\frac{1}{2}} = -R_m \eta_{m+1}^{K+\frac{1}{2}} + S_m \tag{23}$$

where

$$R_m = \frac{a_{m+1}}{\bar{a}_{m+\frac{1}{2}}} \qquad S_m = \frac{\hat{B}_{m+\frac{1}{2}}}{\bar{a}_{m+\frac{1}{2}}} \tag{24}$$

and

$$\hat{B}_{m+\frac{1}{2}} = B_{m+\frac{1}{2}} + a_m \eta_M^{K+\frac{1}{2}} \tag{25}$$

Substitution of equation 23 into the second equation gives

$$-a_{m+\frac{1}{2}} \left(-R_m \eta_{m+\frac{1}{2}}^{K+\frac{1}{2}} + S_m\right) + \eta_{m+1}^{K+\frac{1}{2}} + a_{m+\frac{3}{2}} U_{m+\frac{3}{2}}^{K+\frac{1}{2}} = A_{m+1} \tag{26}$$

or

$$\eta_{m+1}^{K+\frac{1}{2}} = -P_{m+1} U_{m+\frac{3}{2}}^{K+\frac{1}{2}} + Q_{m+1} \tag{27}$$

where

$$P_{m+1} = \frac{a_{m+\frac{3}{2}}}{1+a_{m+\frac{1}{2}} R_m} \qquad Q_{m+1} = \frac{A_{m+1} + a_{m+\frac{1}{2}} S_m}{1 + a_{m+\frac{1}{2}} R_m} \tag{28}$$

Again, the flow rate can be expressed as a function of the next water level:

$$U_{m+\frac{3}{2}}^{K+\frac{1}{2}} = -R_{m+1} \eta_{m+2} + S_{m+1} \tag{29}$$

where

$$R_{m+1} = \frac{a_{m+2}}{\bar{a}_{m+\frac{3}{2}} + a_{m+1} R_{m+1}} \qquad S_{m+1} = \frac{B_{m+\frac{3}{2}} + a_{m+1} Q_{m+1}}{\bar{a}_{m+\frac{3}{2}} + a_{m+1} R_{m+1}} \tag{30}$$

In general, the recursion formulas can be written as:

$$\eta_m^{K+\frac{1}{2}} = -P_m U_{m+\frac{1}{2}}^{K+\frac{1}{2}} + Q_m \tag{31}$$

$$U_{m-\frac{1}{2}}^{K+\frac{1}{2}} = -R_{m-1} \eta_m^{K+\frac{1}{2}} + S_{m-1} \tag{32}$$

where

$$T1 = 1 + a_{m-\frac{1}{2}} R_{m-1} \qquad T2 = \bar{a}_{m+\frac{1}{2}} + a_m P_m$$

$$P_m = \frac{a_{m+\frac{1}{2}}}{T1} \qquad Q_m = \frac{A_m + a_{m-\frac{1}{2}} S_{m-1}}{T1}$$

$$R_m = \frac{a_{m+1}}{T2} \qquad S_m = \frac{B_{m+\frac{1}{2}} + a_m Q_m}{T2} \tag{33}$$

In the numerical model, fractional subscripts are not permitted. For use in the program, a new index system is adopted, whereby water levels, flows, etc., appearing in the shaded area of Figure 6 have the same coordinate index (N,M). Using this notation, the expanded form of the recursion coefficient formulas for the first cycle can be expressed as:

$$P_M = \left\{\frac{\tau}{(\mu_1)_{2M-1}\,\Delta\alpha_1}\right\} \div \left\{1 + \frac{\tau}{(\mu_1)_{2M-1}\,\Delta\alpha_1} R_{M-1}\right\} \tag{34}$$

$$Q_M = \left\{A_M + \frac{\tau}{(\mu_1)_{2M-1}\,\Delta\alpha_1} S_{M-1}\right\} \div \left\{1 + \frac{\tau}{(\mu_1)_{2M-1}\,\Delta\alpha_1} R_{M-1}\right\} \tag{35}$$

$$D1 = 1 + \frac{4g\tau}{[d^*(C_{N,M+1} + C_{N,M})]^2}\left[(U^{K-\frac{1}{2}}_{N,M})^2 + \bar{\bar{V}}^2\right]^{\frac{1}{2}} + \frac{g\tau}{(\mu_1)_{2M}\,\Delta\alpha_1} d^* P_M \tag{36}$$

$$R_M = \left\{\frac{gd^*\tau}{(\mu_1)_{2M}\,\Delta\alpha_1}\right\} \div D1 \tag{37}$$

$$S_M = \left\{B_M + \frac{g\tau}{(\mu_1)_{2M}\,\Delta\alpha_1} d^* Q_M\right\} \div D1 \tag{38}$$

where

$$A_M = \eta^K_{N,M} - \frac{\tau}{(\mu_2)_{2N-1}\,\Delta\alpha_2}\left(V^K_{N,M} - V^K_{N-1,M}\right) + \tau \hat{R}^K_{N,M} \tag{39}$$

$$B_M = U^{K-\frac{1}{2}}_{N,M} + \tau\left\{2f\bar{\bar{V}} - \frac{gd^*}{(\mu_1)_{2M}\,\Delta\alpha_1}\left\{\eta^{K-\frac{1}{2}}_{N,M+1} - \eta^{K-\frac{1}{2}}_{N,M} - 2\left[(\eta_a)^K_{N,M+1}\right.\right.\right. \tag{40}$$

$$\left.\left.\left. - (\eta_a)^K_{N,M}\right]\right\} + 2(F_{\alpha_1})^K_{N,M} - \frac{4gU^{K-\frac{1}{2}}_{N,M}}{[d^*(C_{N,M}+C_{N,M+1})]^2}\left[(U^{K-\frac{1}{2}}_{N,M})^2+\bar{\bar{V}}^2\right]^{\frac{1}{2}}\right\}$$

$$d^* = \tfrac{1}{2}\,(\eta^K_{N,M+1} + \eta^K_{N,M} - h_{N,M+1} - h_{N,M}) \tag{41}$$

$$\bar{\bar{V}} = \tfrac{1}{4}\,(V^K_{N-1,M} + V^K_{N,M} + V^K_{N-1,M+1} + V^K_{N,M+1}) \tag{42}$$

$$\tau = \Delta t/2 \tag{43}$$

The solution equations are given by:

$$\eta^{K+\frac{1}{2}}_{N,M} = - P_M U^{K+\frac{1}{2}}_{N,M} + Q_M \tag{44}$$

$$U^{K+\frac{1}{2}}_{N,M-1} = - R_{M-1}\,\eta^{K+\frac{1}{2}}_{N,M} + S_{M-1} \tag{45}$$

The recursion coefficients, P, Q, R and S, can be computed in succession between boundaries on line N. Depending upon the types of boundary conditions that are applied, various approximations of these coefficients are required. Having calculated the set of coefficients, the solution equation can be solved for all surface elevations and flows in descending order.

The second operation computes η and V implicitly, advancing the time from $(K + \frac{1}{2})\Delta t$ to $(K + 1)\Delta t$. The development of the recursion formulas for this cycle is very similar to that just described. The equations for

the second cycle, applied row-wise along a line m, are:

$$V^{K+1}_{n+\frac{1}{2},m} = V^{K}_{n+\frac{1}{2},m} + \Delta t \left\{ \overline{\overline{fu}}^{K+\frac{1}{2}}_{n+\frac{1}{2},m} + (F\alpha_2)^{K+\frac{1}{2}} - \frac{g}{2\Delta\alpha_2} \left(\frac{\hat{d}}{\mu 2}\right)_{n+\frac{1}{2},m} \right.$$

$$\left\{ \eta^{K+1}_{n+1,m} - \eta^{K+1}_{n,m} + \eta^{K}_{n+1,m} - \eta^{K}_{n,m} - 2\left[(\eta_a)^{K+\frac{1}{2}}_{n+1,m} - (\eta_a)^{K+\frac{1}{2}}_{n,m}\right] \right\} \quad (46)$$

$$\left. + \frac{g(V^{K+1}_{n+\frac{1}{2},m} + V^{K}_{n+\frac{1}{2},m})}{(2\hat{d}\overline{C}^{K+\frac{1}{2}})^2} \left[(\overline{\overline{U}}^{K+\frac{1}{2}}_{n+\frac{1}{2},m})^2 + (V^{K}_{n+\frac{1}{2},m})^2\right]^{\frac{1}{2}} \right\}$$

$$\eta^{K+1}_{n,m} = \eta^{K+\frac{1}{2}}_{n,m} - \frac{\Delta t}{2} \left[\frac{1}{\Delta\alpha_1(\mu_1)_m} (U^{K+\frac{1}{2}}_{n,m+\frac{1}{2}} - U^{K+\frac{1}{2}}_{n,m-\frac{1}{2}}) \right. \quad (47)$$

$$\left. + \frac{1}{\Delta\alpha_2(\mu_2)_n} (V^{K+1}_{n+\frac{1}{2},m} - V^{K+1}_{n-\frac{1}{2},m})\right] + \frac{\Delta t}{2} \hat{R}^{K+\frac{1}{2}}_{n,m}$$

where

$$\overline{\overline{U}}^{K+\frac{1}{2}}_{N+\frac{1}{2},m} = \tfrac{1}{4}(U^{K+\frac{1}{2}}_{n+1,m+\frac{1}{2}} + U^{K+\frac{1}{2}}_{n+1,m-\frac{1}{2}} + U^{K+\frac{1}{2}}_{n,m+\frac{1}{2}} + U^{K+\frac{1}{2}}_{n,m-\frac{1}{2}}) \quad (48)$$

$$\overline{C}^{K+\frac{1}{2}} = \tfrac{1}{2}(C^{K+\frac{1}{2}}_{n+1,m} + C^{K+\frac{1}{2}}_{n,m}) \quad (49$$

$$\hat{d} = \tfrac{1}{2}(\eta^{K+\frac{1}{2}}_{n+1,m} + \eta^{K+\frac{1}{2}}_{n,m} - h_{n+1,m} - h_{n,m}) \quad (50)$$

The recursion coefficients are given by:

$$P_N = \left\{ \frac{\tau}{(\mu_2)_{2N-1}\Delta\alpha_2} \right\} \div \left\{ 1 + \frac{\tau}{(\mu_2)_{2N-1}\Delta\alpha_2} R_{N-1} \right\} \quad (51)$$

$$Q_N = \left\{ A_N + \frac{\tau}{(\mu_2)_{2N-1}\Delta\alpha_2} \right\} \div \left\{ 1 + \frac{\tau}{(\mu_2)_{2N-1}\Delta\alpha_2} R_{N-1} \right\} \quad (52)$$

$$D2 = 1 + \frac{4g\tau}{[\hat{d}(C_{n+1,M} + C_{N,M})]^2}\left[\overline{\overline{U}}^2 + (V^K_{N,M})^2\right]^{\frac{1}{2}} + \frac{g\tau\hat{d}}{(\mu_2)_{2N}\,\Delta\alpha_2}P_N \quad (53)$$

$$R_N = \left\{\frac{g\tau\hat{d}}{(\mu_2)_{2N}\,\Delta\alpha_2}\right\} \div D2 \quad (54)$$

$$S_N = \left\{B_N + \frac{g\tau\hat{d}}{(\mu_2)_{2N}\,\Delta\alpha_2}Q_N\right\} \div D2 \quad (55)$$

where

$$A_N = \eta^{K+\frac{1}{2}}_{N,M} - \frac{\tau}{(\mu_1)_{2M-1}\,\Delta\alpha_1}(U^{K+\frac{1}{2}}_{N,M} - U^{K+\frac{1}{2}}_{N,M-1}) + \tau\hat{R}^{K+\frac{1}{2}}_{N,M} \quad (56)$$

$$B_N = V^K_{N,M} - \tau\left\{2f\overline{\overline{U}} + \frac{g\hat{d}}{(\mu_2)_{2N}\,\Delta\alpha_2}\left\{\eta^K_{N+1,M} - \eta^K_{N,M} - 2[(\eta_a)^{K+\frac{1}{2}}_{N+1,M} - (\eta_a)^{K+\frac{1}{2}}_{N,M}]\right\} - 2(F_{\alpha_2})^{K+\frac{1}{2}}_{N,M} + \frac{4gV^K_{N,M}}{[\hat{d}(C_{N+1,M} + C_{N,M})]^2}\left[\overline{\overline{U}}^2 + (V^K_{N,M})^2\right]^{\frac{1}{2}}\right\} \quad (57)$$

$$\hat{d} = \tfrac{1}{2}(\eta^{K+\frac{1}{2}}_{n+1,M} + \eta^{K+\frac{1}{2}}_{N,M} - h_{N+1,M} - h_{N,M}) \quad (58)$$

$$\overline{\overline{U}} = \tfrac{1}{4}(U^{K+\frac{1}{2}}_{N+1,M} + U^{K+\frac{1}{2}}_{N+1,M-1} + U^{K+\frac{1}{2}}_{N,M-1} + U^{K+\frac{1}{2}}_{N,M}) \quad (59)$$

The solution equations for the second operation are given by:

$$\eta_{N,M}^{K+1} = - P_N V_{N,M}^{K+1} + Q_N \tag{60}$$

$$V_{N-1,M}^{K+1} = - R_{N-1} \eta_{N,M}^{K+1} + S_{N-1} \tag{61}$$

2. Variable Grid

The rectilinear space staggered variable grid system employed by WIFM is developed through the use of a numerical program (MAPIT) designed to calculate the mapping defined by equation (4). Each axis is mapped independently. Figure 7 displays an example of a grid for Mississippi Sound and Mobile Bay. Consider a mapping from left to right of the horizontal (east-west) axis for this case. The mapping is partitioned into 9 regions: a contracting meshsize to Cat Island, constant meshsize to Ship Island Pass, expanding meshsize to Biloxi, contracting meshsize to Dog Keys Pass, expanding meshsize to the middle of Horn Island, contracting meshsize to Horn Island Pass Channel, expanding meshsize to Petit Bois Pass, contracting meshsize to Mobile Main Ship Channel, and finally an expanding meshsize to Bon Secour, Alabama.

It is important to maintain continuity of the mapping function and its derivatives at the partition division points. The objective is to define coefficients (a, b and c) of equation (4) for each partition region along the axis. The procedure is begun by selecting the minimum grid meshsize, locations of partition points in real space (x, y space) and approximate values for μ (rate at which the grid is expanding or contracting) at partition points. The mapping is carried out by varying the number of α-space intervals within a given partition. When the

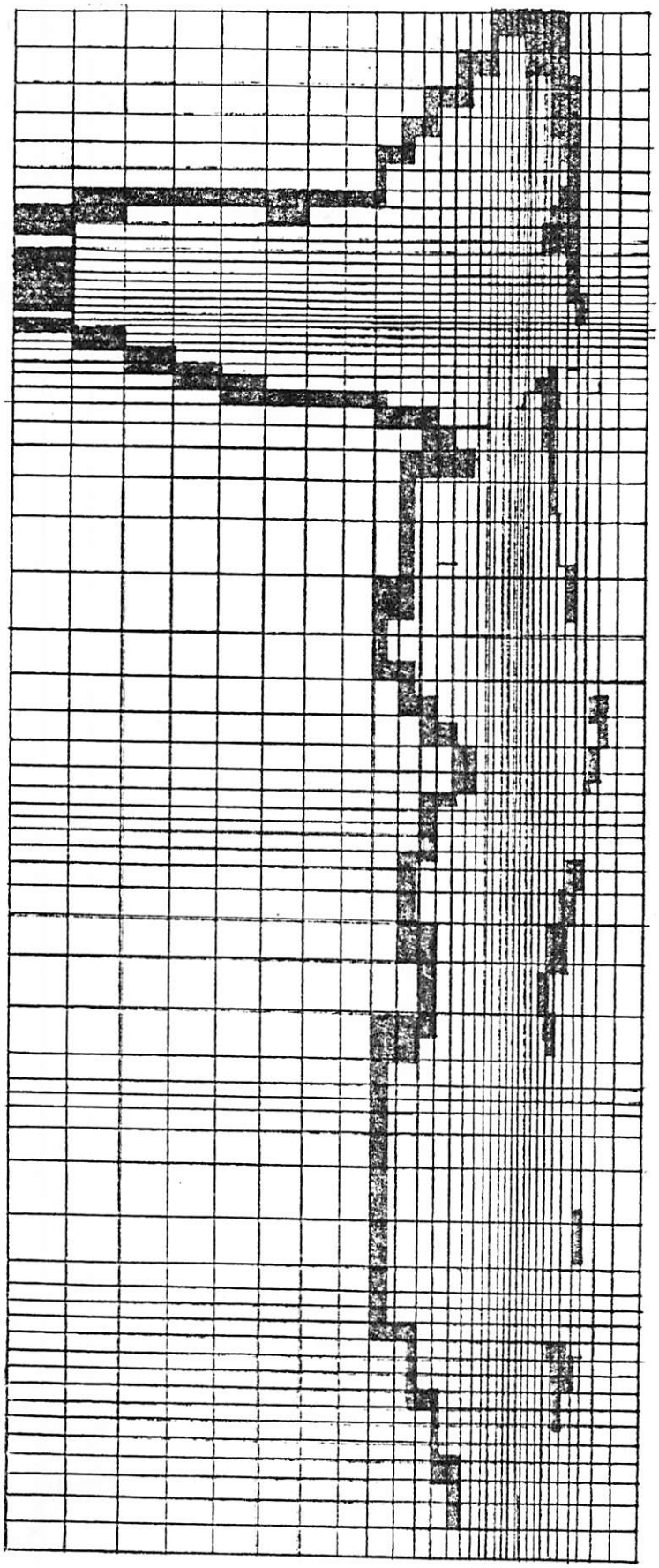

Figure 7. Typical Computational Grid for WIFM II

reverse mapping of a partition point in α-space brackets the actual location of the partition point in real space, an exact mapping is obtained by varying the value of μ at the partition point.

Having finished the mapping of partition points along both axes, a numerical program (TGRID) is used to compute the complete mapping of the study area into a regular computational grid. The code outputs the grid on a pen-plotter for use as an overlay on bathymetric charts for ease of digitizing the water depths. In addition, the coefficients μ_1 and μ_2 for each cell in the appropriate direction are given for direct use by WIFM.

3. Variable Tidal Input

The code WIFM has been changed to permit variable tidal inputs along a computational boundary. To better represent the actual tidal condition, boundary grids for tidal input can be divided into several regions, and the tidal input in each region can be either constant or variable from cell to cell. Given tidal cycles at both ends, the code WIFM will calculate tidal height for each cell in that region. A complete description of how to set up tidal input for the whole system is given in a following discussion of model input data.

4. Boundary Conditions

The boundary conditions can be classified into three general groups: open boundaries, water-land boundaries and subgrid barrier boundaries.

a. Open boundaries

This category includes seaward boundaries terminating the computational grid or channels exiting the two-dimensional grid at any point in the grid system. Water levels or flow rates are prescribed as functions of location and time and are given as tabular input to the code.

b. Water-land boundaries

For these boundaries, the flow normal to the boundary is set to be zero. Low-lying terrain may alternately dry and flood within a tidal cycle or surge history. Inundation is simulated by making the location of the land-water boundary a function of local water depth. The possibility of inundation can be determined by checking water levels in adjacent cells. Initial movement of water on dry cells is controlled by using a broad-crested weir formula,

$$Q_n = \pm C_o d_H \sqrt{d_H} \qquad (62)$$

where

Q_n = the normal component of transport

d_H = the depth of water over the crest of the barrier

C_o = an appropriate admittance coefficient whose units are equivalent to those of $\sqrt{g}$. It's usually less than 5.0 for controlling movement of water onto a dry cell.

Once the water level on the dry cell exceeds some small prescribed value, the boundary face is treated as open, and η, U and V are computed for that cell. The drying of cells is the inverse process. When the water level recedes beyond some small prescribed value, a no-flow condition is applied. A graphic representation of flood cell treatment is shown in Figure 8.

c. Subgrid barriers.

Subgrid barriers are defined along cell faces and have three types: exposed, submerged, and overtopping.

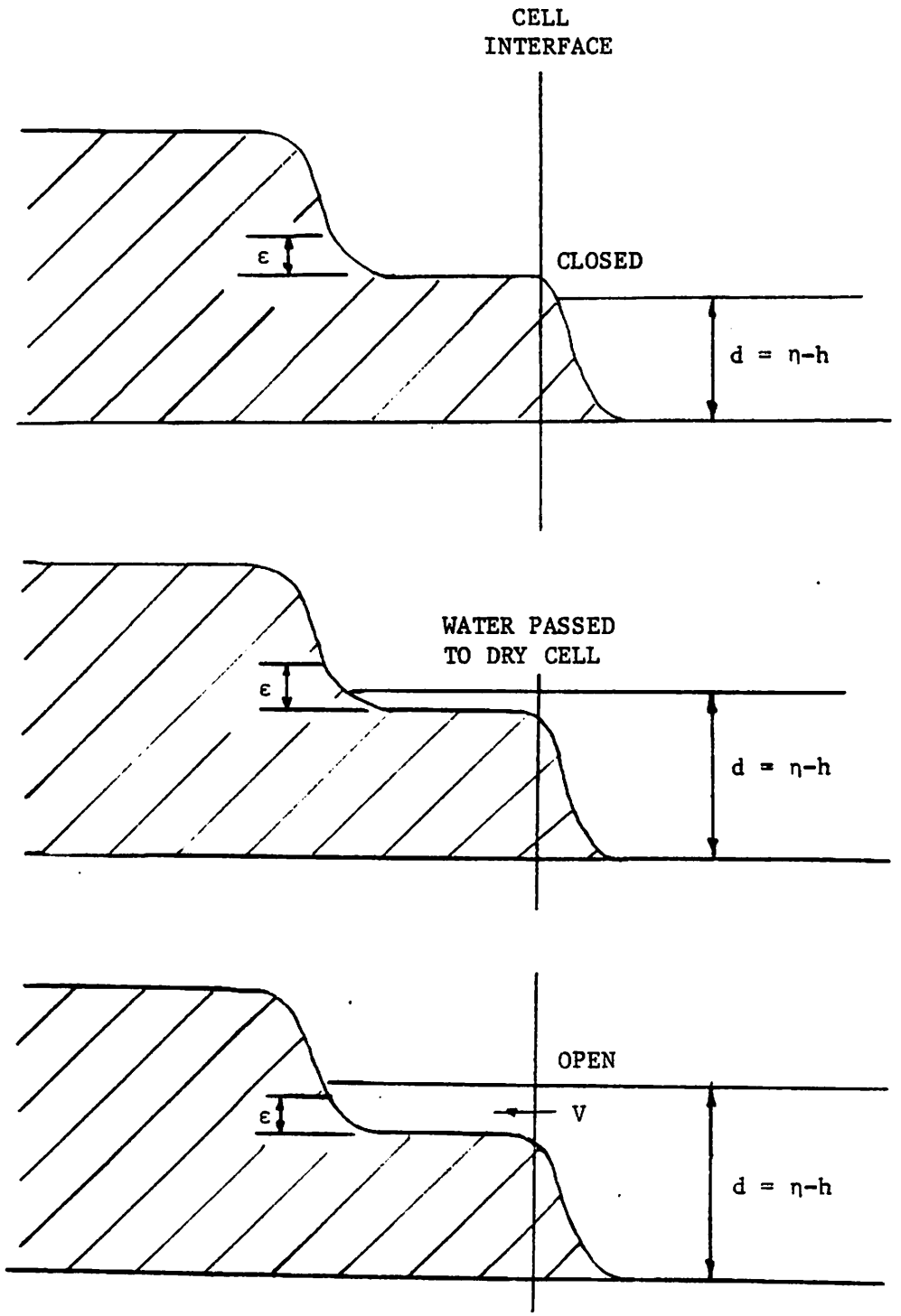

Figure 8. Flood Cell Treatment in WIFM II

(i) Exposed barriers are handled by simply specifying no-flow conditions across the appropriate flagged cell faces.

(ii) Submerged barriers are simulated by controlling flow across cell faces with the use of a time-dependent frictional coefficient.

(iii) Overtopping barrier is a terminology used to distinguish barriers which can be submerged during one segment of the simulation and totally exposed in another. Actual overtopping is treated by using the broad-crested weir formula, equation (62), to specify the flow rate across the barrier. C_o is usually less than 3.0 for a broad-crested barrier. Figure 9 gives a visual description of these barrier conditions.

D. Program Input

WIFM has been constructed as a generalized long-wave model. Associated with WIFM are pre- and post-processing codes which provide data to or a means of interpreting the results of WIFM. Programs MAPIT and TGRID are used to develop the grid system and the expansion coefficients (defining the mapping of prototype to computational space). Having developed a regular or variable spaced grid system, water depth and friction code for each cell must be decided. Friction codes are associated with given bottom surface materials. Other data required include forcing tides or flows and special gage-point locations.

Storage arrays in the code have been defined for a limited number of grid points, gage points, and tabular forcing functions. Large problems can be solved by expanding these dimensions to get sufficient storage.

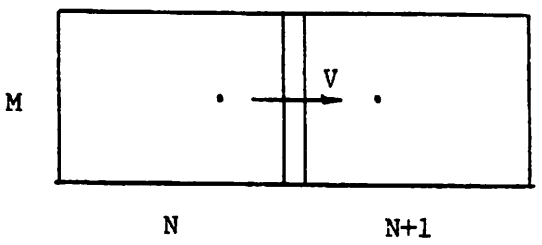

Barrier at Cell Interface (Height b)

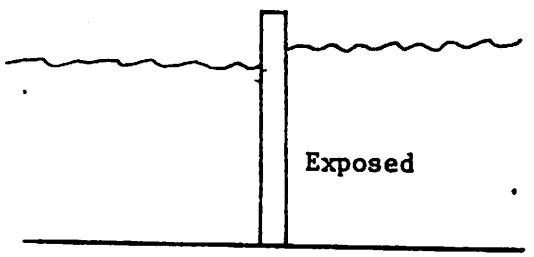

$V = 0$

$\eta_N < b + \varepsilon$

$\eta_{N+1} < b + \varepsilon$

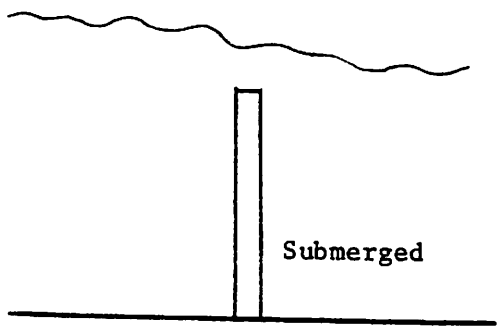

$\eta_N > b + \varepsilon$

$\eta_{N+1} > b + \varepsilon$

V Controlled by Special Chezy Coefficient

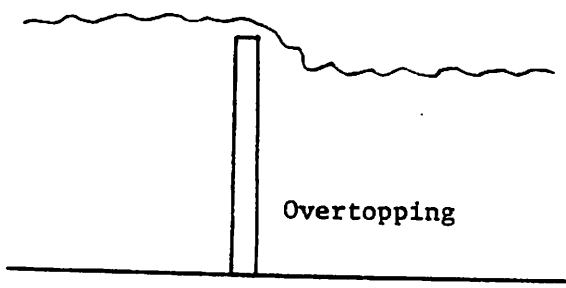

$\eta_N > b + \varepsilon$

$\eta_{N+1} < b + \varepsilon$

$V = C_o d_H \sqrt{d_H}$

Water is passed to Low Side According to Flow Rate V

Figure 9. Barrier Conditions Treated by WIFM II

WIFM consists of a MAIN driver and 12 subroutines. The definitions of major variables are as follows:

SEP,SE,SEM	Surface elevations at time n+1, n, and n-1
UP,U,VP,V	Transport components at time n+1 and n
C,H,ICU,ICV	Chezy, depth, and flag arrays
FXX,FYY,PHED	Wind stress arrays and hydrostatic elevation array
MAN	Coded friction array
JSB	Control array defined in programs DEPTH and MOTION
SURFE,DCHRGE	Forcing function arrays, tide and transports
FRIC	Stores depth-dependent Chezy coefficients at depth intervals of 0.25 ft or 0.1m
XMU,YMU	Expansion coefficients for variable grid
RATIO	Stores the ratio of length of each grid to the length of segment of tidal input. This array will be used to interpolate the tidal height along the tidal boundary.
SAV	Array for saving punch-card output of special gage-point hydrographs
NMAX,MMAX	Horizontal and vertical dimensions of grid
IFLOOD,ZFU,ZFV CHZ,IPAS	Flood cell control arrays
IBARR,IBARX IBARY,IBART	Subgrid barrier control arrays
ITIDE,IFLOW	Location of forcing function boundaries
A,B,P,Q,R,S	Coefficients in recursion formulas for ADI solution scheme

The dimensions within each subprogram are set as follows:

MAIN Variables SEP,SE,SEM,UP,U,VP,V,C,H,ICU,ICV and JSB are set to n_1, where $n_1 \geq$NMAX*MMAX.

Variables FXX,FYY and PHED are set to 1. (No windfield is applied.)

Variable SURFE is set to n_2 where

$n_2 \geq$NTID*(ITID-1)*JTID.

Variable DCHRGE is set to n_3, where

$n_3 \geq$NFLO*(ITID-1)*JTID.

FRIC is set greater than 4* (maximum depth +1)*20 for depth in feet and to 10* (maximum depth +1)*20 for depth in meters.

DUMMY is set to seven times the maximum number of cells along any grid side. XMU,YNU are set to twice that amount.

DRIVE SAVID is set to (n_4,10) assuming 10 gages and $n_4 \geq n_2$/MSKP (see input data definition).

If MSKP = 0, set SAVID to (1,10).

Variables in COMMON blocks V3 and V4 are set up for 70 gage points.

The dimensions for barrier cells, tidal input cells and transport input cells are set up in COMMON block V6.

The dimension for flood cells is set up in COMMON block AA4.

Also set XMU, YNU, DUMMY as in MAIN.

DEPTH Set COMMON blocks V6 and AA4 as in DRIVE. The dimension for RATIO is equal to the number of tidal input cells.

RANGE Set DUMMY, XMU, YNU as in MAIN.

ELEVAT SURIN is set for a maximum of 200 tabular values for any one forcing gage.

POUT The dimension of VK is set to 70 cells.

SAVE — Set COMMON blocks V6, AA5, SAV and V8.

PRINPT — Set COMMON blocks V3, V6, AA4, SAV and RATIO.

PRGRID — Set COMMON block VK.

MOTION — Set COMMON blocks V6, AA4, V3 and RATIO. Variables in blocks V7 and V8 are set for a maximum of 70 cells on either axis. Note that V8 is now defined in terms of the recursion coefficients.

Logical unit numbers for use in WIFM tape and file manipulation are defined as:

TAPE 2 — Save restart data at defined time increments.

TAPE 3 — Save punch output for special gages. Send to punch with control cards.

TAPE 5 — Normal input file

TAPE 6 — Normal output file

TAPE 7-15 — Nine scratch files for concatenating special point gage data. Printed by use of control cards.

TAPE 18 — Save η, U, V, h at defined time increments for later plotting.

TAPE 20 — Special sea-boundary input data (usually from another model to drive WIFM).

TAPE 21 — Additional input data, if any.

TAPE 22 — Input data on restart tape.

TAPE 23 — Scratch file.

Definition of Input Data

The input data for WIFM have been assembled into card groups which may consist of one or more data cards. The following text delineates each card group and Fortran format.

Card Group (Format)	Variable	Description
1 (11A4)	ITL	Identification title card (up to 44 characters).
2 (3I5)	NMAX	Horizontal grid dimension) must be less than 100
	MMAX	Vertical grid dimension) must be less than 100
	INITL	0 -- Initial condition on input file.
		1 -- Restart conditions on TAPE 22. Omit input for card groups 13-17 and 21-22.
		-m -- As for 0, but save restart data on TAPE 2 every mτ.
3 (16I5)	ITID	Number of entries in tidal input vectors or flow vectors.
	JTID	Number of τ's between entries in tide or flow input vectors.
	NTID	Number of distinct tidal input vectors.
	NFLO	Number of distinct flow input vectors.
	NP1) NP2) NP3)	Print output grid from N = NP1 to NP2 in steps of NP3.
	NPR	2 -- Print full grid of η only.
		1 -- Print from NP1 to NP2 -η only.
		-1 -- As for NPR = 1 - prints η, U, V.
		-2 -- Print full grid of η, U, V.

Card Group (Format)	Variable	Description
3 (16I5) cont'd.	MPR	|MPR| - 1 -- Print flag arrays only.
		|MPR| = 2 -- Print depth and Chezy, also.
		MPR<0 -- Also print flood, barrier, and tidal or flow data.
	MSURF	Print SURFE or DCHRGE vectors in steps of MSURF.
	KS1	=m -- Hold cell face closed for $m\tau$'s.
	KS2	=m -- Hold cell face open for $m\tau$'s.
	KS3	=m -- Hold barrier characteristic for $m\tau$'s (submerged barrier).
	KS4	=m -- As for KS3 (overtopping barrier).
	KS5) KS6)	Not used.
4 (8E10.1)	TAU	Time step ($\tau=\Delta t/2$) for 1 cycle (sec.)
	DX	Vertical spatial stepsize (minimum stepsize for α-space) (ft or m).
	DY	Horizontal spatial stepsize (minimum stepsize for α-space) (ft or m).
	G	Acceleration of gravity (ft/sec^2 or m/sec^2).
	ALAT	Average latitude of study region (degree).
	XI	Constant rate of rainfall (in/day or cm/day).
	WA	Not used, set to 0.
	THETA	Not used, set to 0.
	EPSD	ε_d -- Minimum amount of water defining a dry cell (ft or m).
	APSD	ε_b -- Minimum amount of water over a barrier for submergence (ft or m).

Card Group (Format)	Variable	Description
4 (8E10.1) cont'd.	DCONI	Add DCONI to water depths and tidal input to translate datum (ft or m).
	DMPX	Value of still water land elevation assigned artificially to areas that will never flood (ft or m).
	ROTA	Not used.
	TPRO	Start of prototype time (time of day, hours).
	ADV	Set to 0.0 -- advective terms are omitted.
	VIS	Set to 0.0 -- flux terms are omitted.
	XLAND	A value of h>XLAND defines a cell that will never flood (ft or m).
	XSCOUR	A value of h<XSCOUR defines a cell that will never go dry (ft or m).
	SMAX	If η>SMAX cease computation and print η.
	SINIT	Set η = SINIT as initial conditions.
	DMAXG	Bound on maximum total water depth that will be experienced during simulation (ft or m).
5 (16I5)	MAXTIM	Number of τ's to run simulation.
	INTAP	=m -- Save η, U, V on TAPE 18 every mt. = -1 -- No data is saved on TAPE 18.
	IDELAY	Delay saving information on TAPE 18 until ITIME = IDELAY (Note: ITIME counts the number of cycles).
	IPLOT	Set to zero.
	IXPAN	=0 -- Constant spatial steps. $\neq$0 -- Read in variable grid expansion coefficients.

Card Group (Format)	Variable	Description
5 (16I5) cont'd.	NGAGE	Number of special gage points.
	IGS	The first IGS special gage points will have corresponding special treatment (see group 9).
	NFREQ	Frequency to print hydrodynamics at gage points (every NFREQ τ's).
	KREST	Start run at ITIME = KREST -- Set to zero except for a restart run.
	NZP	Number of corrections to input depth grid.
	NDTAP	Logical tape unit for depth and coded friction input data (normally 5).
6 (4G20.11)	YNU_i	Expansion coefficients for horizontal direction -- variable grid.
	XMU_i	Same for vertical direction (start new card).

NOTE: Group 6 is created by program TGRID and is omitted for IXPAN = 0.

7 (16I5)	$INPRINT_i$	Time step index to print grid -- present version permits 32 printouts -- two cards must be included.
8 (16I5)	$NPOT_i$	Special gage points -- horizontal indices.
	$MPOT_i$	Same for vertical -- NGAGE in number (start new card).

NOTE: Group 8 is omitted if NGAGE = 0.

9 (16I5) and (16F5.2)	$IGAGE_i$	Codes for methods of computing flows at first IGS special gage points --

Card Group (Format)	Variable	Description
9 (16I5) and (16F5.2) cont'd.		=1 -- U, $\overline{\overline{V}}$ =2 -- $\overline{\overline{U}}$, V =3 -- $\overline{U}$, $\overline{V}$ =4 -- U, V =5 -- U =6 -- V =7 -- $\overline{U}$ =8 -- $\overline{V}$
	$DGAGE_i$	Water depth used in computing velocity for first IGS special points (ft or m) (start new card).
	NOTE: Group 9 is omitted if IGS = 0.	
10 (5I5,F5,0) and (16I5)	NDIV NH NLAB NVD INUM HOUR KPLOT	This group is omitted.
11 (16F5.2)	WAT_i DIR_i	This group is omitted.
12 (10E8.1) (20 values for each variable.)	$XMAN_i$	Manning's n for each code i, i = 1, 20 used for defining friction.
	ZB_i	Barrier height for each code i, i = 1, 20 (ft or m).
	CO_i	Chezy coefficient to approximate an exposed barrier for each code i, i = 1, 20
	CD_i	Admittance coefficient for overtopping barrier for each code i, i = 1, 20 (see formula for broad-crested weir equation).
	CAYD	Recession coefficient for draining of flood cell - keyed by friction codes for each code i, i = 1, 20.

Card Group (Format)	Variable	Description
12 (10E8.1) (20 values for each variable.) cont'd.	CD_i	Admittance coefficient for limiting movement of water onto flood cells -- keyed by friction codes for each code i, i = 1, 20.
13 (15F5.1)	$D_{N,M}$	Depths at center of each grid cell -- for each $N=N_i$, read in a group of cards containing $D_{N,M}$, M = 1, MMAX (ft or m) (start new card for each N_i).

NOTE: Group 13 is omitted for a restart case, INITL = 1. Data for D is usually included with the other data but may be read in from TAPE 21 by setting NDTAP = 21.

14 (2I5,F5.1)	N M D(N,M)	Corrections to depth grid. Grid indices N, M and corrected depth D(N,M) (ft or m) (NZP in number).
	NOTE: Group 14 is omitted if NZP = 0.	
15 (35I2)	$MAN_{N,M}$	Friction codes (1 to 20) -- for each $N = N_i$, read $MAN_{N,M}$, M = 1, MMAX (start new card for each N_i).

NOTE: Group 15 is omitted for a restart case, INITL = 1. MAN data may also be placed on TAPE 21 when NDTAP is set to 21.

16 (4I2,4I4)	ITYP	Barrier type =1 -- Exposed barrier at all times =2 -- Overtopping barrier =4 -- Submerged barrier at all times

Card Group (Format)	Variable	Description
16 (4I2,4I4) cont'd.		Input type
		=8 -- Tidal input
		=9 -- Flow input
		=99 -- End of group 16 data
		=0 -- Permits special corrections to flag arrays (ICU and ICV) (see note).
	INDX	Keyed index for variables in group 12 or index for tidal or flow input arrays.
	INDXL	For ITYP $\neq$ 8, INDXL = 0. For ITYP = 8, the tidal input arrays which are equal to INDX and INDXL will be used to interpolate the tidal height for each cell along the tidal input boundary in that segment. For constant tidal input, set INDX = INDXL.
	IDIR	=1 -- Flow in vertical direction.
		=2 -- Flow in horizontal direction.
	I1	Grid index of boundary line.
	I2) I3)	Boundary extends from I2 to I3.
	I4	=0 -- Lower boundary - applicable for input boundaries only -- input directed toward the right or bottom of the cell.
		=1 -- Upper boundary -- input directed toward the left or top of the cell.

NOTE: Group 16 is omitted for a restart case, INITL = 1. If ITYP is set to zero, corrections are read in as: ICU(I1,I2) = 10*INDX + IDIR and ICV(I1,I2) = 10*I3 + I4.

Card Group (Format)	Variable	Description
17 (16I5)	N M ICU(N,M) ICV(N,M)	Additional corrections to ICU, ICV flag arrays. Keyed by setting I1 = number of corrections in last data card of group 16.

NOTE: Group 17 is omitted if I1 = 0 on last card of group 16 (ITYP = 99).

18 (2I5)	NBG)) MBG)	NBG, MBG are N,M indices of a special point for which the tide record is known and is subsequently backed-off to the seaward boundary according to the free gravity wave speed.
19 (15F5.2)	$SURIN_i$	Input NTID vectors of tidal elevation -- index location in SURFE array chosen by order of input (keyed in group 16) -- start each distinct tide on a new card. (ITID*JTID in number for each tide and NTID different tides)
	NOTE: Group 19 is omitted if NTID = 0.	
20 ((15F5.2)	$SURIN_i$	As in group 19 for input vectors of flow quantities (NFLO different vectors).
	NOTE: Group 20 is omitted if NFLO = 0.	
21A (2I5)	INITL)) NCH)	Redefine INITL -- restart run corrections to flag, depth, or chezy arrays of NCH $\neq$ 0.
21B (4I5,3F5.1)	N M ICU(N,M) ICV(N,M) H(N,M) MAN(N,M) SE(N,M)	Corrections to various arrays - indices N,M -- correct flag arrays, still-water depth, Manning's n, and surface elevation.

NOTE: Group 21A and 21B are included for a restart run only. Group 21B is omitted if NCH = 0.

Card Group (Format)	Variable	Description
22 (16I5)	JNS	Number of ranges for computing volumetric discharge.
	JT1	Time index marking beginning of discharge computation.
	JPER	Period of discharge cycle in time index units.
	JDT	Sampling time step in time index units.
	JMUL	Number of sec in sampling period.
	JDELAY	Delay print of special gage data until ITIME = IDELAY.
23 (16I5)	$JDIR_i$	Direction of flow in discharge range, 1 -- Vertical direction 2 -- Horizontal direction
	JMN_i	Coordinate index of range line.
	$JMN1_i$	Range line extends from JMNI to JMN2
	$JMN2_i$	(JNS sets of data).
	NOTE: Group 23 is omitted if JNS = 0.	
24 (16I5)	NNPOT	Number of special gage points for punching surface elevation data.
	MSKP	Frequency to punch surface elevation (every MSKP τ's)
	MDLY	Delay punch of special gage data until ITIME = MDLY.
25 (16I5)	$INPOT_i$	Special gage points for punch data -- horizontal indices.
	$JNPOT_i$	Same -- vertical indices (start new card).
	NOTE: Group 25 is omitted if NNPOT = 0.	

V. Mobile Bay - Mississippi Sound System

Mobile Bay is approximately 1000 km^2 in area, has an average depth of 3 m, and is located on the northeastern shoreline of the Gulf of Mexico east of the Mississippi River delta. The estuary is about 50 km long and varies in width from 13 km to 16 km in the north half to about 38 km wide in the southern portion. The southeastern region of the estuary is referred to as Bon Secour Bay. The southern end is blocked from the open Gulf by land barriers: Gulf Shores to the east and Dauphin Island to the west. There are two passes located in this area, also: the main pass which connects the bay with the Gulf at Mobile Point and the pass which connects the bay with Mississippi Sound at Cedar Point.

The bay is the terminus of the Mobile River Basin which consists of more than 114,000 km^2 of drainage area, the fourth largest in the United States. Variations in river discharge rate from a normal high of 3850 m^3/s in March to a normal low of 450 m^3/s in September have been recorded. Gauging stations at Jackson (or Coffeeville), Alabama and Claiborne, Alabama provide continuous discharge records for the Tombigbee and Alabama Rivers, respectively.

Mississippi Sound is a uniquely expanded, shallow, estuarine environment created by the occurrence of a series of offshore barrier islands which limit the exchange of fresh water from local runoff with higher-salinity water offshore. Mississippi Sound extends about 110 km in the east-west direction, the barrier islands running parallel to and 13 to 19 km from the coast. Water depths in the Sound are mostly 2.7 - 4 m except for channels.

The Mississippi Sound shoreline consists of a number of bays, marshes, bayous and rivers and serves as the drainage basin for much of Mississippi, Alabama and some of Louisiana. Fresh water enters the Sound primarily through the Pascagoula and Pearl Rivers, with lesser flows from Biloxi Bay and St. Louis Bay. Water also enters the Sound from Mobile Bay, from the Pontchartrain-Lake Borgne drainage and possibly some Mississippi River water through Chandeleur Sound. In addition, tidal water exchange occurs through passes between the barrier island chain that serves as the southern boundary of Mississippi Sound.

Circulation patterns within Mississippi Sound have not been well documented. More information is available for Mobile Bay; however, the effects of current and future development projects on the system create a need for numerical models to predict tidal hydrodynamics.

To simulate tidal hydrodynamics of Mobile Bay and Mississippi Sound, three separate cases have been considered: (1) a combined Mobile Bay-Mississippi Sound model, (2) a model of Mobile Bay alone, and (3) a model of Mississippi Sound alone. The discretized representations of these three cases are shown in Figures 10 through 12.

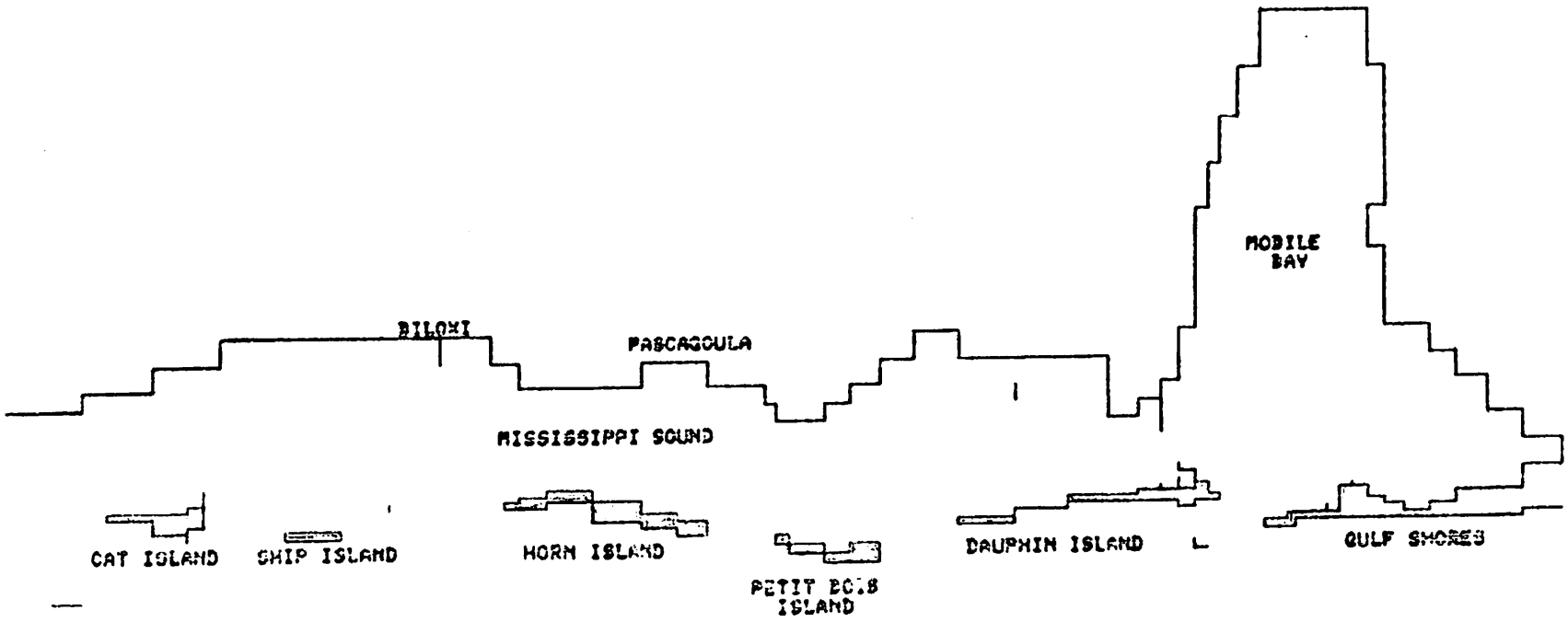

Figure 10. Numerical Model Representation of Mobile Bay and Mississippi Sound

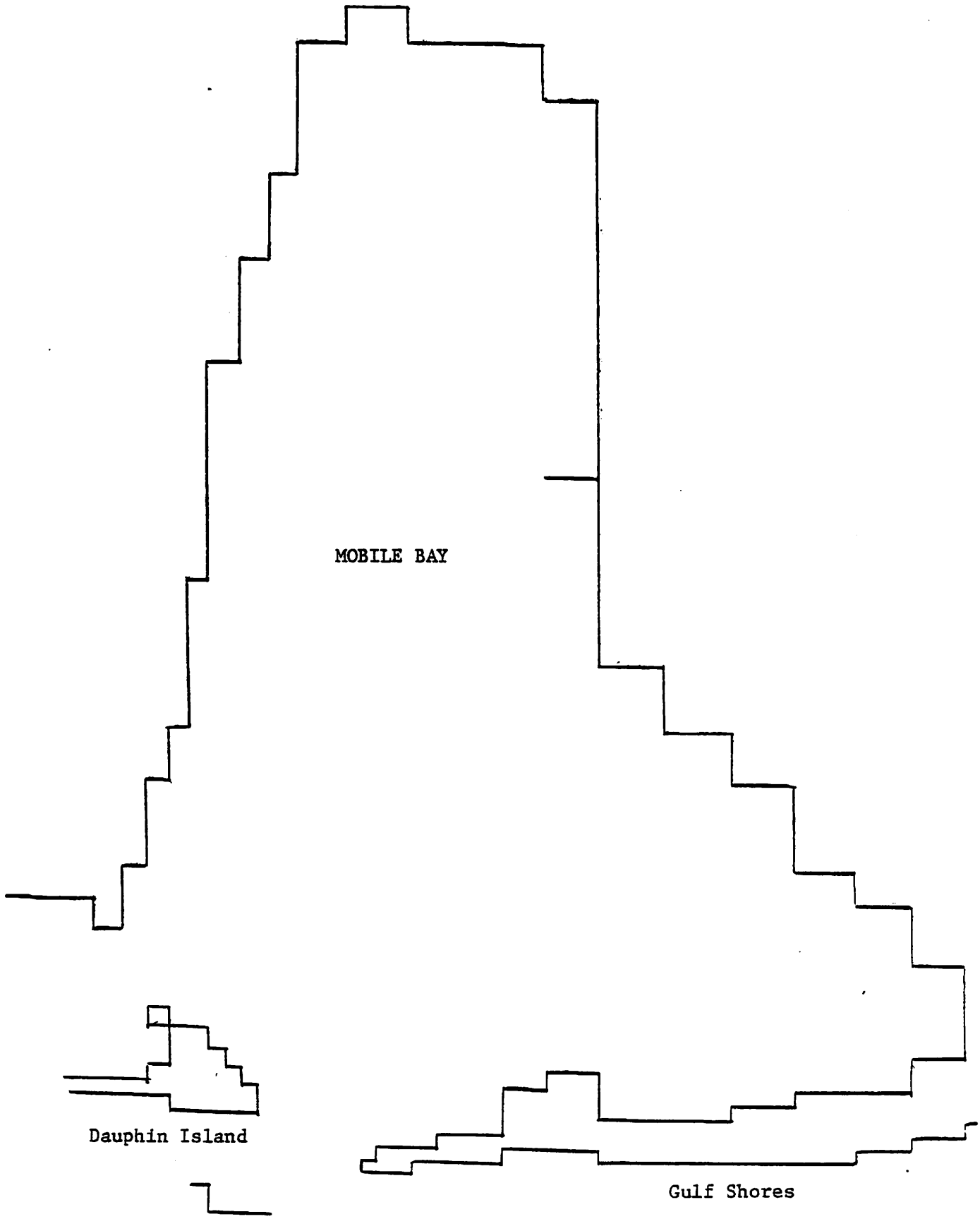

Figure 11. Numerical Model Representation of Mobile Bay

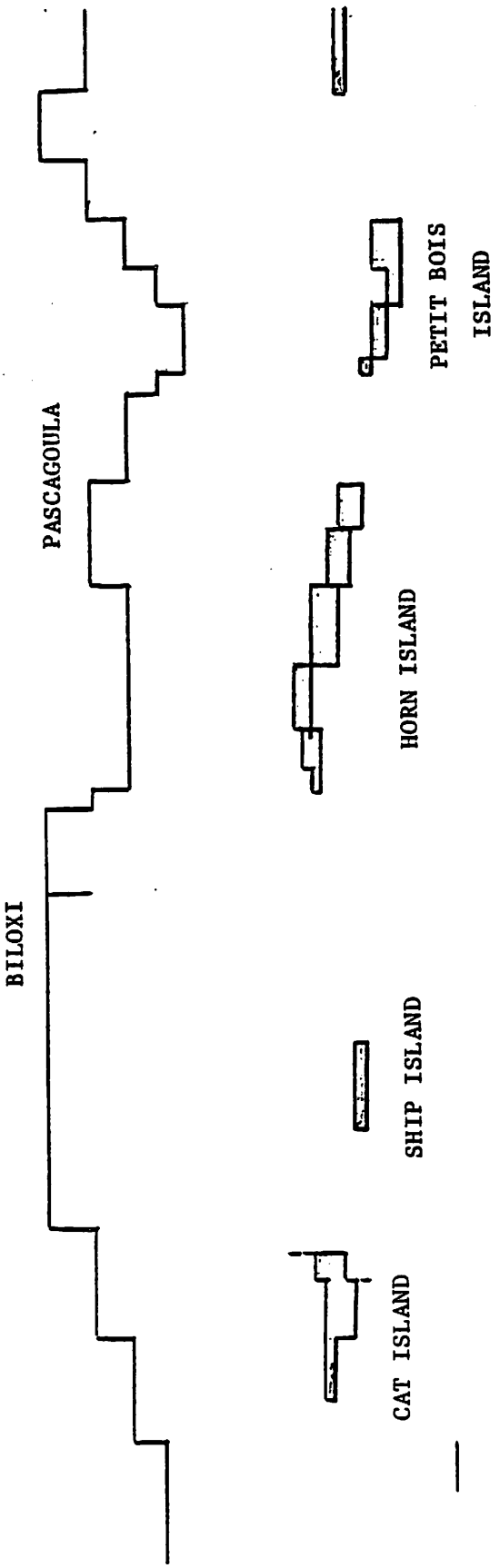

Figure 12. Numerical Model Representation of Mississippi Sound

VI. MODEL APPLICATIONS

The WIFM II hydrodynamic model has been applied for the three separate regions: Mobile Bay-Mississippi Sound combined, Mobile Bay alone, and Mississippi Sound alone. Due to a lack of prototype data for model calibration and verification, model applications have basically been limited to establishing trends in the system, improving graphical output techniques for presenting model results and attempting to improve model operation. Only for the Mobile Bay model has any attempt been made to begin the calibration and verification process. A very limited amount of prototype data were obtained from the Mobile District, Corps of Engineers, and preliminary comparison with model results have been made.

A. Mobile Bay Application

In the first attempts to apply the WIFM II model to Mobile Bay, an effort was made to limit the number of grid cells to no more than 1000, while still attempting to adequately represent the physical characteristics of the Bay. This limit was desirable to reduce memory-core requirements of the program to a level that would not pose undue constraints upon the availability of computer time. A large number of computer runs are required to determine the model reaction to various changes in input data. A standard navigational chart of Mobile Bay was used as a basis for establishing the grid utilized in the study. The result was a grid with 990 cells (33 divisions in the east-west direction and 30 in the north-south). The variable grid capability of the model was used to reduce the grid-cell size in the area of the Main Pass and Pass Aux Herons (Dauphin Island Bridge) to allow the model to more accurately represent these

critical areas. A larger cell size was used in the mid- and upper-bay as well as in the Bon Secour area because of the relatively uniform depths and regularity of the shoreline. The resulting variable grid representation is shown in Figure 13. The model provides many features that were used to represent various features of the bay system. The different bottom compositions (from oyster beds around Cedar Point to mud and sand in other parts of the Bay) were approximated by assigning appropriate Manning friction factors to each cell in the bay.

The subgrid boundary conditions available in the model allow better representation in areas such as Point Clear and Sand Island than would be possible from cell geometry alone. Combinations of exposed and overtopping barriers are used to represent features that are smaller in size than the grid cells.

The number of grid cells used in the model required termination of the grid at the mouth of the northern river system of the bay, resulting in a rough representation of the river. Four cells in the vicinity of the Mobile River and Tensaw River openings into the Bay were chosen to depict the total width of the river. In terms of real distance, this "river mouth" is 8750 ft wide. Because of the relatively small contributions of the other river system, such as Dog and Fowl River, to the total influx of water into the Bay, these were omitted from consideration in the model. Later models in the development sequence will represent this upper bay river system more accurately.

The depths associated with each cell in the grid were assigned by overlaying the grid on the navigational chart and determining a weighted average of the depths within each cell. This procedure was particularly important in representing the narrow ship channel.

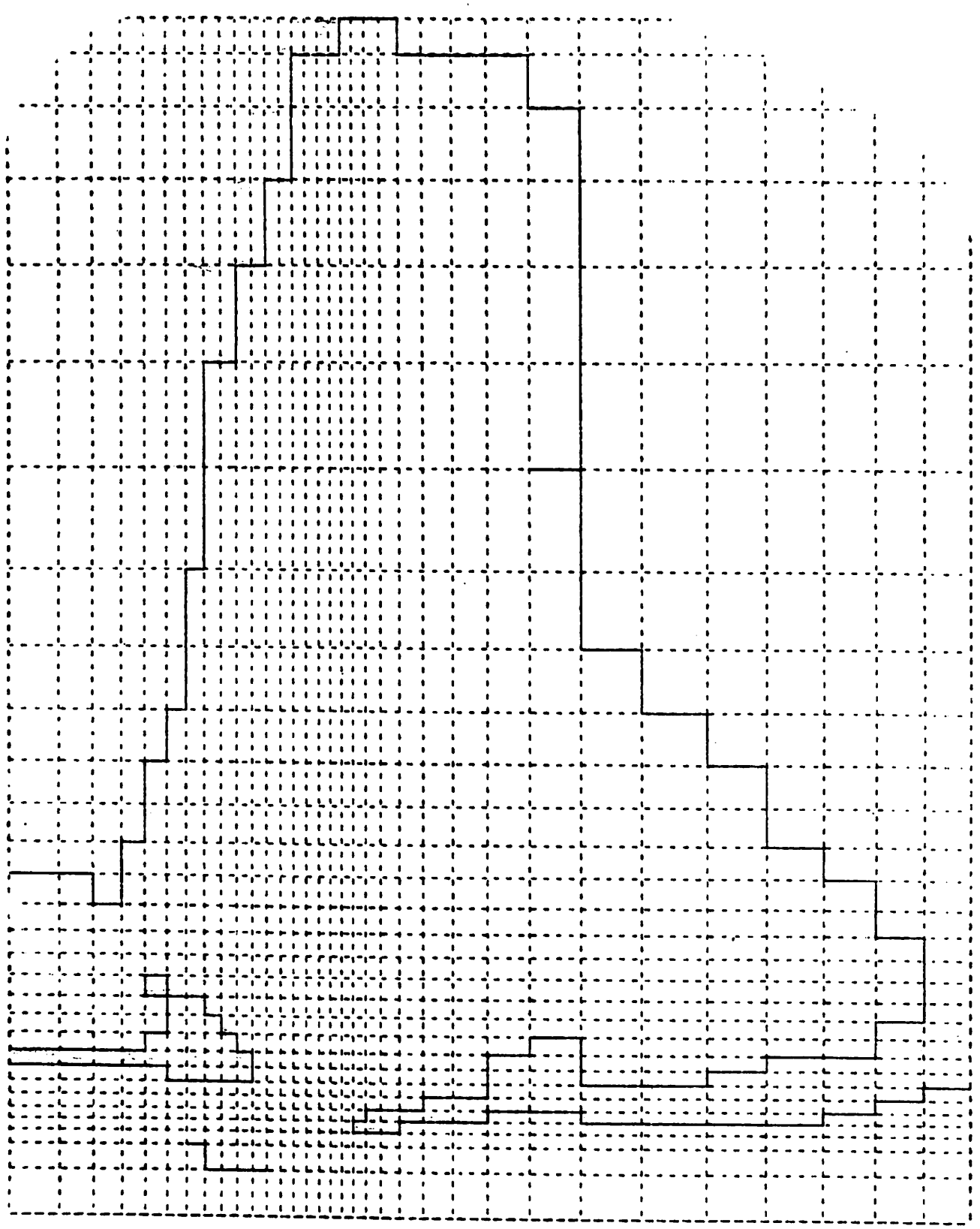

Figure 13. Variable Grid System for Mobile Bay

The model allows specification of special gage points at any given location of the grid where more detailed calculations are made for elevations and velocities. Velocity ranges may also be established across which the volumetric discharge of water can be calculated at any time, as well as the accumulated flow for a specified time period. Gage points in the grid were located at the Alabama State Docks, East Fowl River, Point Clear, Cedar Point, the east end of Dauphin Island, and in Bon Secour Bay. Discharge ranges were used across the Dauphin Island Bridge Pass and the Main Pass. The southern boundary of the grid and the position of the western boundary corresponding to Mississippi Sound are the locations for the appropriate tidal-forcing functions. These locations are shown in Figure 14.

Results

The first series of computer runs with the previously described grid system involved use of "average" river inflow conditions and an "average" tidal cycle for the month of December. Several years of river-flow data for the Alabama River at Claiborne Lock and Dam and the Tombigbee River at Coffeeville Lock and Dam were examined and the flows averaged to give an approximate average river flow of 59150 cfs. This value was input to the model as a constant influx to the model at the "river mouth".

The tide cycle chosen had a high tide of 1.6 ft and a low tide of -0.5 ft from the standard tide tables. This tide was made to fit a cosine curve with a period of 24 hours. Data from the tide tables for the tide phase differences between Dauphin Island and the Port of Mobile were used to estimate a 15-minute phase difference between Dauphin Island and Cedar Point. The same tidal cycle in terms of elevations was thus used for both Dauphin Island and Cedar Point with a 15-minute delay in phase. No wind field or precipitation rate was input to the model.

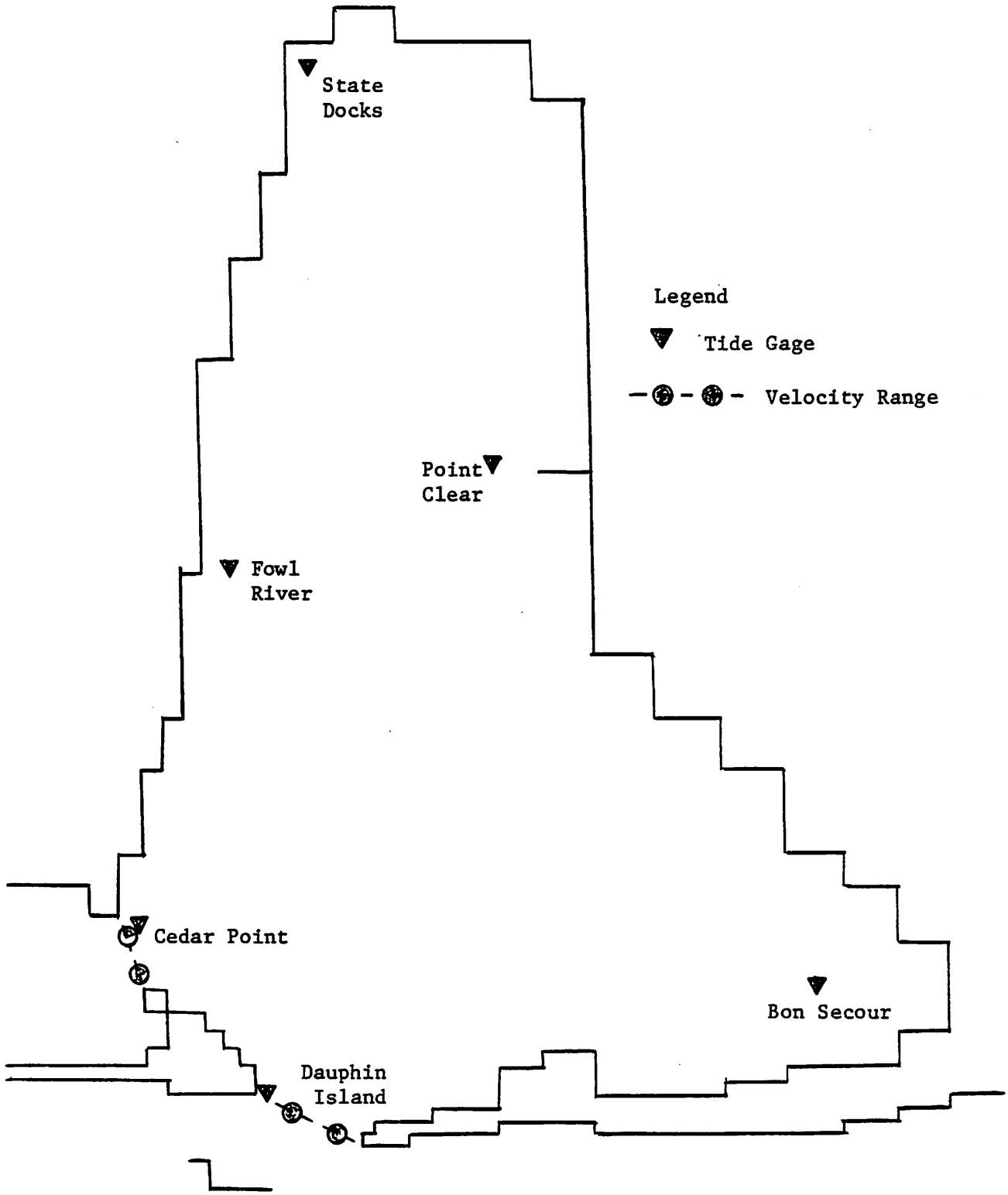

Figure 14. Gage Points and Discharge Ranges for Mobile Bay

The purpose of this study was to establish the trends of the model in terms of the velocity patterns for the Bay. As can be seen from the representative flood-and-ebb velocity profiles generated by the model (Figures 15 through 17), the general pattern of water movement in the Bay, at least qualitatively, matches the pattern observed in the field. The size and direction of the vector in the plots represent the magnitude and direction of the flow at the point for a specific time in the tidal cycle.

The second series of runs was made, using a series of field data from the Mobile Corps of Engineers for May 15 and 16, 1972. The purpose of this application was a preliminary attempt at verifying the model through duplicating field data. The field data were taken over the time period from approximately 0800 May 15 to 1400 May 16. The availabale data consist of hydrographs of the water elevation as a function of time at all special gage-point locations mentioned previously. Velocity and cross-sectional data were provided for Mobile River, Tensaw River, Apalachee River and Blakely River at the causeway. In addition, volumetric discharge as a function of time was provided at Pass Aux Herons and Main Pass. The data indicate Dauphin Island reaching high tide at 1000 May 15 and again at 1100 May 16. All inputs to the model are based on the cycle for this 25-hour period. The data do not represent a true 25-hour cycle because high tide at 1000 is 2.4 ft and that for 1100 is 2.1 ft., with similar discrepancies in the other curves. Therefore, a cycle was forced for all data sets by fitting a smooth curve to match the values at the end of the cycle with those at the beginning. All the pertinent data sets were taken as cycles derived from the time period beginning at 1100 May 15 and ending at 1100 May 16.

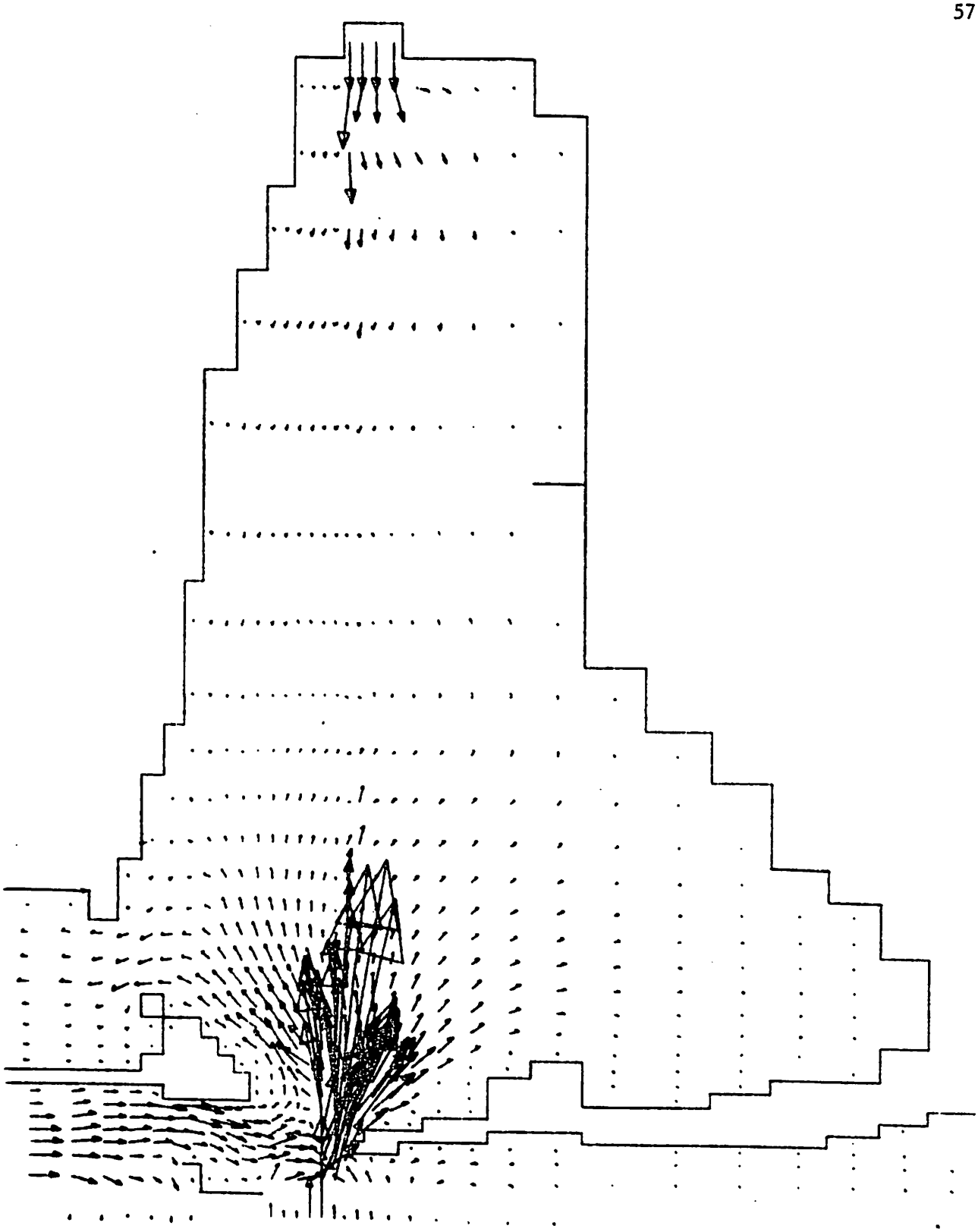

Figure 15. Typical Circulation Pattern for Flood Tide

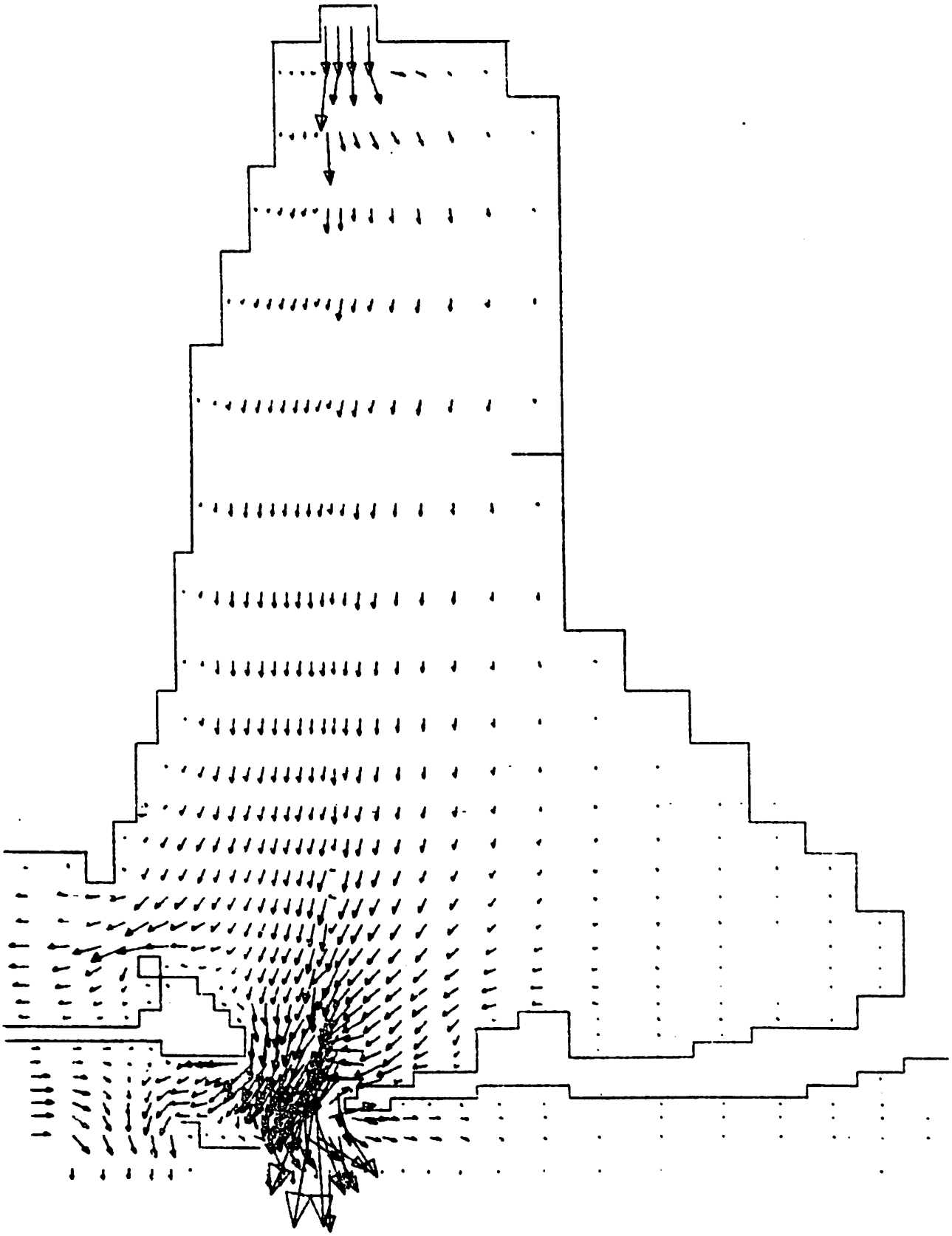

Figure 16. Typical Circulation Pattern for Ebb Tide

Figure 17. Typical Circulation Pattern Near Slack Tide

The river input was calculated by multiplying the velocity for each river every hour beginning with 1000 May 15 by the cross-sectional area of the respective river at the elevation for that hour from the Alabama State Docks gaging station. The volumetric flows for each river were then added to give the total volumetric flow at each hour for the river system at the upper end of the Bay. These total flows were used as input to the program at the "river mouth" in the model.

The program was run for 52 hours of prototype time so the model would stabilize over the input data cycles. This stabilization could be seen in the plots of the tidal elevations over time for each gage point (Figures 18 through 21). Correlation of the model data with field data is shown in Figures 22 through 27. Correlation for Dauphin Island and Cedar Point was excellent as would be expected since field data for these points were the basis for the tidal boundary input. The correlation of elevation for Fowl River, Point Clear, and Bon Secour was very good in terms of the magnitudes of the high and low tide and in the slopes of the curves. However, a phase shift is noticed. The gage point at the Alabama State Docks revealed the poorest comparison between model and field data. This is almost certainly due to the proximity of this gage point to the river input boundary of the model, since only one cell separates these two points. As indicated previously, the representation of the river will be improved in later applications.

No attempt was made to correlate the volume discharge data through the two passes. Additional work is required in interpreting field data and how to compare it with model results. Typical velocity vector plots produced by the numerical model for this application are shown in Figures 28 through 30.

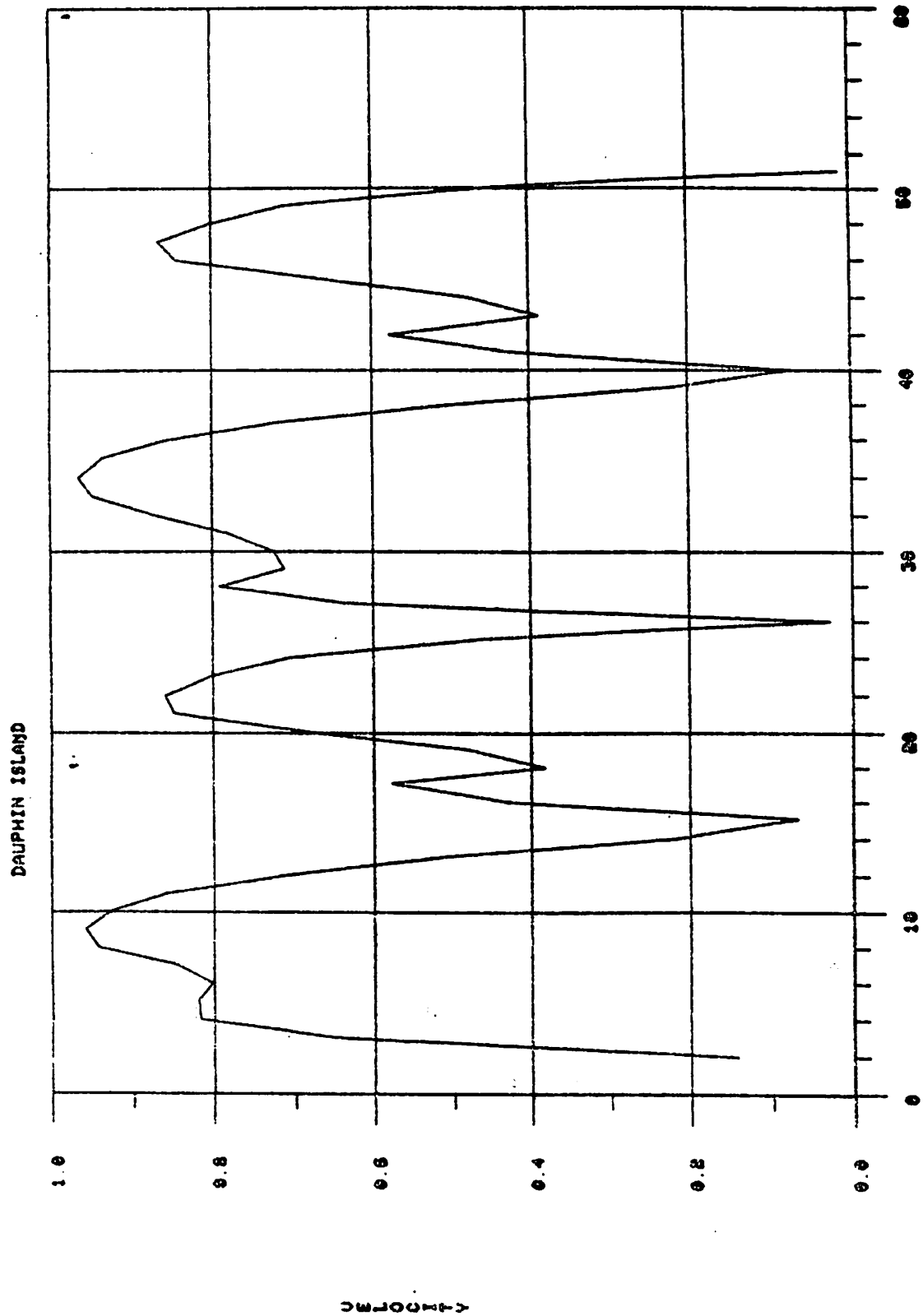

Figure 18. Tidal Height Fluctuation at Dauphin Island Gage Point

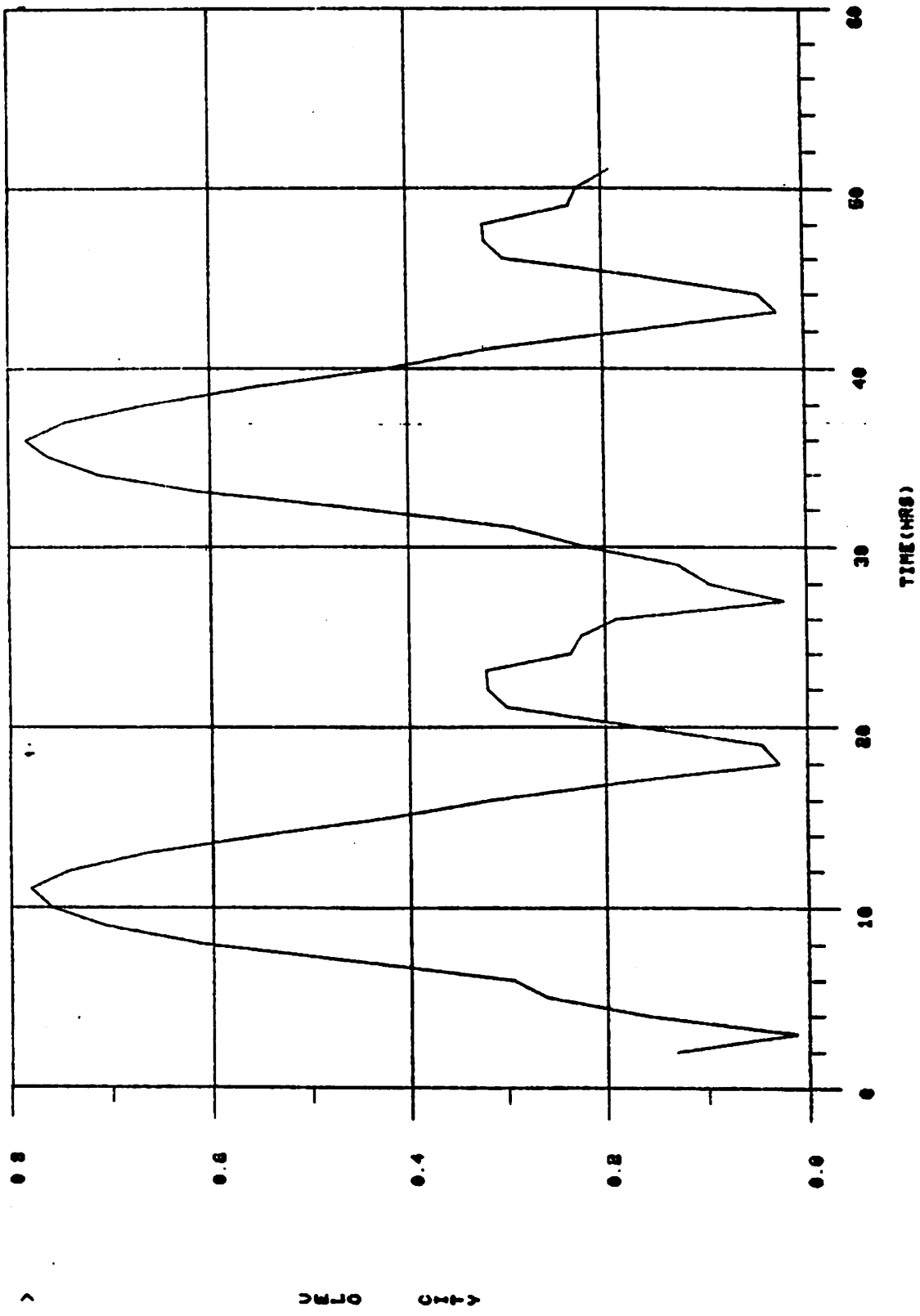

Figure 19. Tidal Height Fluctuation at Point Clear Gage Point

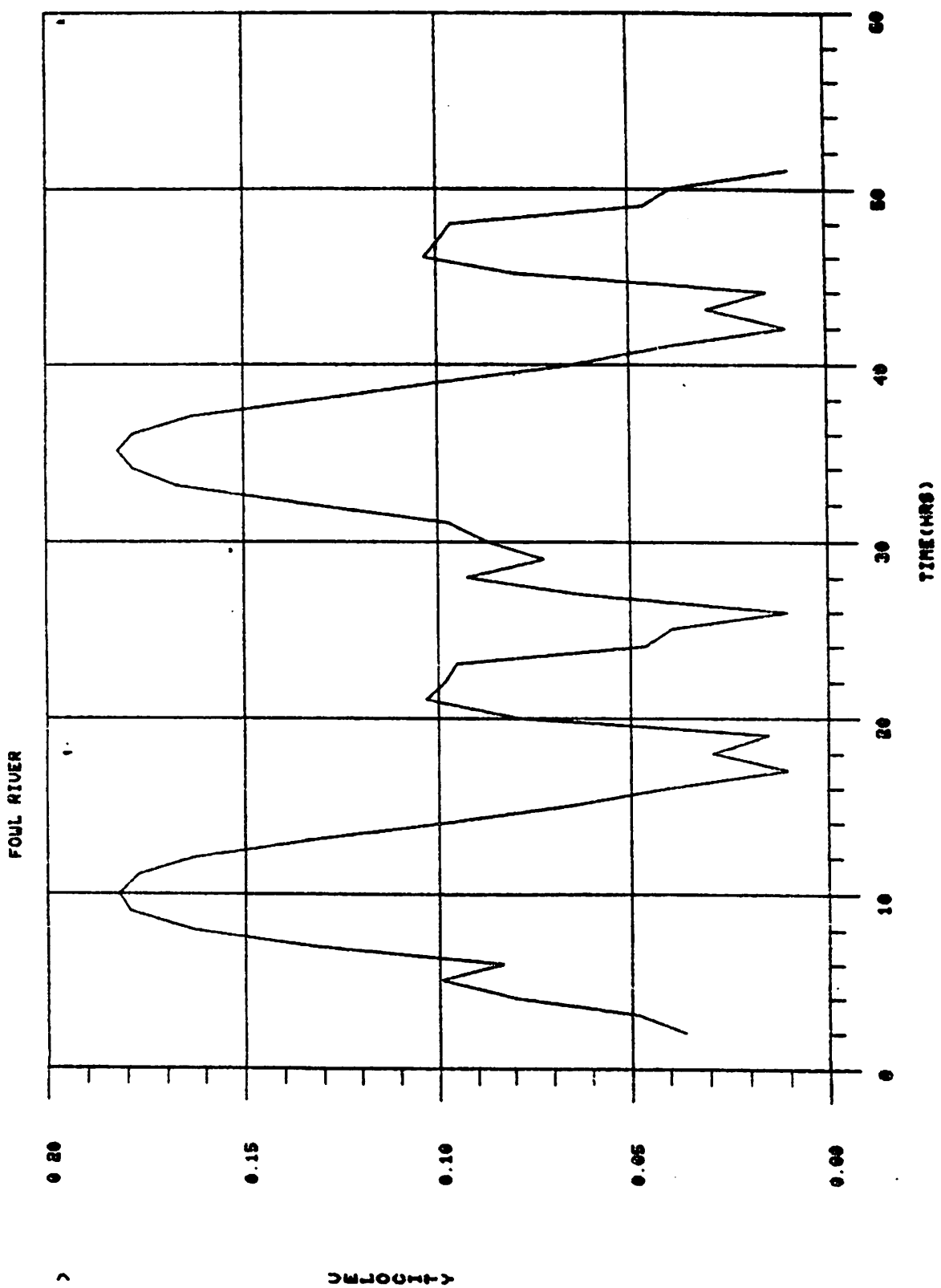

Figure 20. Tidal Height Fluctuation at Fowl River Gage Point

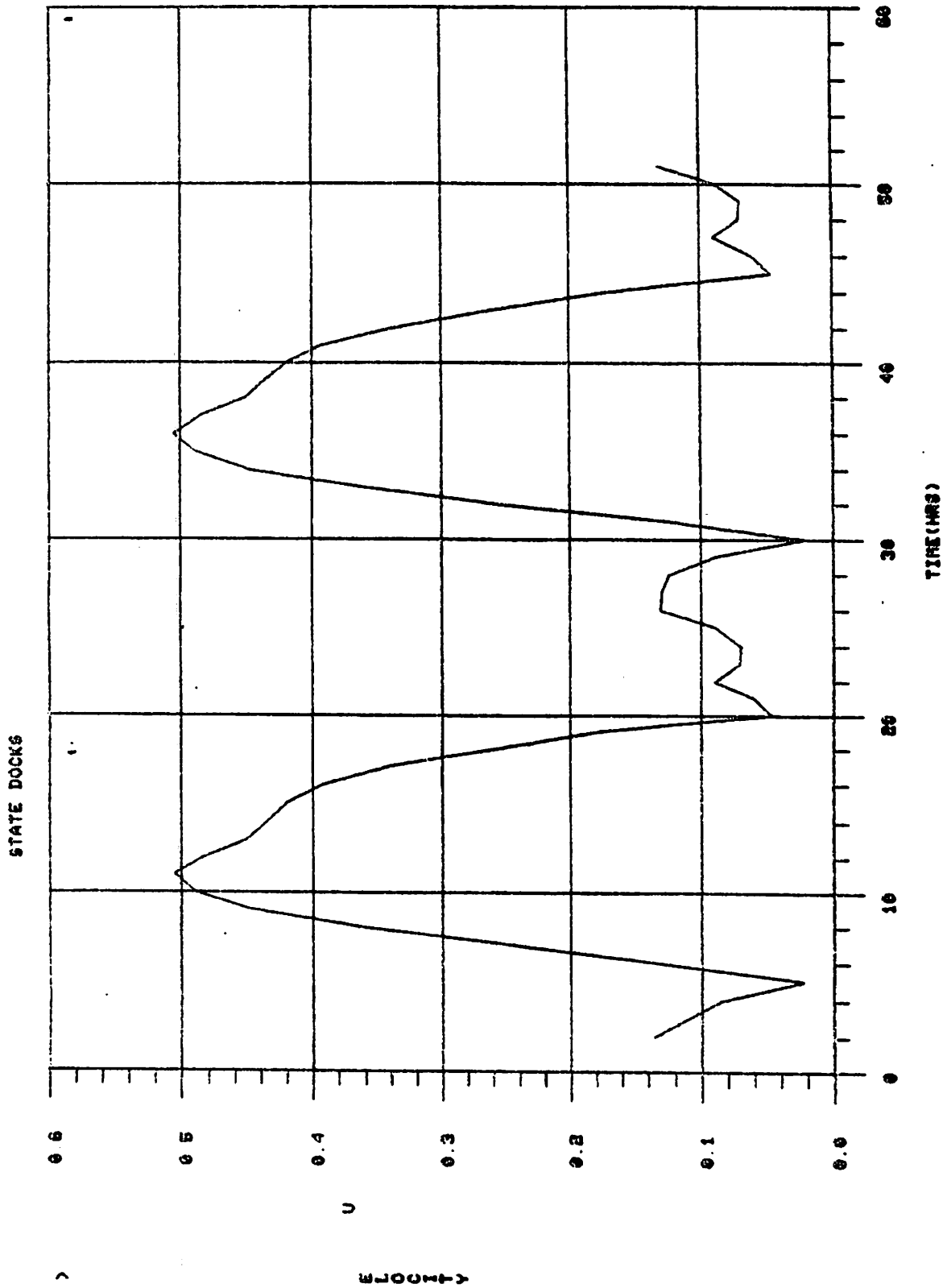

Figure 21. Tidal Height Fluctuation at State Docks Gage Point

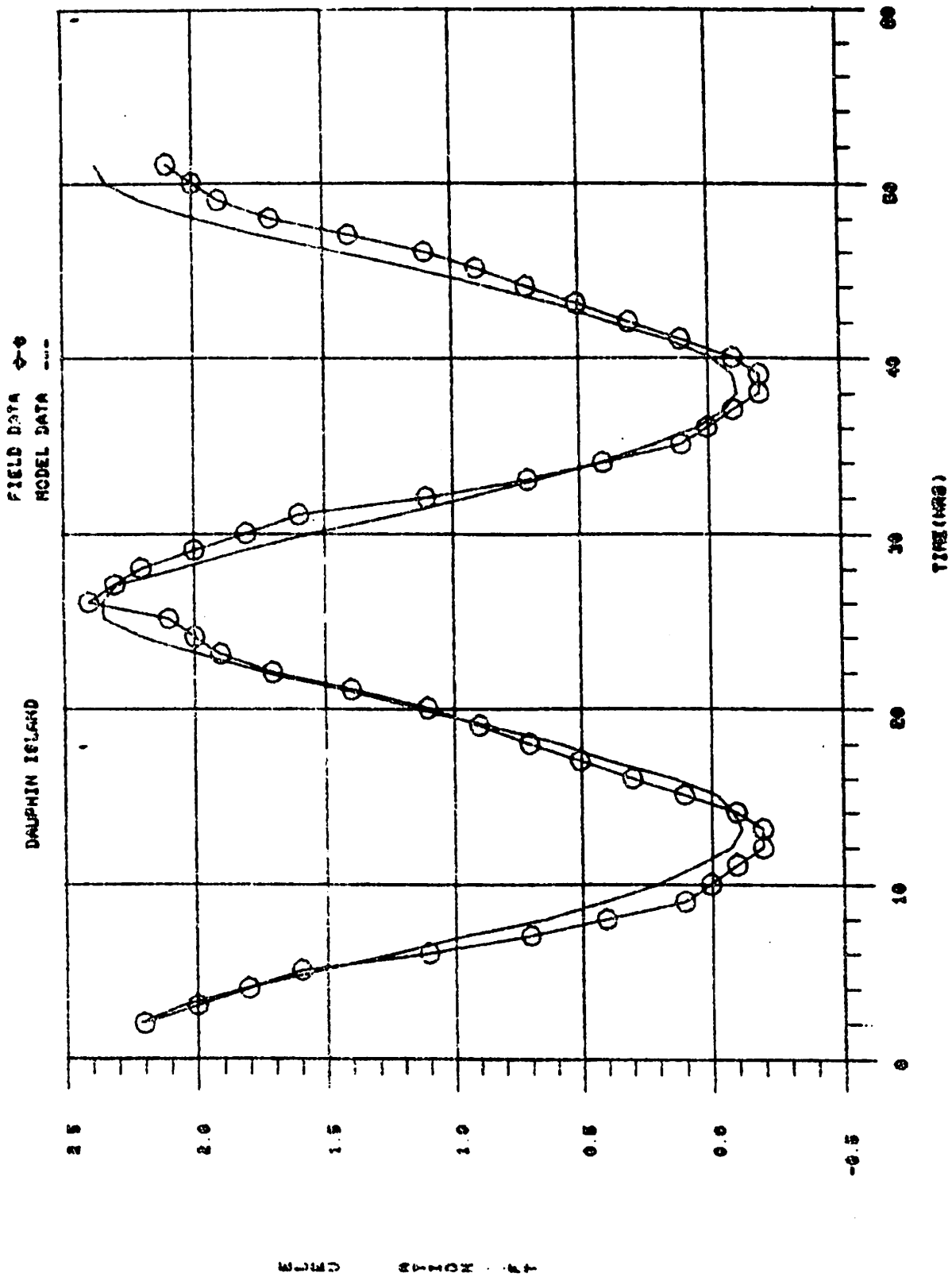

Figure 22. Correlation of Model Results and Field Data at Dauphin Island

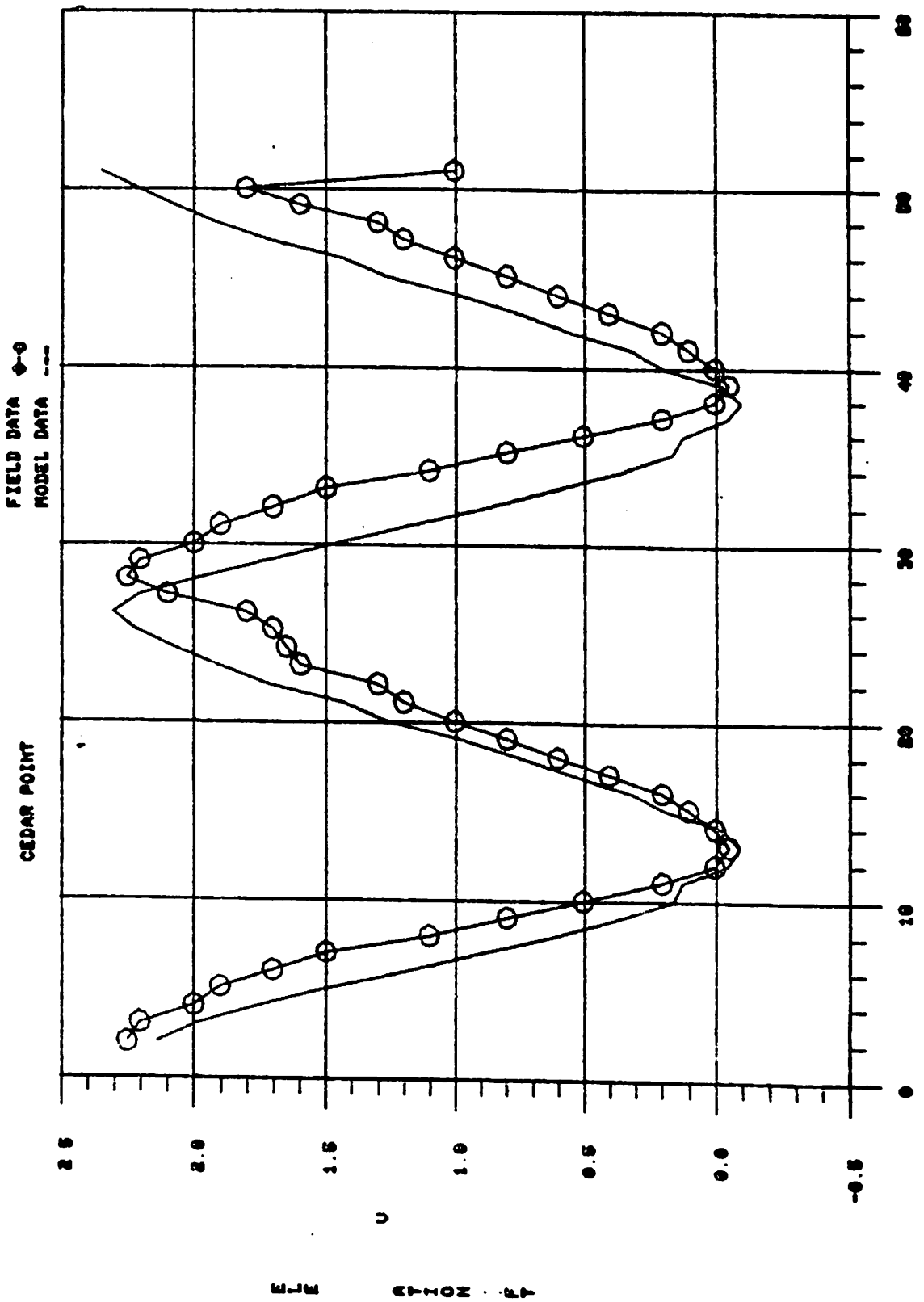

Figure 23. Correlation of Model Results and Field Data at Cedar Point

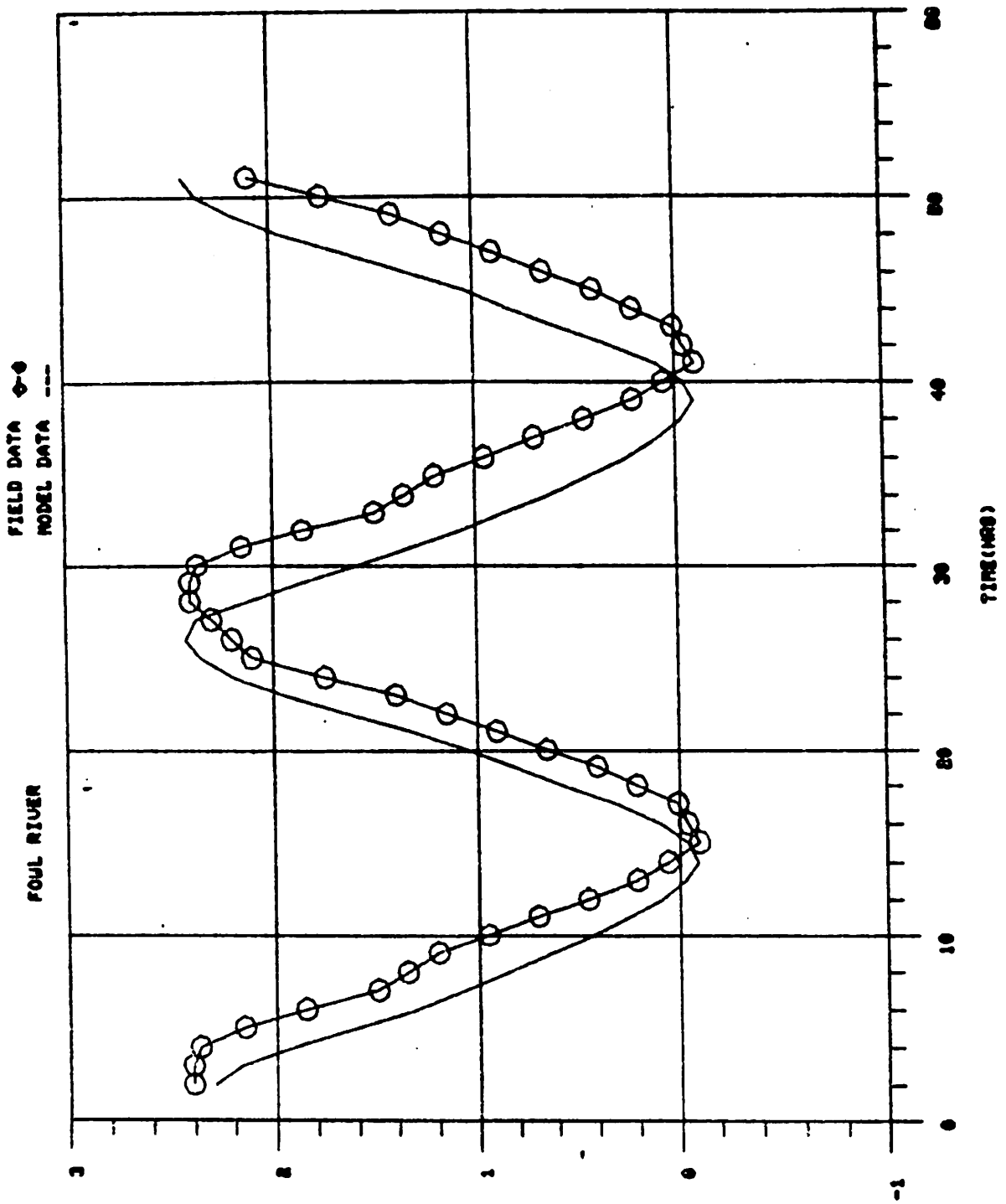

Figure 24. Correlation of Model Results and Field Data at Fowl River

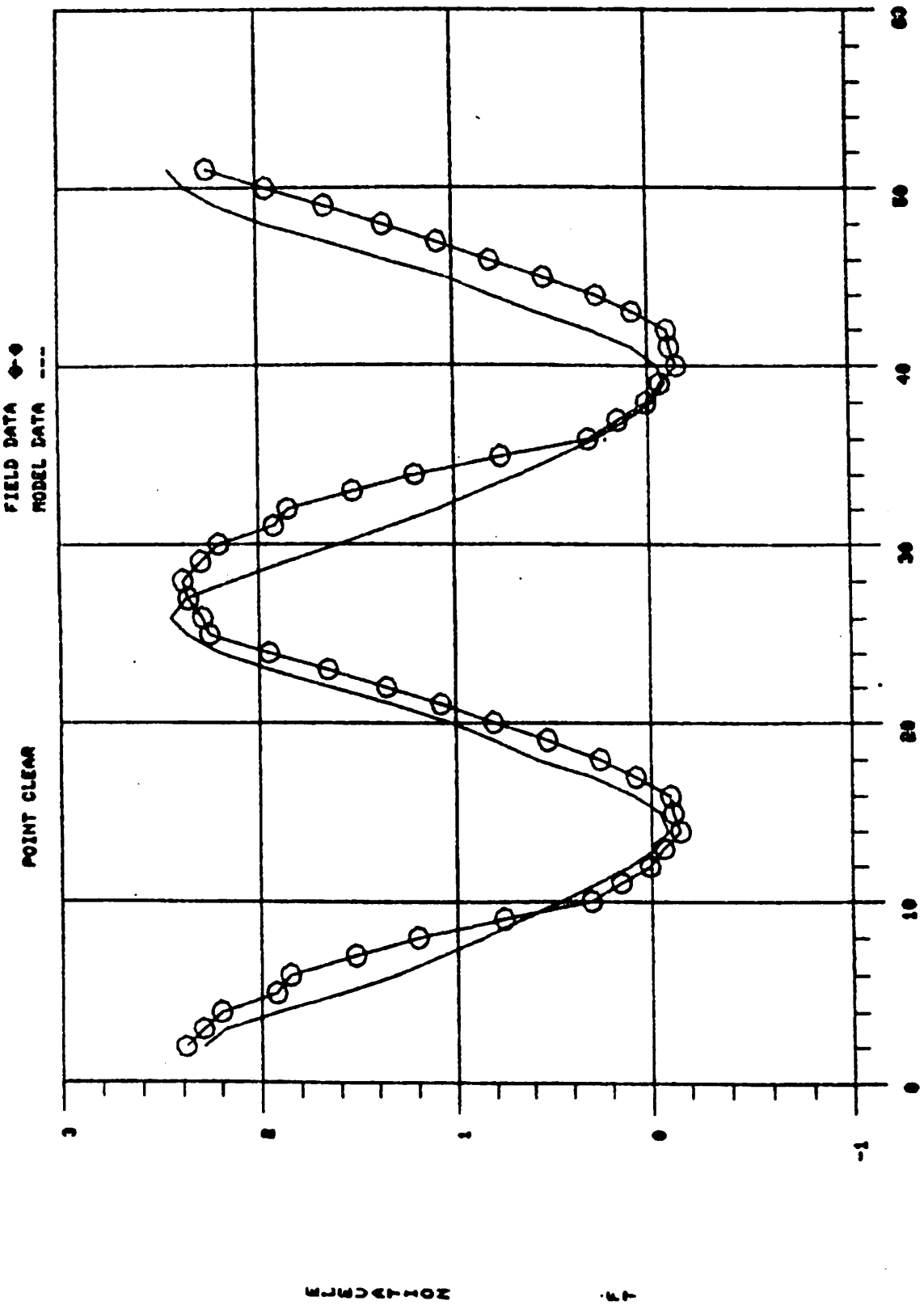

Figure 25. Correlation of Model Results and Field Data at Point Clear

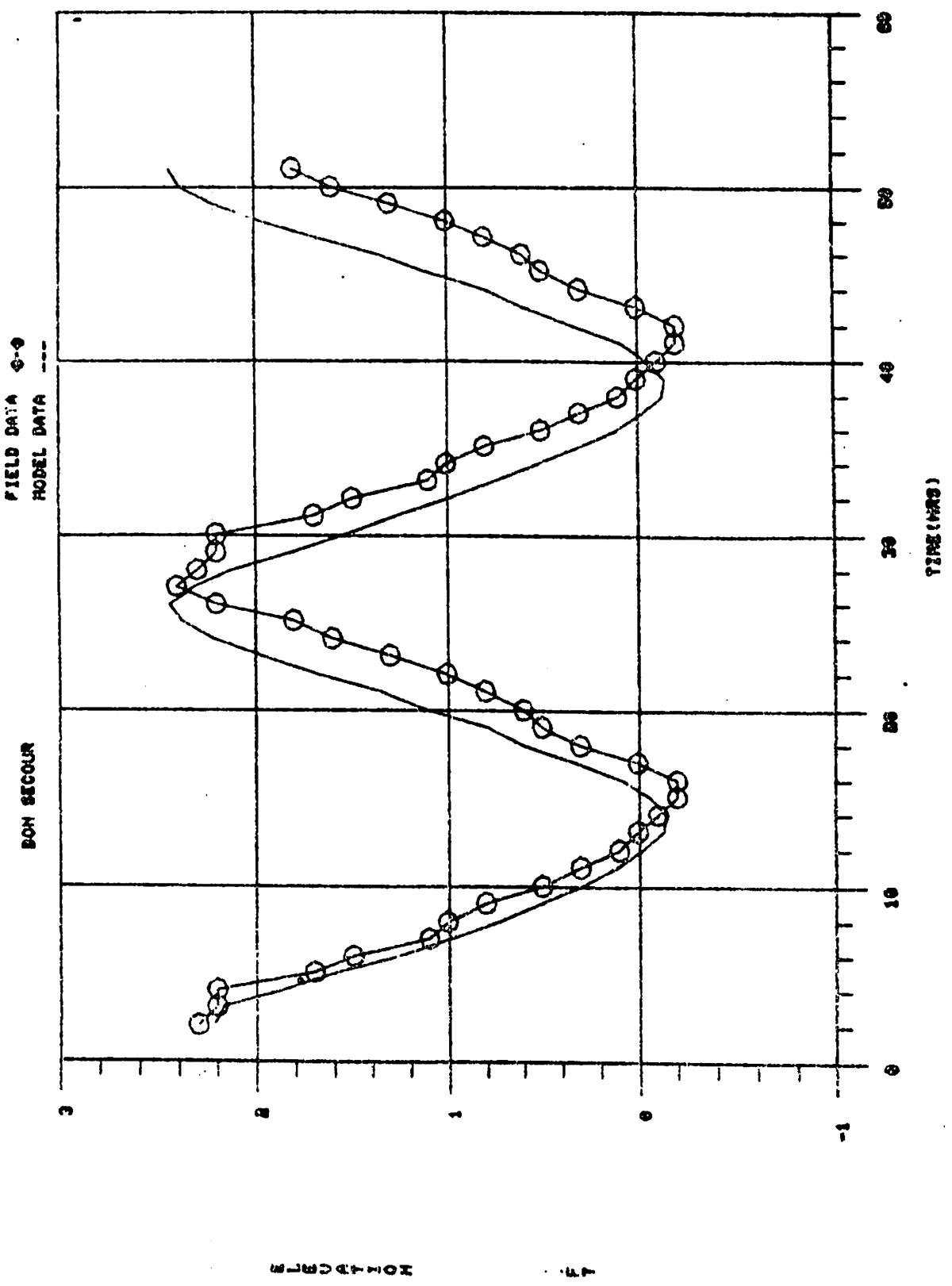

Figure 26. Correlation of Model Results and Field Data at Bon Secour

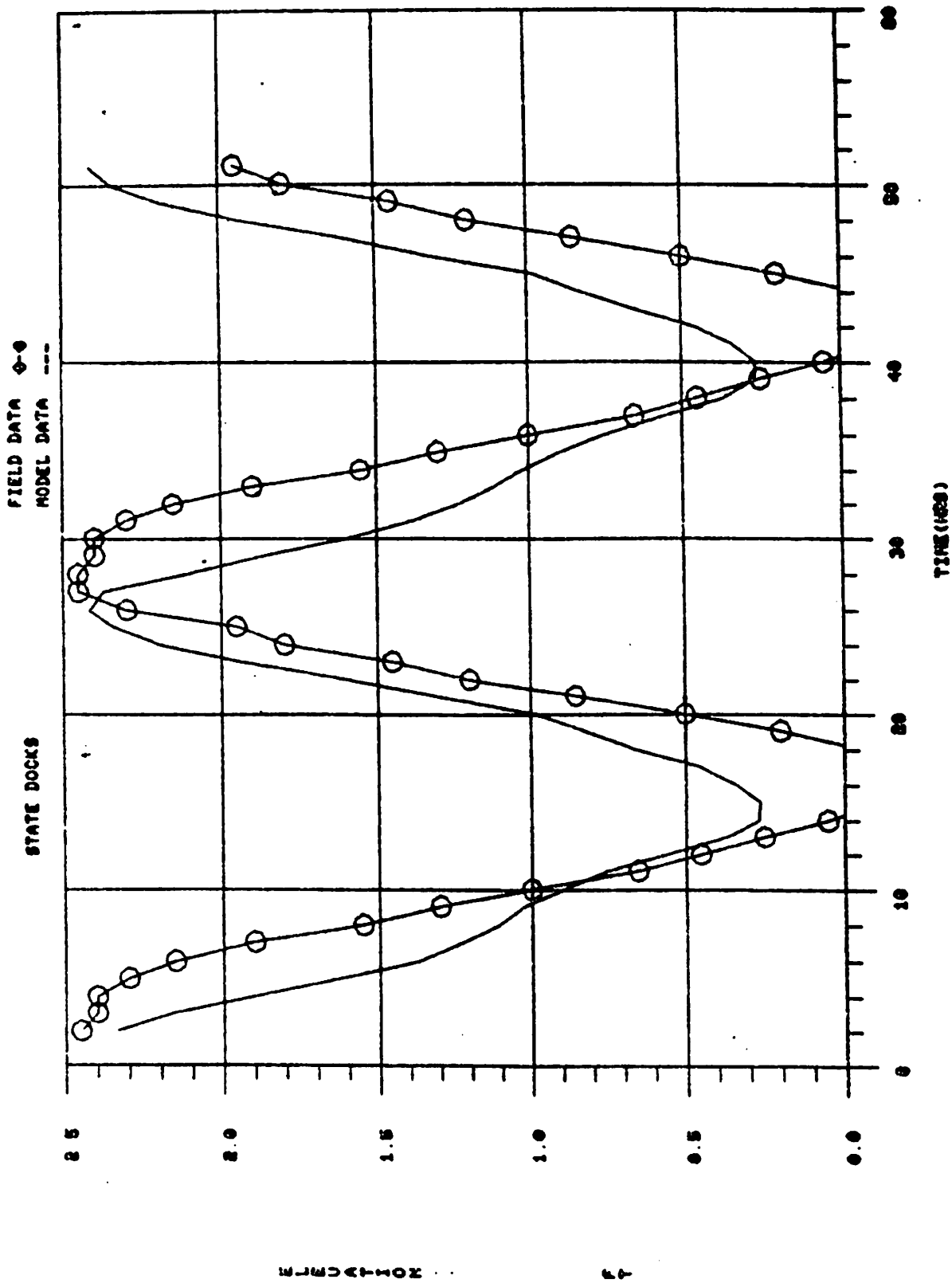

Figure 27. Correlation of Model Results and Field Data at State Docks

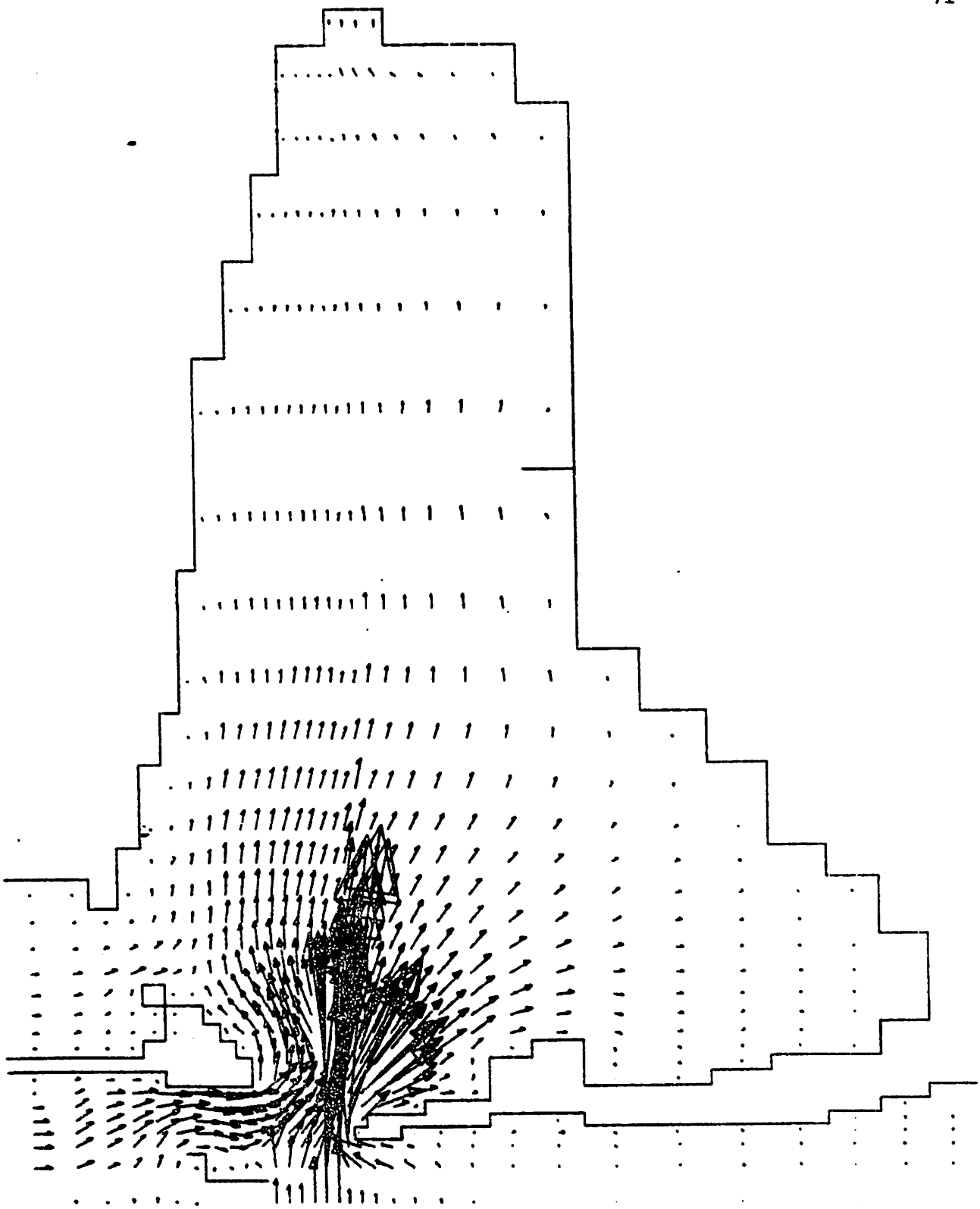

Figure 28. Circulation Pattern at Flood Tide

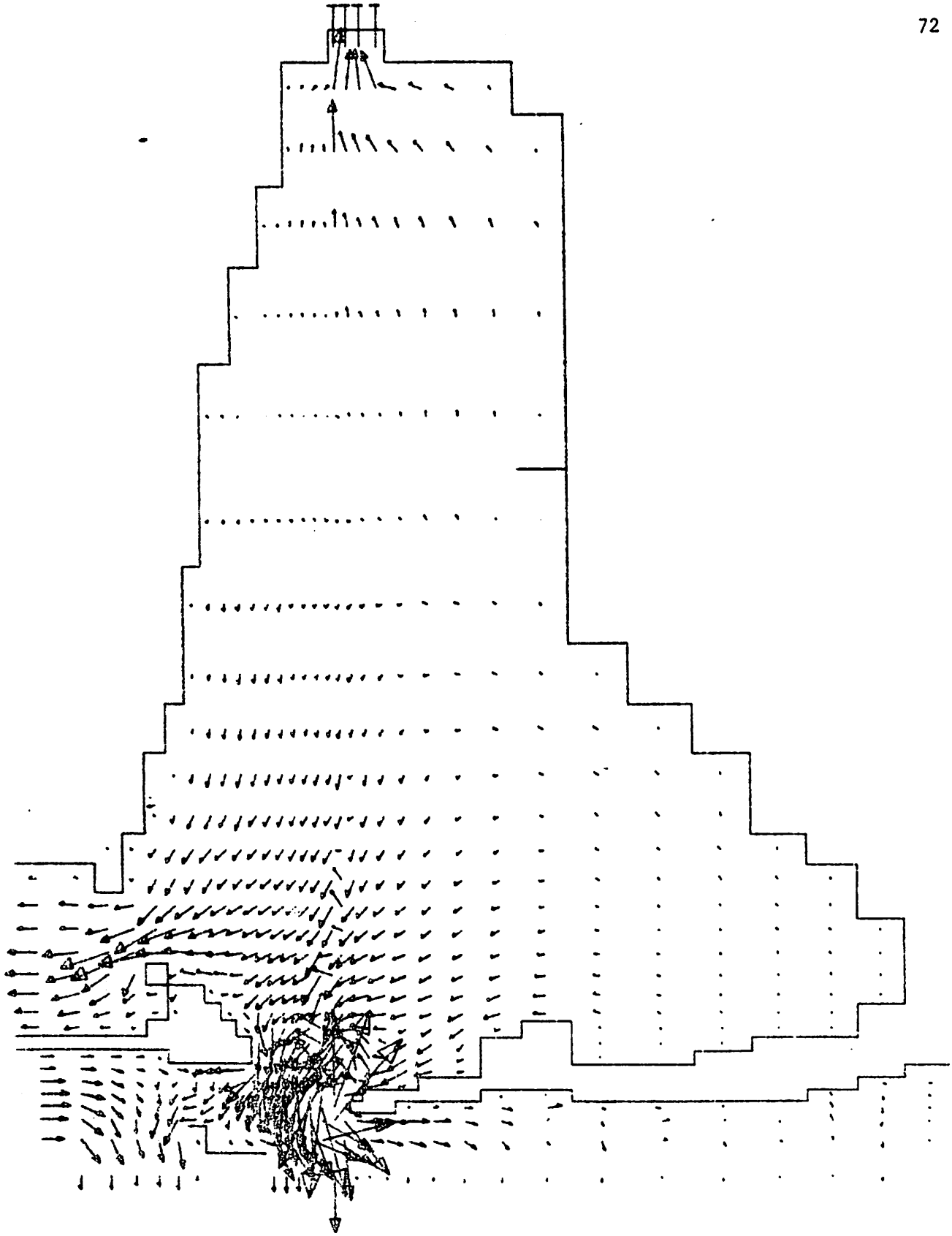

Figure 29. Circulation Pattern at Ebb Tide

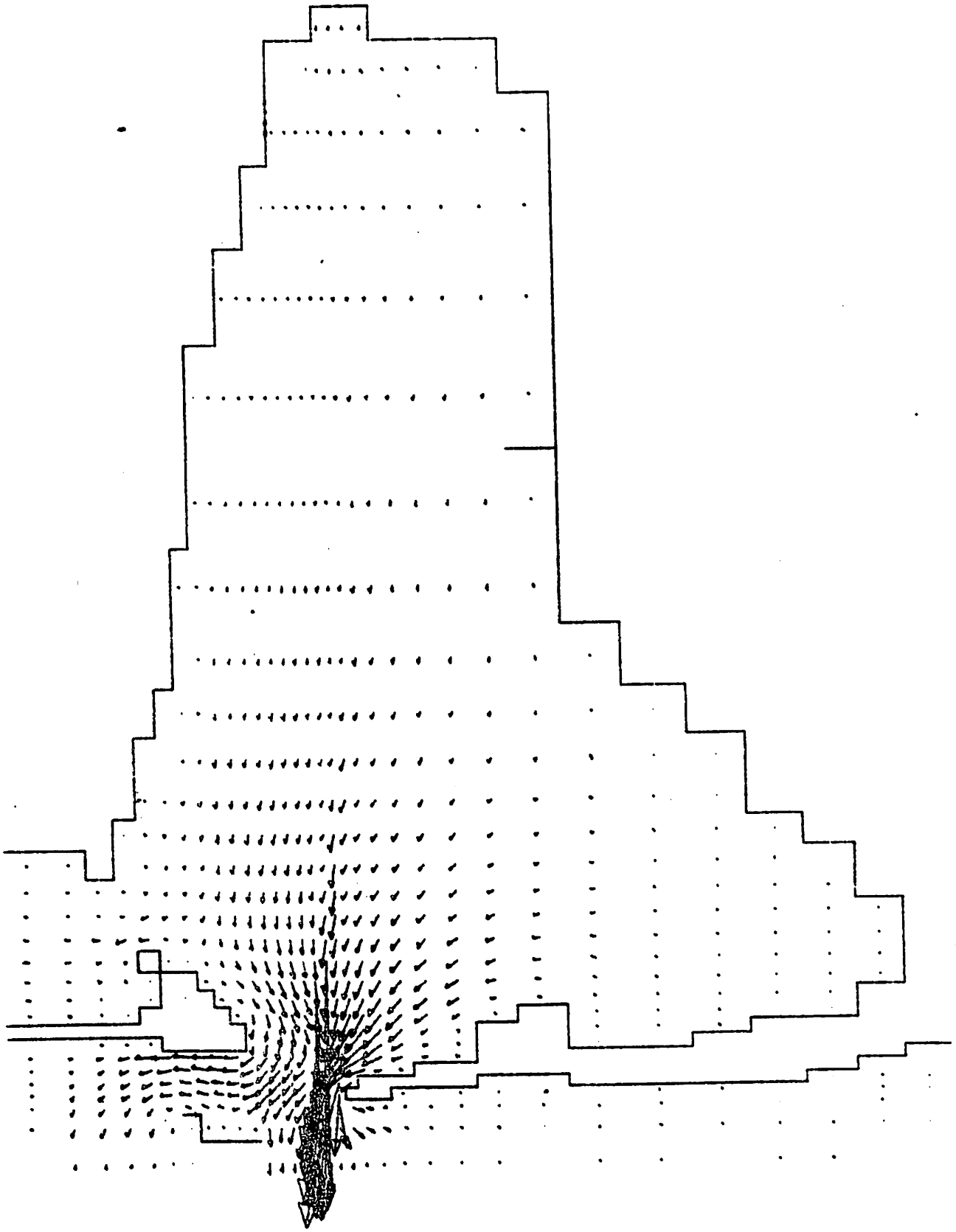

Figure 30. Circulation Pattern Near Slack Tide

Further refinement of the model applied to the Mobile system will necessitate refinement of the grid representation and the acquisition of more field data for comparison studies. It would be desirable to use as river input the data from the continuous monitoring stations at Coffeeville and Claiborne rather than velocity information at the mouth of the Bay, which are unavailable in most circumstances. Therefore, the grid system will need expansion northward to insulate the point of river input to the model from the Bay. Several techniques will be investigated for achieving this desired result. A one-dimensional river model coupled to the two-dimensional model is one possibility. Various modifications of the basic grid system and representation of various phenomena will evolve as calibration of the models proceed.

One problem associated with presenting overall circulation patterns in a graphical format is the wide range of velocities present. If the major velocities are plotted to an appropriate scale, then the smaller velocities become almost points rather than vector. On the other hand, if the smaller velocities are plotted to an appropriate scale, the major velocities become unreasonably large. To alleviate this problem, it may be necessary to focus in on some particular section of the overall system and plot the sub-system to an appropriate scale. This is illustrated in Figure 31.

B. Mobile Bay-Mississippi Sound Application

Model applications have been restricted to a preliminary investigation of tidal circulation, tidal elevations, velocity fields, and flow rates in Mobile Bay and Mississippi Sound. There are three main entrance channels to the Mobile Bay-Mississippi Sound system.

(1) Main ship channel, average depth 40 ft.

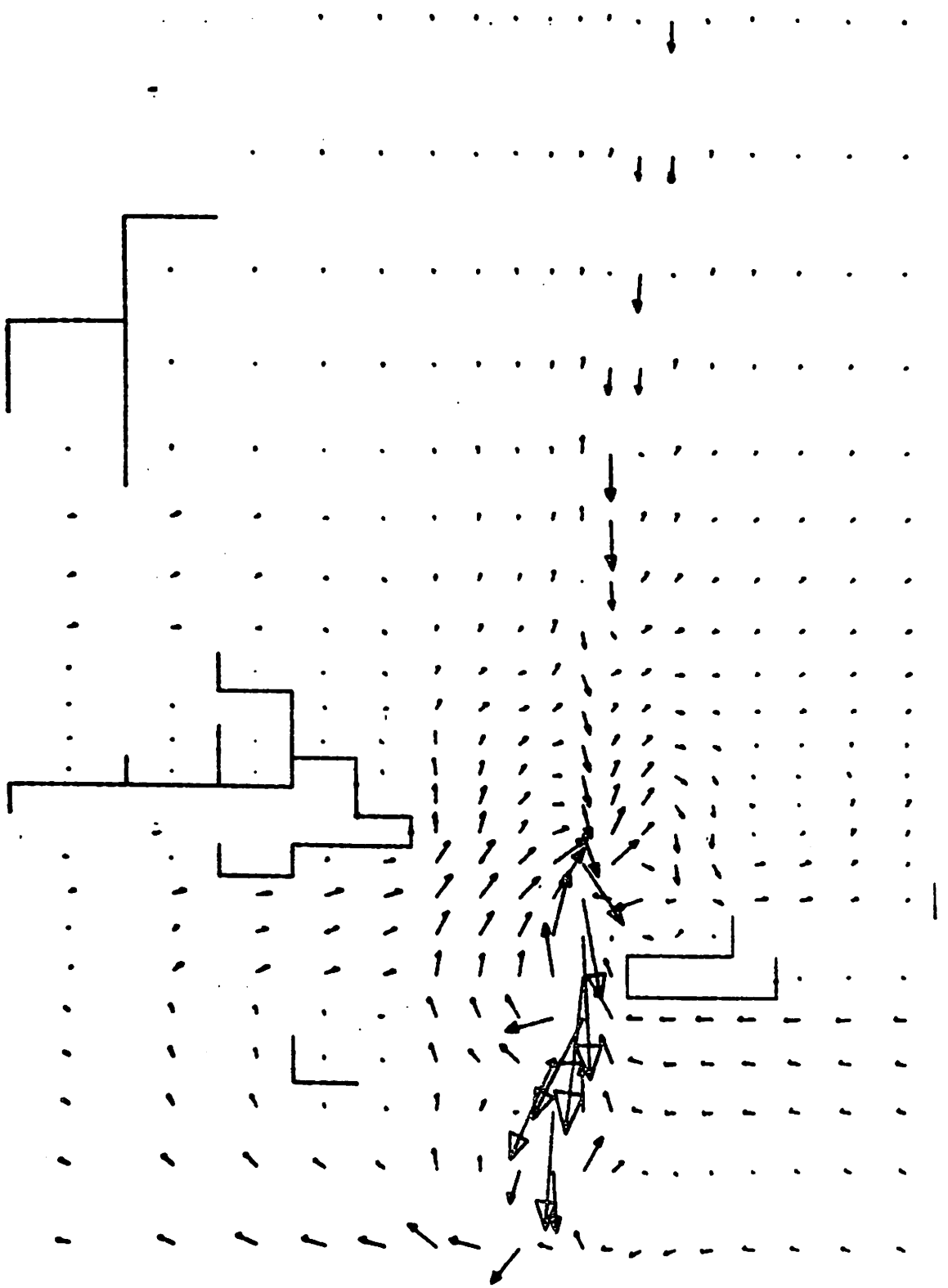

Figure 31. Expanded Scale Plot of Local Circulation Patterns

(2) Horn Island Pass Channel, average depth 36 ft.

(3) Ship Island Pass Channel, average depth 28 ft.

The main entrance channels and the numerical representation of the system are shown in Figure 32.

Several rivers discharge into the system but only two major rivers, Mobile River and Pascagoula River, are included in this simulation.

A variable grid consisting of 2170 grid cells (31 x 70) was developed for the system region. Programs MAPIT and TGRID were used for grid development. The minimum cell width is 1667 ft and the maximum is 17500 ft. Figure 33 displays the computational grid and Figure 34 shows the location of gage points. Various subgrid barriers were used throughout the grid system to represent features such as sand bars and small islands. A time step of 180 seconds per time cycle was selected.

The river discharge was determined from an average inflow between December 5 and December 11, 1976. The discharge during this period was steady and close to the long-term-average value. The river discharge information was obtained from references (3) and (4) and is summarized in Table A.

Three different tides, which were simulated by a cosine function $0.55 + 1.05 \cos (0.2618t + \theta)$ θ phase difference, were employed in the system. Referring to Figure 32, tidal inputs which vary from cell to cell were applied to region I and region II, whereas a constant tide was applied to region III.

Typical tidal circulation plots are shown in Figures 35 through 37. These flow patterns appear reasonable; however, no attempts to calibrate the model have been made due to a lack of suitable prototype data.

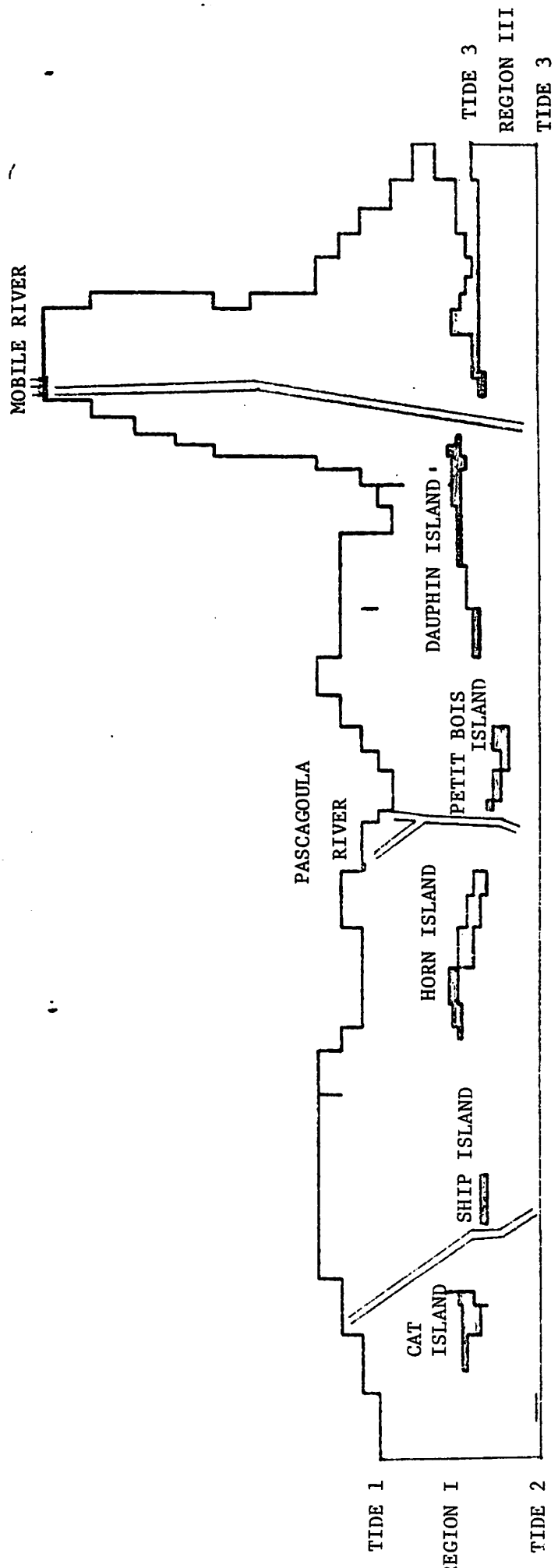

Figure 32. Main Entrance Channels to Mobile Bay-Mississippi Sound

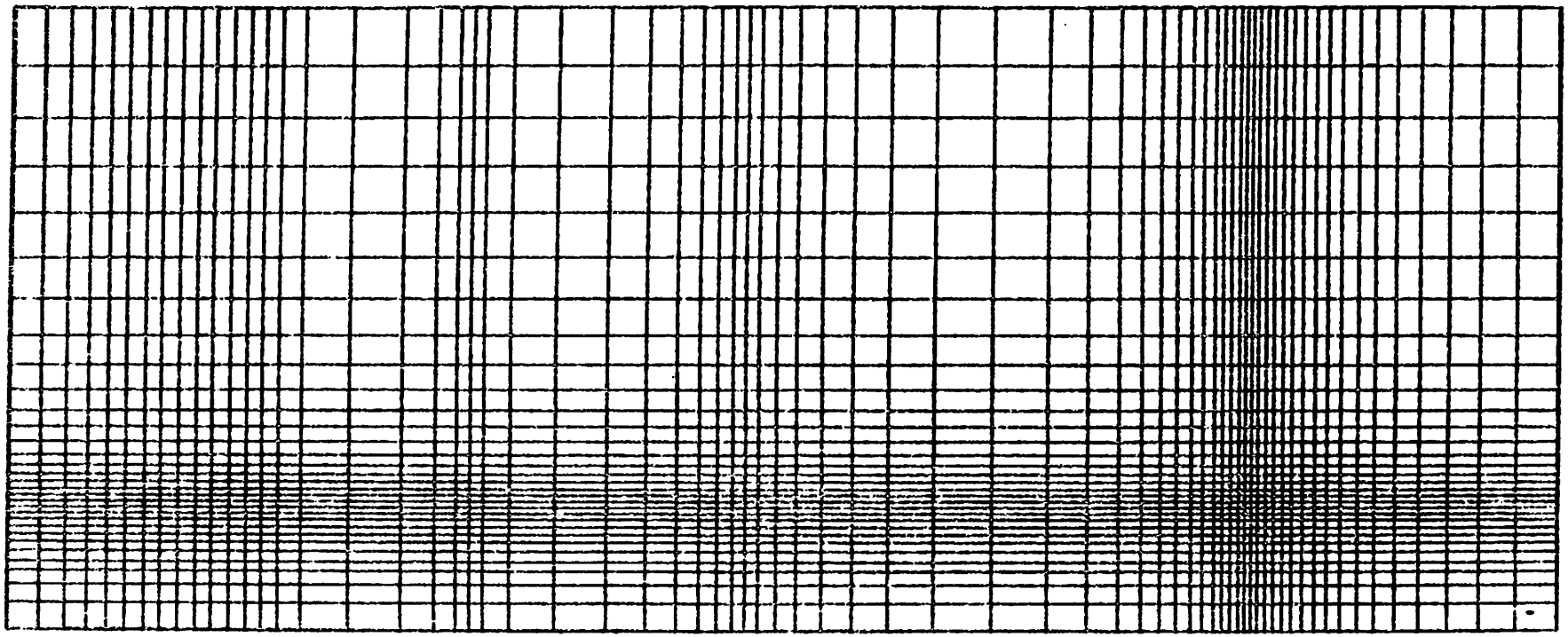

Figure 33. Computational Grid for Mobile Bay and Mississippi Sound

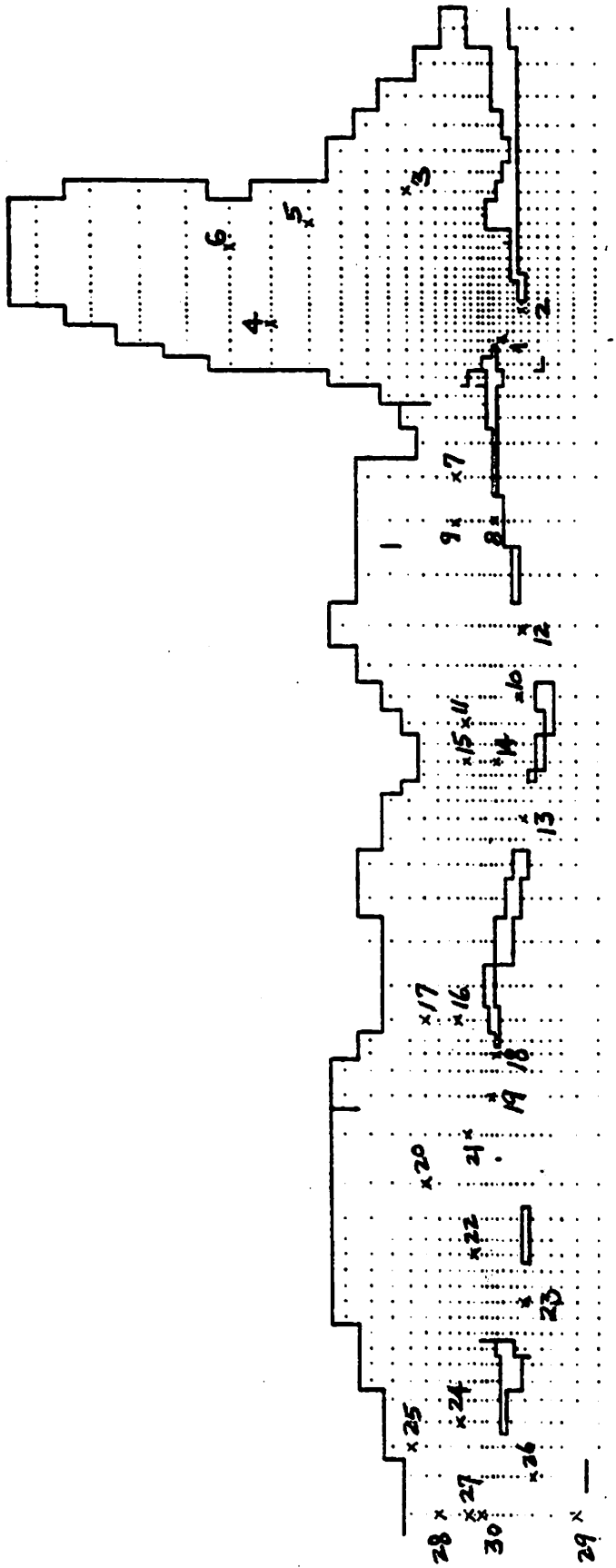

Figure 34. Gage Point Location for Hydrodynamic Output

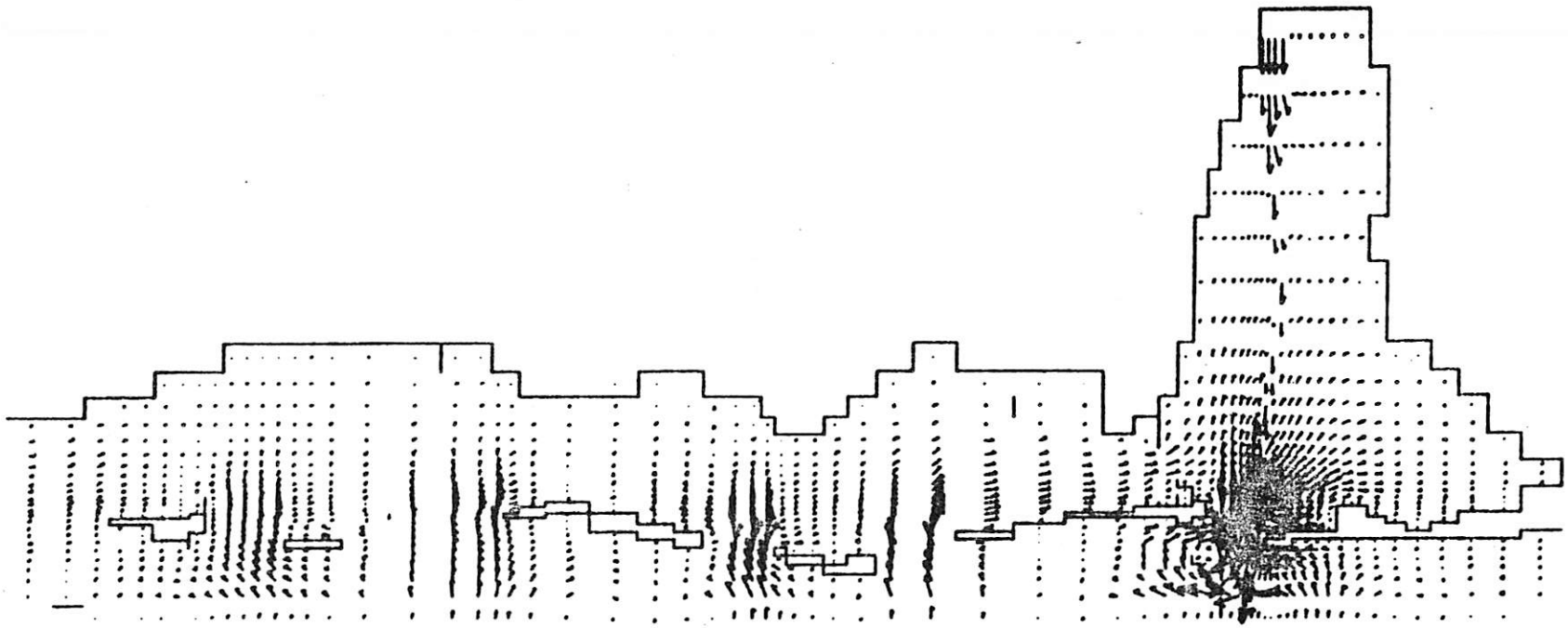

Figure 35. Typical Circulation Plot for Flood Tide

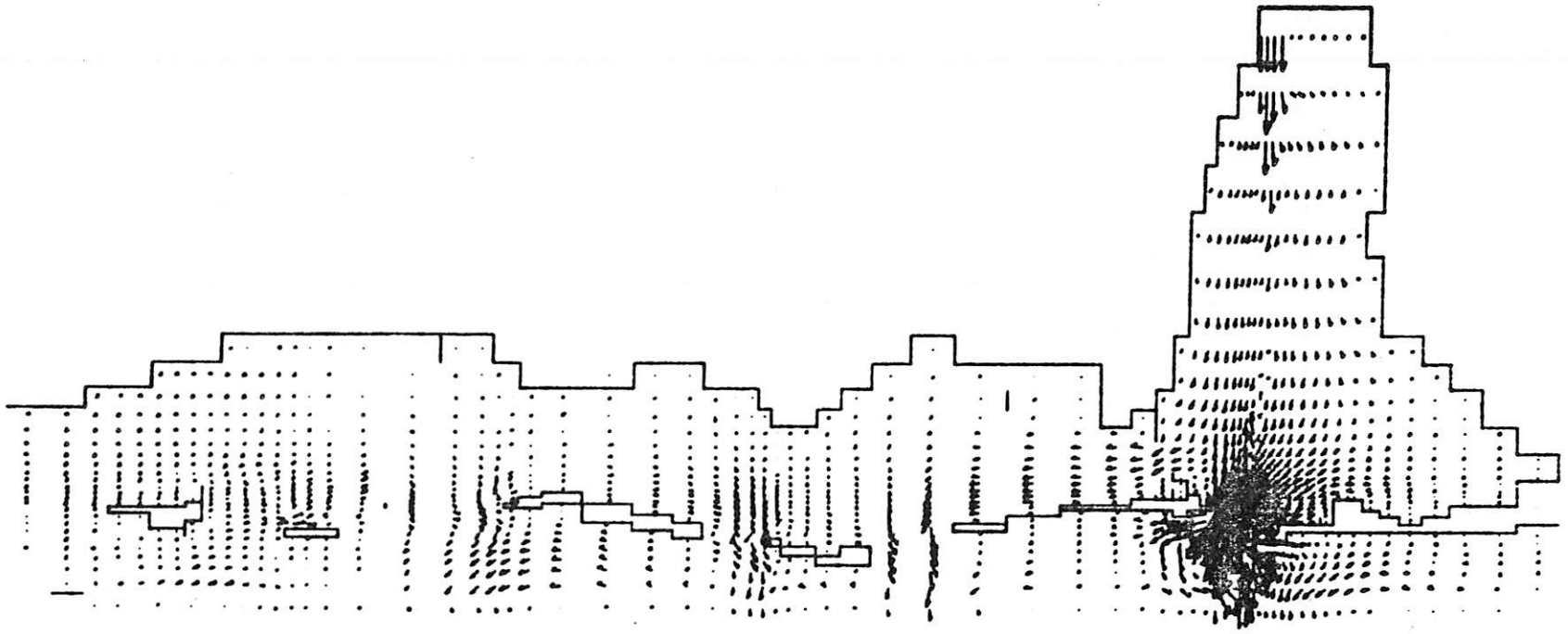

Figure 36. Typical Circulation Plot for Ebb Tide

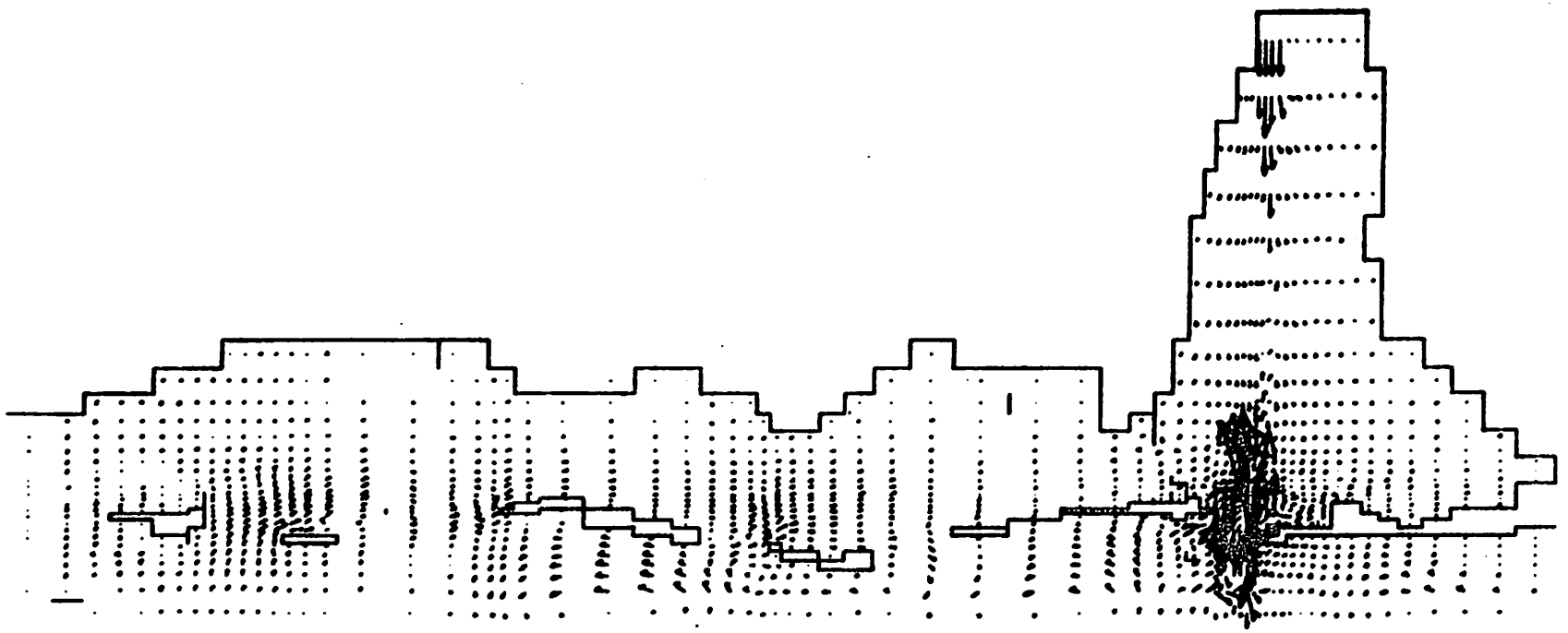

Figure 37. Typical Circulation Plot Near Slack Tide

WATER YEAR 1976 unit: ft^3/sec

PASCAGOULA RIVER (MS)									
Day / Station No.	Dec. 5	Dec. 6	Dec. 7	Dec. 8	Dec. 9	Dec. 10	Dec. 11	Average Value (Dec. 5 11)	Average for long-term
02479000	7500	6660	7060	8810	9530	8390	6710	7808	9667
02479160	748	687	1250	1880	1380	1070	900	1132	1028
02479300	594	558	638	1320	1190	920	736	851	836
02479560	1010	894	1050	1220	1260	1280	1260	1138	968
02480250	50	64	110	90	70	60	50	71	114
Total Inflow	9902	8873	10108	13320	13430	11720	9656	11000	12613

MOBILE RIVER (AL)									
Day / Station No.	Dec. 5	Dec. 6	Dec. 7	Dec. 8	Dec. 9	Dec. 10	Dec. 11	Average Value (Dec. 5 11)	Average for long-term
02428400	47900	47300	42800	36500	29300	28000	25500	36757	36200
02469761	29000	26300	26400	24200	21800	21800	22200	24528	31850
Total Inflow	76900	73600	69200	60700	51100	49800	47700	61285	68050

The width of Pascagoula River: 7290 ft. inflow = $\frac{11000\ ft^3/sec}{7290\ ft} = 1.51\ ft^2/sec$

The width of Mobile River: 8646 ft. inflow = $\frac{61285\ ft^3/sec}{8646\ ft} = 7.09\ ft^2/sec$

Table A. Summary of River Data

C. Mississippi Sound Application

In the initial application of WIFM II to Mississippi Sound, a grid with 975 cells was used. The discretization of the shoreline and the variable grid for Mississippi Sound are shown in Figures 38 and 39.

The model has been run, using average conditions similar to those used for the combined Mobile Bay - Mississippi Sound model. Typical circulation patterns are shown in Figures 40 through 42. No attempt has yet been made to calibrate or verify the model.

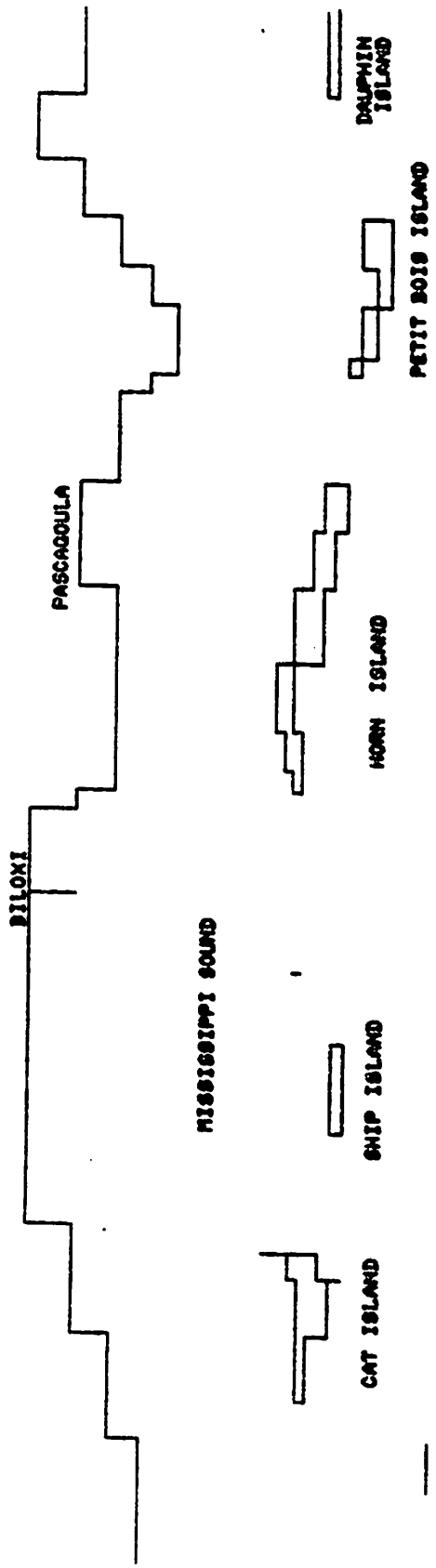

Figure 38. Mississippi Sound Model Representation

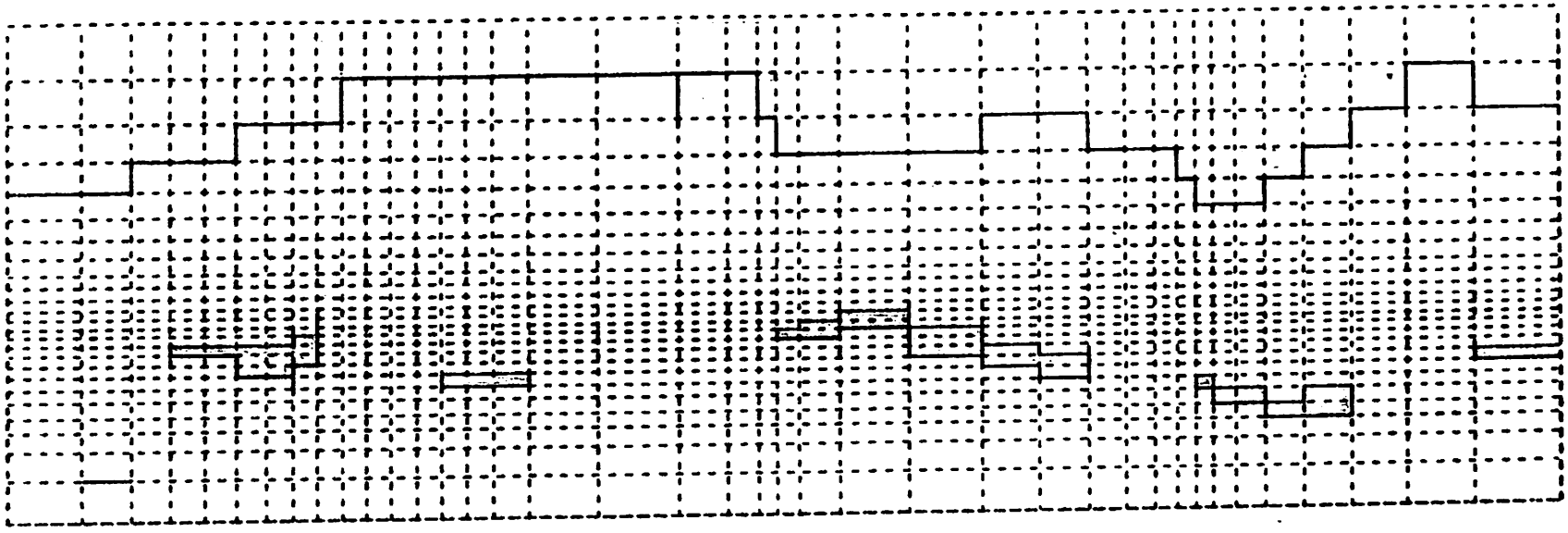

Figure 39. Variable Grid System for Mississippi Sound

Figure 40. Typical Circulation Pattern for Flood Tide

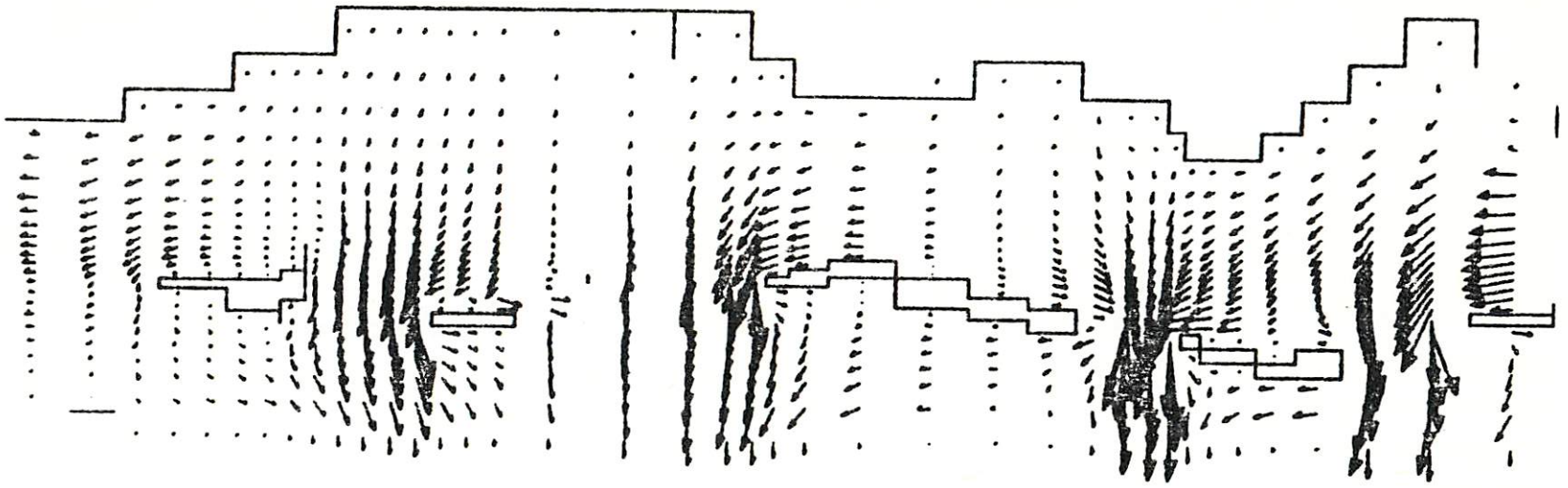

Figure 41. Typical Circulation Pattern for Ebb Tide

Figure 42. Typical Circulation Pattern Near Slack Tide

VII. ADDITIONAL STUDY AREAS

A. Spectral Analysis Techniques

Long waves penetrating an estuary from the ocean will not only change in amplitude but also transfer energy from one wave frequency to another. This wave-dispersion process is very complex. As a wave propagates, the non-linear advective terms in the equation of motion generate higher harmonics of the fundamental frequency. In particular, the second harmonic increases in amplitude with the distance of propagation. Similarly, bottom friction and changes in bottom slope generate various harmonics. The varying depth and complicated boundaries also generate dispersion of energy in frequency. If several frequencies are present simultaneously, frequency sums and differences can be generated as the tide travels through the estuary. Thus, energy can be transferred from one frequency to higher and lower frequencies by interaction of waves with different frequencies.

The classical method for verifying and calibrating hydraulic models has been to compare model results with field measurements. Generally the comparison has been made subjective by comparing data in various graphic form, then concluding that the model is or is not verified. The subjective analysis of whether the model is verified or not can be enhanced by determining some statistical properties of the differences between observed and computed values. Model parameters can be adjusted to bring the statistical results into better agreement with prototype results. For example, the energy spectra of the model at various locations in the estuary can be compared with the prototype energy spectra

to determine how well the model represents the complex frequency dispersion of energy which takes place when a wave propagates through the estuary.

The general subject of statistical or probabilistic methods is a complex subject and will not be treated in this report. The reader is referred to standard textbooks such as that by Papoulis (4) for a general treatment of the subject or to Rand Reports by Liu (5), and Leendertse and Liu (6) for general methods of application to hydrodynamic systems. In this report application will be limited to mentioning some basic spectral analysis techniques which may be useful in verifying and calibrating numerical models. This is the context from which spectral analysis techniques are being investigated for this project.

The spectrum of a data set describes the general frequency composistion in terms of the mean square value of each individual component. For example, if a record exists from a combination of two sinusoidal components

$$A_1 \sin (2 f_1 t) + A_2 \sin (2 f_2 t) \quad ,$$

then the spectrum would be two values on the graph shown in Figure 43.

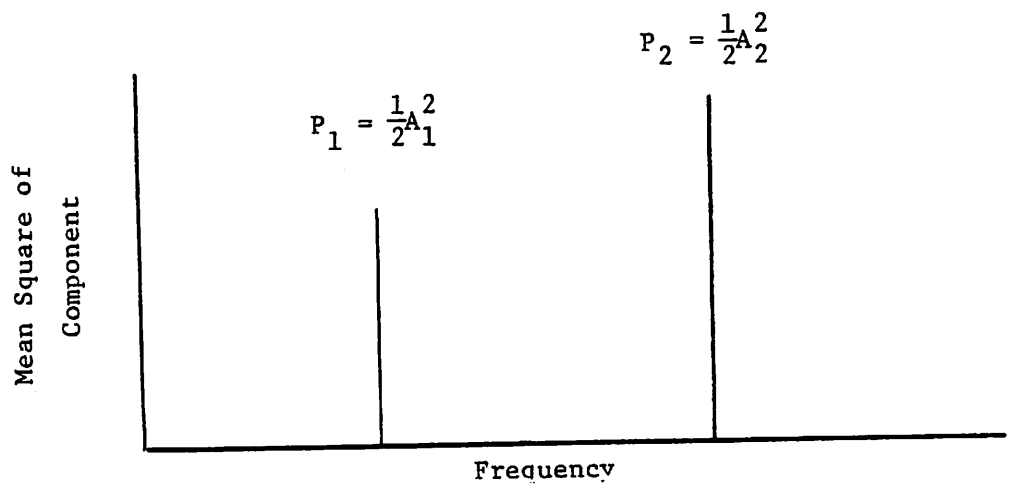

Figure 43. Line Spectrum of Data Set

The line spectrum is computed by integrating the squared components of the data set over its period and subsequently determining its mean value.

$$P_1 = \frac{1}{T} \int_0^T \left| A_1 \sin (2 f_1 t) \right|^2 dt = \frac{1}{2} A_1^2$$

Because of traditional use with currents in electrical engineering where power is proportional to $(\text{Current})^2$, the line spectrum is often called the power spectrum. The power spectrum, when divided by the frequency, yields energy associated with that particular frequency; this is often called the power spectral density or energy spectrum. These terms are often used for convenience even if the actual input and output quantities are not necessarily associated with power or energy.

In work with field data and real physical systems, inputs generally do not consist of a limited number of sinusoidal components. It is more appropriate to work with the concept of random or stochastic data for inputs and outputs. If the random data are considered to be stationary (by which is meant that certain statistical properties are invariable if sampled over sufficient time), then the data can be described as being composed of an infinite number of sinusoidal components. The power spectrum of the data then becomes continuous. Rather than plotting the power associated with a particular frequency, as is done for a line spectrum, one plots the power spectral density as indicated on Figure 44. The power spectral density or energy spectrum can be thought of as the data set components mean square value within a narrow frequency interval between f and $f+\Delta f$, divided by the frequency interval.

$$P_{xx}(f) = \lim_{\Delta f \to 0} \frac{1}{\Delta f} \lim_{T \to \infty} \frac{1}{T} \int_0^T X^2(t,f,\Delta f)\, dt$$

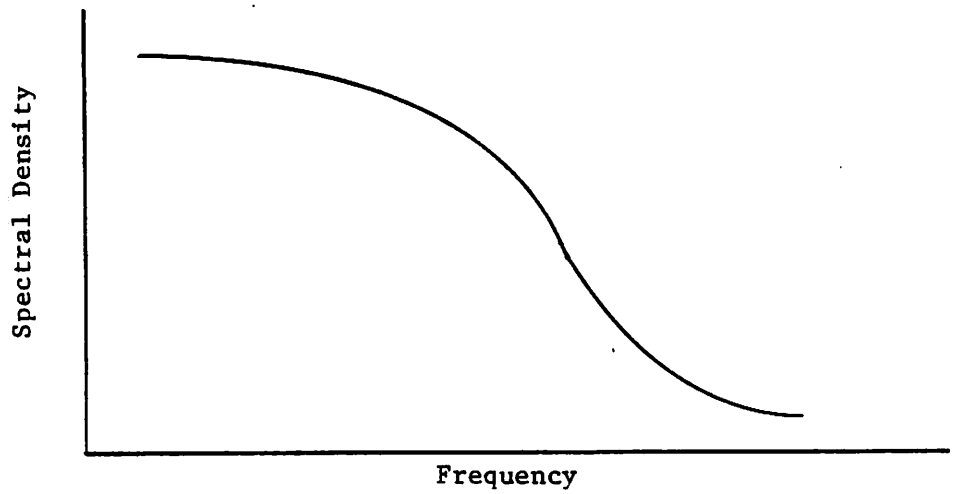

Figure 44. Energy Spectrum of a Data Set

In this equation $x(t,f,\Delta f)$ represents that part of the data set after all components not present in the frequency interval between f and $f+\Delta f$ are removed. Thus the integral under the curve of the spectral density function represents the mean square value $(\sigma_x)^2$ of $x(t)$.

$$\int_0^\infty P_{xx}(f)\, df = (\sigma_x)^2$$

The power spectral density or energy spectrum can thus be thought of as energy associated with a particular frequency.

By comparison of the energy spectra at various locations in a hydrodynamic system, it may be possible to associate any observable differences with physical or geometric characteristics of the system. A typical input energy spectrum to a numerical hydrodynamic model is shown in Figure 45 while Figure 46 indicates a typical model output

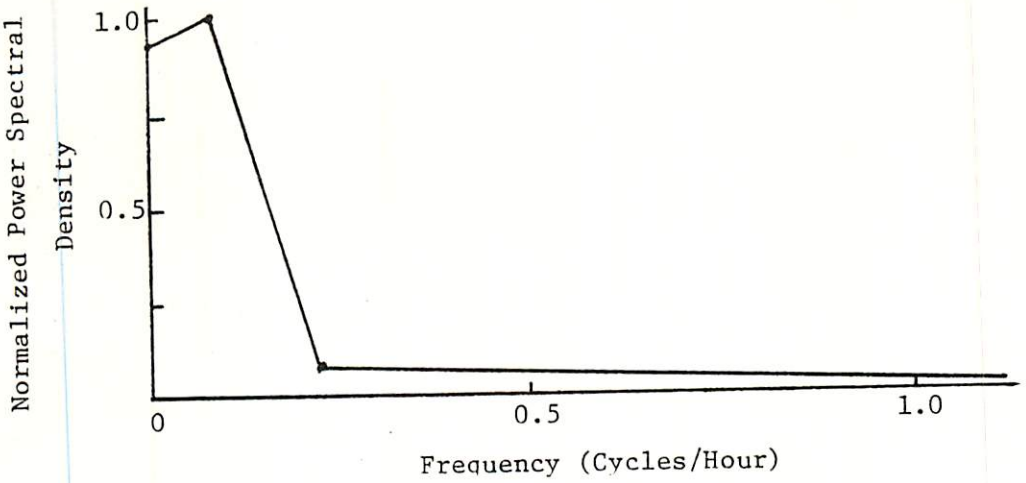

Figure 45. Typical Input Energy Spectrum

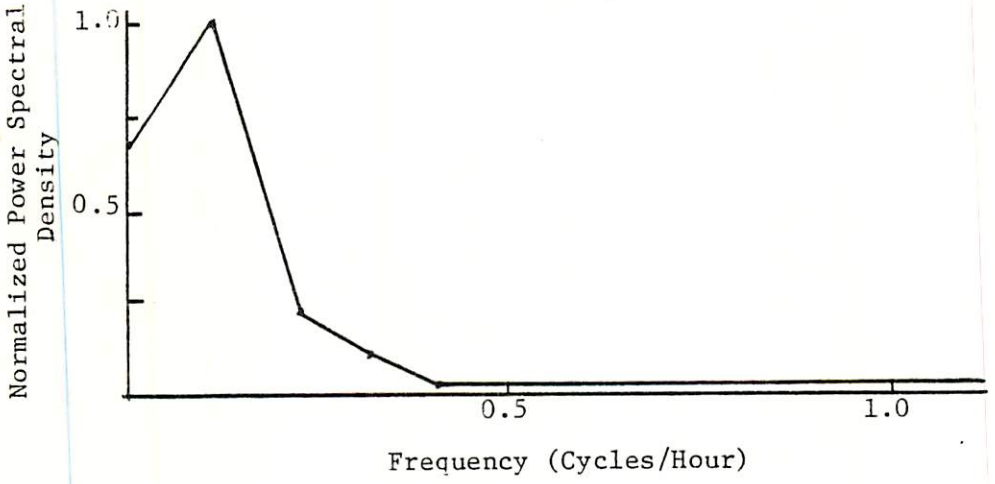

Figure 46. Typical Output Energy Spectrum

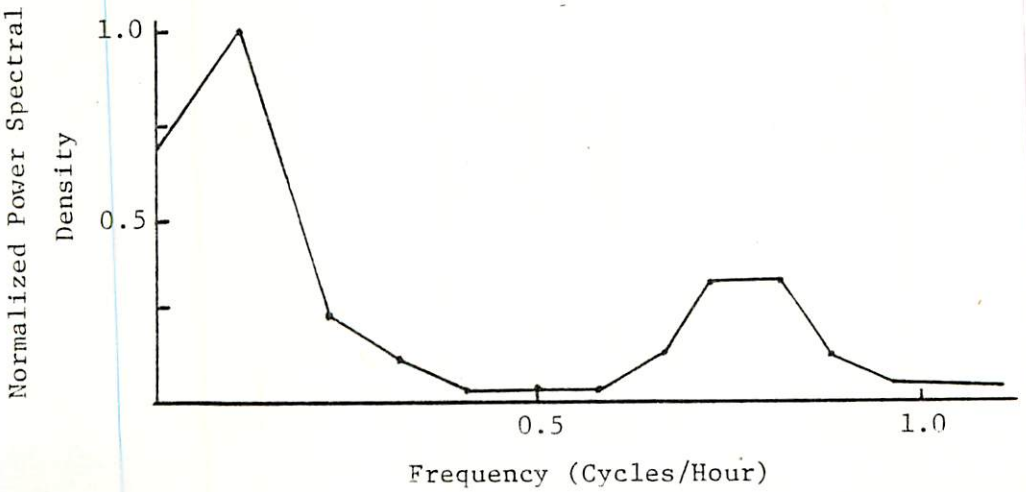

Figure 47. Distorted Output Energy Spectrum

energy spectrum at some location in the estuary. Any tendency of the system to oscillate at some fundamental mode or to distribute the energy to other frequencies can be detected. This is illustrated in Figure 47.

B. Three-Dimensional Models

Many estuaries are basically well-mixed with little stratification from salinity or temperature effects. These systems can be considered adequately with two-dimensional-depth-averaged hydrodynamic models similar to the WIFM II currently being used on this project. There are cases, however, where three-dimensional effects are present and two-dimensional considerations cannot adequately define the process. Investigation of three-dimensional models will proceed to provide insight into methods for considering three-dimensional effects in estuaries.

C. Water-Quality Models

Once a calibrated and verified hydrodynamic model predicting surface elevations and velocities is available, it can be coupled with a water-quality model to predict salinity patterns, bacterial concentrations, spread of oil spills and similar phenomena. These models represent sophisticated planning tools, and specialized models for Mobile Bay and Mississippi Sound should be developed as a natural progression from the hydrodynamic models.

D. Sediment Processes

One of the major deficiencies of numerical modeling at the present time is in the area of sediment transport. The process by which sediment is suspended in the water column, how its movement is related to the water movement and under what conditions the sediment is deposited out of the water column make the sediment-transport model difficult to formulate.

In addition, the time frame for sediment movement is very long compared with most hydrodynamic processes which are modeled. The calibration and verification process for models is therefore more difficult. A great deal of effort is currently being devoted to the sediment problem by the Corps of Engineers and other investigators. The literature on sediment processes in estuaries will be monitored to keep abreast of current activity and the potential for applications to Mobile Bay and Mississippi Sound.

VIII. CONCLUSIONS

The first year of this project has been completed essentially as planned. The WIFM II model developed at the U. S. Army Waterways Experiment Station was selected as the basic hydrodynamic model. This model has been made operational at The University of Alabama. Required input data for the model have been developed and necessary modifications to the model were accomplished. Graphical programs for convenient visual display of model output have also been developed. Three model applications have been made: Mobile Bay alone, Mississippi Sound alone, and Mobile Bay-Mississippi Sound combined. These models have all been run for several tidal cycles and are producing results which appear reasonable. Of course, the accuracy of the results can be established only by comparing them with prototype data. The only part of the first year's program not completed was due to a lack of prototype data with which to begin the detailed calibration and verification process.

Detailed investigations have been initiated into spectral analysis techniques, three-dimensional models, one-dimensional river models, water-quality models and sediment processes. These investigations will contribute to future efforts on the project.

IX. REFERENCES

1. Butler, H. L., "WIFM II - WES Implicit Flooding Model; Theory and Program Documentation," Report to be published, U. S. Army Waterways Experiment Station, CE, Vicksburg, Mississippi.

2. Raney, D. C., Durham, D. L., and Butler, H. L., "Lake Erie International Jetport Model Feasibility Investigation: Numerical Model Feasibility Study," Technical Report H-74-6, Report 17-4, U. S. Army Engineer Waterways Experiment Station, CE, Vicksburg, Mississippi, April 1977.

3. Wanstrath, J. J., Whitaker, R. E., Reid, R. O., and Vastano, A. C., "Storm-Surge Simulation in Transformed Coordinates, Vol. I - Theory and Application," Technical Report 76-3, U. S. Army Coastal Engineering Research Center, CE, Fort Belvoir, Virginia, November 1976.

4. Papoulis, Anthanasios, "Probability, Random Variables, and Stochastic Processes," McGraw-Hill Book Company, 1965.

5. Liu, S. K., "Stochastic Analysis and Control of Urban Estuarine Water-Quality Systems: Vol. 1 - Estimation and Prediction," Report R-1622-NYC, The New York City Rand Institute, December 1974.

6. Leendertse, J. J. and Liu, S. K., "A Water-Quality Simulation Model for Well-Mixed Estuaries and Coastal Seas: Vol. VI, Simulation, Observation and State Estimation," Report R-1586-NYC, The New York City Rand Institute, September 1974.

THE UNIVERSITY OF ALABAMA
COLLEGE OF ENGINEERING

The College of Engineering at The University of Alabama has an undergraduate enrollment of more than 1,800 students and a graduate enrollment exceeding 100. There are approximately 100 faculty members, a significant number of whom conduct research in addition to teaching.

Research is an integral part of the educational program, and research interests of the faculty parallel academic specialities. A wide variety of projects are included in the overall research effort of the college, and these projects form a solid base for the graduate program which offers twelve different master's and five different doctor of philosophy degrees.

Other organizations on the University campus that contribute to particular research needs of the College of Engineering are the Charles L. Seebeck Computer Center, Geological Survey of Alabama, Marine Environmental Sciences Consortium, Mineral Resources Institute—State Mine Experiment Station, Mineral Resources Research Institute, Natural Resources Center, School of Mines and Energy Development, Tuscaloosa Metallurgy Research Center of the U. S. Bureau of Mines, and the Research Grants Committee.

This University community provides opportunities for interdisciplinary work in pursuit of the basic goals of teaching, research, and public service.